March 2020

CHARACTERIZATION OF BIODISTRIBUTION OF TRANSFERRIN AND RECEPTOR BINDING MECHANISM BY MASS SPECTROMETRY

Hanwei Zhao

CHARACTERIZATION OF BIODISTRIBUTION OF TRANSFERRIN AND RECEPTOR BINDING MECHANISM BY MASS SPECTROMETRY

A Dissertation Presented

by

HANWEI ZHAO

Submitted to the Graduate School of the

University of Massachusetts Amherst in partial fulfillment

of the requirements of the degree of

DOCTOR OF PHILOSOPHY

February 2020

Department of Chemistry

CHARACTERIZATION OF BIODISTRIBUTION OF TRANSFERRIN AND RECEPTOR BINDING MECHANISM BY MASS SPECTROMETRY

A Dissertation Presented

By

HANWEI ZHAO

Approved as to style and content by:

_____
Igor A. Kaltashov, Chair

_____
Richard W. Vachet, Member

_____
Lynmarie K. Thompson, Member

_____
Stephen J. Eyles, Member

_____
Ricardo B. Metz, Department Head

Department of Chemistry

DEDICATION

To my dear husband who has always supported, encouraged, and stood by me.

To my precious kids who are the joy of my life.

To my loving mom and dad for making me be who I am.

ACKNOWLEDGMENTS

First of all, I would like to thank my advisor, Prof. Igor A. Kaltashov, for his constant professional guidance, suggestion, encouragement, and support throughout my graduate study and research. He is such a good mentor who doing things for his students' benefit. I would also like to express my sincere appreciation to Prof. Cedric E. Bobst for his patient and careful guidance in instrument handle, experimental design, data analysis, and discussion. I also want to thank Dr. Rinat Abzalimov who gave me technical support and hands-on help on the mass spectrometer. Many thanks go to the rest of the group members and alumni, Adriana Kita, Burcu Baykal, Guanbo Wang, Shunhai Wang, Nguyen Son, Ololade Fatunmbi, Khaja Muneeruddin, Jake Pawlowski, Shengsheng Xu, Yunlong Zhao, Chengfeng Ren, and Honglin Yao. You made Kaltashov's group a peaceful and great community.

My special appreciation goes also to my committee members, Prof. Richard W. Vachet, Prof. Lynmarie K. Thompson, and Prof. Stephen J. Eyles, for their useful comments and suggestions on all stages of my work. Special thanks to Prof. Anne B. Mason (University of Vermont, College of Medicine) for generously providing protein samples for my study, as well as for many helpful discussions; to Prof. Vachet for his poignant comments on my work; and to Prof. Eyles for helping me with multiple instruments.

It has been a pleasure to work with colleagues in Prof. Vachet and Prof. Rotello's group, they are Gokhan Elci, Bo Yan, Yuqing Xing, Dr. Sung Tae Kim, Krishnendu Saha, and Dr. Chang Soo Kim.

I would express my gratitude to all my friends. You have filled my mind with such beautiful memories at Amherst.

Finally, my deepest appreciation is expressed to my extended family, my parents, my parents-in-law, my husband and my lovely kids, for their love, understanding, and encouragement. It is your support and sacrifice that makes me focus on this dissertation.

ABSTRACT

CHARACTERIZATION OF BIODISTRIBUTION OF TRANSFERRIN AND RECEPTOR BINDING MECHANISM BY MASS SPECTROMETRY

FEBRUARY 2020

HANWEI ZHAO, B.S., CAPITAL MEDICAL UNIVERSITY, CHINA

M.S., UNIVERSITY OF MASSACHUSETTS LOWELL

Ph.D., UNIVERSITY OF MASSACHUSETTS AMHERST

Directed by: Professor Igor A. Kaltashov

Protein-based therapeutics have emerged as a key driver of rapid growth in drug development pipelines. However, developing such protein drugs is not straightforward in most cases, the existence of physiological barriers greatly restricts the efficient delivery of many therapeutic molecules, and therefore limits their clinical applications. A promising way to address this challenge takes advantage of certain transport protein which can effectively across and enhance the permeability of these barriers, such as transferrin (Tf) which can be internalized by malignant cells and cross physiological barriers via transferrin receptor (TfR)-mediated endocytosis and transcytosis. However, developing such products is impossible without successfully understanding the molecular mechanisms governing Tf/TfR interactions and the ability to monitor the biodistribution of Tf. In this work, hydrogen/deuterium exchange mass spectrometry (HDX MS) is used to investigate TfR higher order structural and dynamic changes in different Tf/TfR models that mimic various stages encountered during endocytosis. Detailed characterizations of TfR gained by HDX MS reveal the regions located at the

interdomain cleft exhibiting bimodal exchange patterns may be responsible for the loss of its enzyme function in the molecular evolution. At neutral pH, a movement at the TfR/TfR interface helps to stabilize the holoTf/TfR complexation. At acidic pH, the pH-induced conformational changes at the TfR helical domain trigger a series of movements that lead to specific binding properties for holo- and apoTf C-lobe. Obtaining this information greatly enhances our understanding of the pH-dependent Tf binding properties and how TfR facilitates iron release at acidic pH. Another aspect of this dissertation work is utilizing the ability of Tf to bind to noncognate metals to trace the biodistribution of Tf. Particularly, indium has been evaluated and demonstrated as an ideal tracer of exogenous Tf in complex biological matrices using inductively coupled plasma mass spectrometry (ICP MS) as a detection tool. In addition, combining laser ablation (LA) with ICP MS detection allows distribution of exogenous Tf to be mapped within animal tissue cross-sections. The high sensitivity and selectivity of this novel approach make it an ideal quantitation/imaging tool for *in vivo* studies of biodistribution of Tf and Tf-based therapeutics.

TABLE OF CONTENTS

Page

LIST OF FIGURES

Figure **Page**

CHAPTER 1

INTRODUCTION

1.1 Transferrin-Based Drug Delivery and Transferrin/Transferrin Receptor System

1.1.1 Protein Drugs and Drug Delivery

Since the introduction of the first recombinant protein therapeutics, human insulin (1), protein drugs have emerged as an important class on the pharmaceutical market serving patients most in need of novel therapies, including monoclonal antibodies as well as large or fusion proteins. Protein drugs generally have high molecular weights, complex secondary and tertiary structures and post-translational modifications. Due to the complexity of protein drugs, they are engineered to be more specific with the molecular target and have enhanced potency and functionality as well as fewer site-effects. Understanding the protein structure/function and the mechanism of action leads to the customization of existing proteins or the development of next-generation biological therapeutics strategies for specific clinical use. The recent US-FDA approved therapeutic proteins have been developed to treat a wide variety of therapeutic areas, including metabolic/hormonal disorders, cancers, hematology/oncology, cardiology/vascular diseases, autoimmunity, genetic disorders, and infectious disease (2,3).

While the protein drugs have developed significantly in the past decades, the inability for efficient and accurate delivery has limited their use. Despite significant investments and extensive R&D efforts, there are several challenges that make the development of biopharmaceuticals slow down, such as the presence of the scavenger

proteins and various filters (glomerular filter) and barriers (enzymatic barrier and physiological barriers) in the body. A common problem encountered in these areas is the inability of most proteins to cross physiological barriers, such as the gastrointestinal epithelial barrier and the blood-brain barrier (BBB) which restrict the development of protein drugs for oral administration and targeting pathologies in the central nervous system (CNS), respectively.

A receptor-mediated delivery system is one of the attractive strategies to overcome the limitation in drug absorption that enable the endocytosis/transcytosis of the proteins across physiological barriers in the body. This provides a promising approach for the treatment of brain diseases and the development of a viable mechanism of oral delivery. Examples of transported substances to CNS via receptor-mediated transcytosis include insulin (4), transferrin (Tf) (5), leptin (6), and the low-density lipoprotein receptor-related protein (LRP) (7). These proteins can be utilized as drug delivery vehicles, and the therapeutic protein can be tethered to them as payload by either conjugation (chemical cross-linking) or expression as a recombinant fusion protein. It is clear that the successful implementation of this route in drug delivery strategies needs a better understanding of the interactions between the receptors and protein-based therapeutics. In this dissertation, we focus on evaluating the molecular mechanisms of Tf and transferrin receptor (TfR) system.

1.1.2 The Role of Tf/TfR System in Drug Delivery

Tf is a very promising target for a growing number of therapeutic strategies for the purpose of devising highly efficient and selective drug delivery systems, as indicated by numerous reviews (8-10), due to its ability to enter the cell or cross physiological barriers in the process of TfR-mediated endocytosis or transcytosis (Figure 1-1). TfR performs as a cellular iron homeostasis adjustor: the low iron concentrations inside the cell increase the level of TfR expression by increasing the half-life of the TfR message translation in order to increase the iron intake into the cell. Therefore, the level of the soluble form of TfR can be used to monitor erythropoiesis (11). Besides this, TfR appears to be ubiquitously expressed in almost all nucleated cells, for example, red blood cells, thyroid cells, hepatocytes, brain, intestinal cells, and monocytes (12), but is overexpressed in various types of cancer cells, such as immature erythroid cells, placental tissue, and rapidly dividing cells, due to their high rates of proliferation and increased demand for iron (8,13-15). As a result of its differential expression in normal and malignant tissues, TfR has been investigated as a target for pharmacological intervention for several decades (16) and TfR-mediated pathway has also been explored for efficient therapeutic molecules and protein delivery (17-19).

A wide range of therapeutic agents (such as chemotherapeutic drugs, protein toxins, radionuclides, DNA, modified viral particles, and nanoparticles) can be tethered to Tf and delivered to malignant cells by targeting TfR on the cell surface (8,10). The therapeutic efficacy of drug delivery via TfR-mediated pathway can be enhanced due to more effective tumor targeting and less nonspecific toxicity. For example, the cisplatin-Tf conjugate, MPTC-63, which has already entered the clinical trials showed an anti-

tumor response in human epidermoid cancer with minor side effects (20). Another example for Tf-conjugates is MBP-426, a liposome-Tf conjugate for the delivery of oxaliplatin, which is in a Phase II clinical trial for patients with gastric, gastroesophageal, or esophageal adenocarcinoma (8). Normally, the receptor-mediated endocytosis is a saturable process, because of the limited number of the receptors on the cell surface. The nonlinear pharmacokinetics of the recombinant human erythropoietin (rh-EPO) (21) can be used to support this. This trait may limit the dose and efficacy of the drugs, but on the other hand, it can be used to reduce the drug clearance by inhibiting certain receptor-mediated endocytosis (22).

In addition, Tf is often considered as a promising metal-based drug delivery vehicle (10,23). Metal ions are fundamental components of cells and have been frequently incorporated into pharmaceuticals for therapeutic or diagnostic purposes. However, due to the severe side effects and the unstable ionic states of certain metal ions, many metals are investigated for improved pharmacological profiles. In the serum of healthy human subjects, only approximately 30% of Tf is saturated with iron (24), which provides a potential ability for the protein to bind and transport other metal ions from blood to tissues. Indeed, Tf can also bind with a wide range of other metals ions due to their biochemical similarities with iron and serve as a noniron metal mediator. This extends its function to deliver certain metals, including essential elements other than iron (e.g., Mn), therapeutic metal ions (e.g., Bi^{3+}, Ru^{3+} and Ti^{4+}), radio diagnostic metal ions (e.g., $^{67}Ga^{3+}$ and $^{111}In^{3+}$), and some toxic metal ions (e.g., Th^{4+} and U^{6+}), with

various affinities (25-27). Importantly, many of these metal-Tf complexes can still be recognized by TfR (26).

Since TfR is also overexpressed in the brain capillaries, TfR-mediated transcytosis (Figure 1-1B) has been focused as one of the most efficient pathways for the delivery of therapeutic molecules to CNS. Briefly, Tf binds to TfR on the apical membrane. Subsequently, the membrane invaginates to form an intracellular vesicle through endocytosis. The vesicle migrates across the cytoplasm and fuses with the basolateral membrane. Then Tf is released from the receptor on the abluminal surface. Although a detailed understanding of cellular mechanisms associated with TfR-mediated uptake pathway at the BBB remains unclear, several studies have demonstrated the ability of TfR to deliver Tf-drug conjugates (9,28) and TfR-antibody conjugates (29,30) into the brain. The former is achieved either by chemical conjugation of therapeutic drugs, proteins with Tf or by genetic infusion of therapeutic peptides or proteins into the structure of Tf; while the latter is using engineered anti-TfR antibodies as artificial ligands which can be used to shuttle therapeutic molecules into the brain. Furthermore, in addition to mediating transcytosis across BBB in blood-to-brain direction, TfR can also mediate reverse transcytosis of Tf in brain-to-blood direction, as the evidence of the efflux of both apo- and holoTf across BBB (31). Numerous efforts aiming at utilizing this unique trait for the purpose of targeted drug delivery that ranges from small molecules to macromolecular drugs and supramolecular assemblies (32,33) are underway, with the ultimate goal of developing therapeutic agents that can reach targets shielded from the vast majority of existing drugs. Contributing to this goal, our group has started exploring

a possibility of conjugating a bacteriolytic enzyme, lysozyme, to Tf for targeting microbial infections in the central nervous system (34,35).

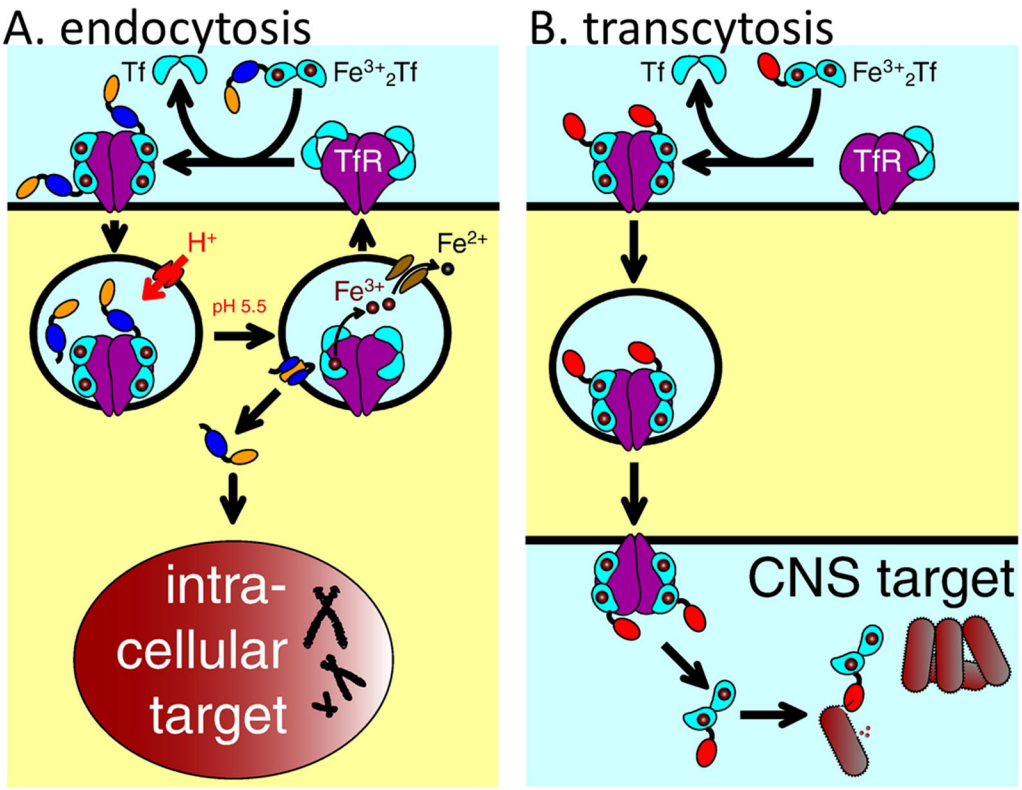

Figure 1-1 Schematic diagram of (A) TfR-mediated endocytosis and (B) transcytosis for Tf-based therapeutic delivery to intracellular targets and CNS targets, respectively. Figure is from Reference (35).

1.1.3 Characterization of TfR-Mediated Endocytosis

Iron is an essential nutrient that participates in various biological processes. Mammalian cells utilize multiple mechanisms to acquire inorganic iron. The primary route for most cells to uptake circulating iron is via Tf/TfR-mediated endocytosis (Figure 1-1A), which is negatively modulated by HFE (the hereditary hemochromatosis protein, which is related to class I major histocompatibility complex proteins (36) and is mutated in the iron-overload disease hereditary haemochromatosis) in transfected cells (37,38)

due to the same or significantly overlapping TfR binding sites for Fe_2Tf and HFE. TfR binds two molecules of Fe_2Tf at the cell surface. The initial stage of the binding mechanism of Fe_2Tf to TfR at neutral pH is the loss of protons from TfR at the Tf binding sites with a proton loss pK_a =8 (39). Upon addition of Fe_2Tf, an intermediate of Tf/TfR where the C1-subdomain of Tf is bound to TfR is formed within microsecond range. Then this intermediate undergoes a slow change in its conformation bringing to the final thermodynamic state where both N- and C-lobe of Tf are bound to TfR (39).

The Tf/TfR complex is then internalized through clathrin-coated pits to form a vesicle, which buds from the plasma membrane, at the cell surface, and subsequently transported to endosomes. Protons are pumped into the endosomes through the action of an ATP-dependent proton pump resulting in a decrease in pH to about 5.5, which triggers the conformational change of the complex and the subsequent release of iron from Tf. The free ferric iron (Fe^{3+}) released to endosomes is reduced to ferrous iron (Fe^{2+}) by the endosomal metalloreductase STEAP3 (six-transmembrane epithelial antigen of the prostate 3) (40) and Fe^{2+} is subsequently transported out of the endosome into the cytoplasm by DMT1 (divalent metal transporter 1) (41). By an iron transport molecule, the cytosolic iron is shuttled to various intracellular locations, including the mitochondria (for heme and ribonucleotide reductase incorporation) and ferritin (for storage) (42,43).

After the iron is released from Tf, the resultant apoTf remains bound to TfR with high affinity. Then the apoTf/TfR complex is quickly recycled back to the cell surface through exocytic vesicles and apoTf is released into the serum either through

dissociation from TfR or displacement by Fe_2Tf or monoferric-Tf (44) due to its weak receptor binding affinity at neutral pH. The apoTf molecule then circulates until it couples to free irons, and the cycle is continued. The entire iron uptake cycle lasts only 4 to 5 minutes (45).

TfR's preference for apoTf at endosomal pH not only facilitates iron release from Tf, but also saves it from inevitable degradation in the lysosomal compartment after endocytosis, where most internalized proteins end up unless they keep bound to a membrane-associated receptor, and recycles back to the cell surface for recycling. Once such "recycling" is no longer needed, the protein is serviced by a different receptor. An example is the lactoferrin (Lf), one of the four distinct members of the transferrin family in mammals (46). It arose from a duplication of Tf gene in the ancestor of mammals approximately 160 million years ago (47). Despite its affinity for iron, Lf is not required for iron homeostasis in the body (48). Instead, it is functioned as part of the innate immune and catalytic response (49). Unlike Tf, Lf cannot bind to TfR but it binds to a number of receptors from unrelated protein families, such as low density lipoprotein receptor-related protein 1 and 2, which are expressed in the bone, cartilage, fibroblasts and brain cells (50). In contrast to Tf, iron is released from Lf when a portion of the endocytosed Lf is routed to the lysosomal compartment and the Lf/receptor complex is degraded. Of course, TfR is not unique in its "guardian" role: the neonatal Fc receptor (FcRn) accomplishes a similar task, which rescues phagocytosed IgGs and serum albumin from being routed to lysosomes (51). However, the structures of the FcRn/IgG and

FcRn/albumin complexes are very different from that of Tf/TfR, and the mechanism of pH-dependent binding is different.

1.1.4 The structures of Tf, TfR and the Tf/TfR Complexes

1.1.4.1 Tf

Human Tf is an 80 kDa monomeric bilobal glycoprotein that transports otherwise insoluble ferric ions (Fe^{3+}) through the bloodstream to cells and crosses the physiological barriers via receptor-mediated endocytosis/transcytosis. Tf has two structurally similar lobes, generally termed the N- and C-lobe, and each lobe is composed of two subdomains (N1 (residues 1-92 and 247-331), N2 (residues 93-246), and C1 (residues 339-425 and 573-679), C2 (residues 426-572)), forming an interdomain cleft which provides a distinct binding site for a ferric ion. It has an extremely high affinity for ferric ions (K_d is 10^{23} M^{-1} at pH 7.4 (52)) and forms holo-Tf at neutral pH. Fe^{3+} is held tightly within one or both homologous N- and C-lobes of Tf (Fe_2Tf, Fe_NTf, and Fe_CTf). Each lobe undergoes a significant conformational change upon Fe^{3+} binding (the two subdomains in each lobe rotate towards each other by approximately 50°), which results in a closing of the metal binding cleft (Figure 1-2). In each lobe the bound ferric ion is coordinated in a near octahedral geometry, with four ligands provided by the protein (one aspartate residue, Asp63/392 in N1/C1, one histidine residue, His249/585 in N1/C1, and two tyrosine residues, Tyr188/517 in N2/C2 and Tyr95/426 in N2/C2) and the two remaining ligands provided by the synergistic carboxylic anion (carbonate or oxalate) (Figure 1-3). The synergistic anion is essential for Tf to facilitate specific and strong ferric ion binding

(53). In the absence of a synergistic anion, the ferric ion has no affinity for the metal binding site which results in nonspecific binding and hydrolytic polymerization at the physiological pH (54). Substitution of carbonate by oxalate anion can effectively lock the iron into each lobe of Tf which results from a symmetric bidentate interaction with iron and the low p*Ka* of the oxalate anion (4.2 for oxalate vs 6.4 for carbonate) (55,56). Although the two lobes are highly homologous (49% homology (57)), their metal-binding properties are significantly different. The C-lobe of the protein has a higher affinity for ferric ion (58), and the iron release from the C-lobe of the protein occurs at a more acidic pH than the N-lobe (59). The transition from the closed to the open state of Tf upon mild acidification is due to the protonation of the residues K534, R632, and D634 in the C-lobe which serves as the pH-sensitive triad, and the pH-dependent dilysine trigger (K206 and K296) in the N-lobe (60). Mutating any of these residues to the dysfunctional pH-sensitive element will effectively lock the lobe in the closed conformation, even at endosomal pH, by reducing the iron release rates by 2-4 orders of magnitude compared to the wild-type Tf (45,61). The R632A mutation transforms a pH-sensitive triad in the C-lobe to a strong salt-bridge K534···D634 favoring the closed conformation, while mutating K206 to an acidic residue, glutamic acid, can convert the dilysine trigger to a very stable salt-bridge E206···K296 and nearly irreversibly lock the N-lobe in the closed conformation.

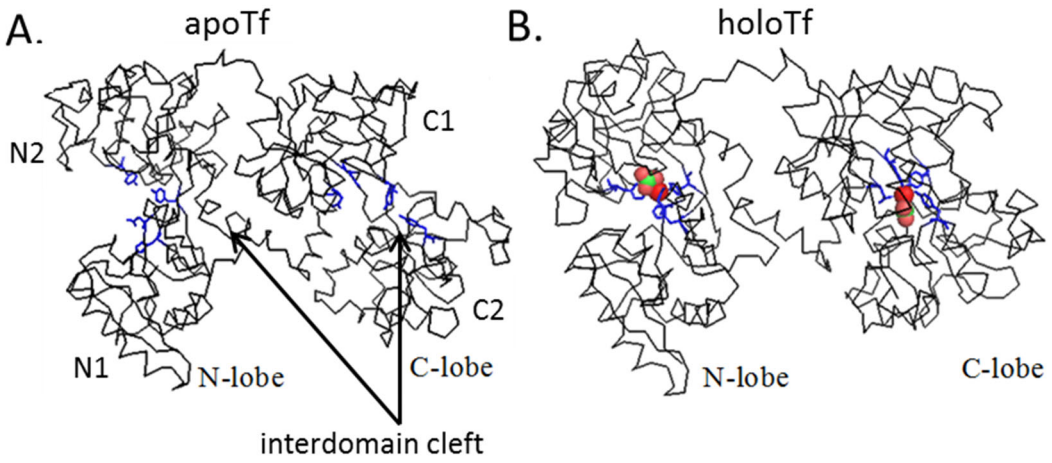

Figure 1-2 Crystal structures of the apo- (A, PDB: 2HAV) and holo-form (B, PDB: 3V83) of human Tf showing the details of iron binding. Side chains coordinating with iron are shown as blue sticks; both ferric ions and the synergistic anions are shown as spheres (Fe: red; C: green; and O: brown).

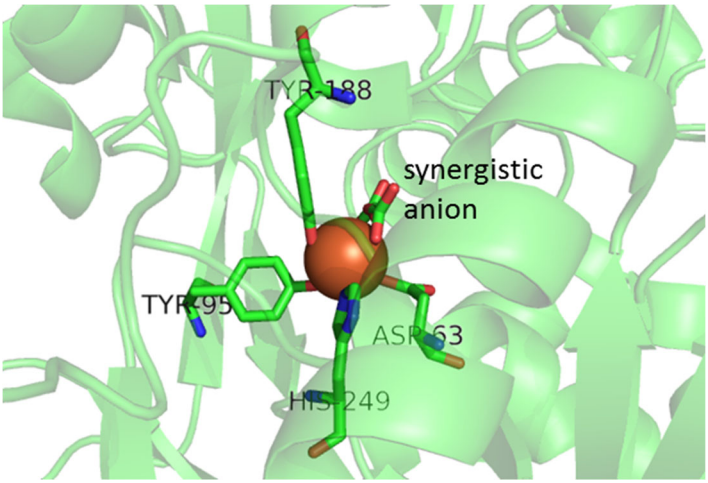

Figure 1-3 Zoomed-in view of the Fe^{3+} binding site of the N-lobe of Tf (PDB: 1A8E). Side chains coordinating with iron are shown as stick structures, and Fe^{3+} is shown as a brown sphere.

1.1.4.2 TfR

TfR is a homodimeric type II transmembrane glycoprotein on the cell surface. A full-length TfR is made up of a short N-terminal cytoplasmic tail (residues 1-67) with an internalization motif (YTRF), a single hydrophobic transmembrane region (residues 68-88), and a stalk (residues 89-120) connected to the Tf binding ectodomain (residues 121-

760) (62) (Figure 1-4A). The stalk contains the trypsin cleavage site which results in the release of the soluble ectodomain. The ectodomain is a dimer and each TfR monomer contains three distinct domains (Figure 1-4B): the protease-like domain (residues 121-188 (PA1) and 384-606 (PA2)), the apical domain (residues 189-383), and the helical domain (residues 607-760) (63). There are three *N*-linked glycosylation sites in TfR (Asn251, Asn317, and Asn727), while only Asn317 shows a significant effect on TfR solubility and can stabilize the apoTf bound to TfR at endosomal pH (64).

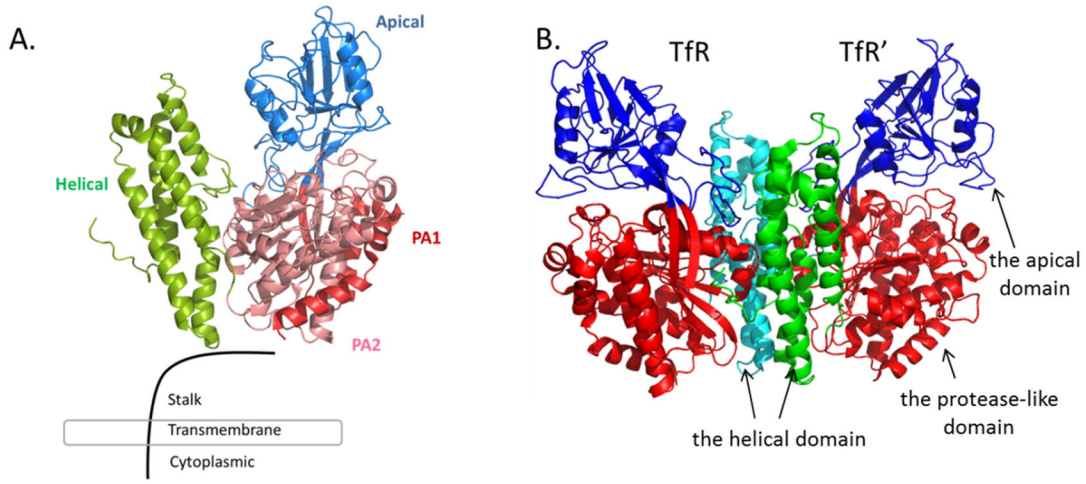

Figure 1-4 The structure of TfR. (A) The schematic figure of the full-length TfR. (B) The crystal structure of the ectodomain of TfR (PDB: 1CX8). The TfR homodimer is colored according to the domains: the apical domain is blue, the protease-like domain is red, and the two monomers of the helical domain are green and cyan, respectively.

1.1.4.3 The Tf/TfR complexes

As the function of receptor, the soluble ectodomain of TfR can bind two Tf molecules. Both the N-lobe and C1-subdomain of Tf are required for maximal TfR binding, and the C-lobe is the primary receptor recognition site and contributes approximately 60% to the Tf/TfR interface (65). At neutral pH, TfR prefers to bind with Fe_2Tf with the dissociation constant (K_d) at 10^{-9} M level (66,67), about 30 times greater

compared to the dissociation of apoTf/TfR (68,69) and 8-9 times greater than that with monoferric-Tf; while these two monoferric species have similar receptor binding affinity (67). In contrast, at acidic pH, the affinity of apoTf for TfR is about 7 times higher than holoTf (70), but about 2-4 times lower than the holoTf and TfR at neutral pH (66,69,71).

The first publication of the structure of the Tf/TfR complex was a 7.5 Å resolution cryo-electron microscopy (EM) model of Fe_2Tf/TfR in 2004 (PDB: 1SUV) (Figure 1-5A) (72). Due to the lack of the crystal structure of either full-length human apoTf or Fe_2Tf at that time, this cryo-EM model was built by docking the crystal structures of the TfR alone and the isolated N-lobe of iron-loaded human Tf and the C-lobe of rabbit Tf (78% sequence identity and 92% sequence similarity to the C-lobe of human Tf (73)) into the electron density map. This model shows that the N-lobe of Tf is sandwiched between the membrane and the TfR and that the C1-subdomain is contacted with the helical domain of TfR. Comparison of the structures of the free rabbit Fe_2Tf with the docked model shows a ~9 Å shift between the N- and C-lobe of Tf (Figure 1-5A). The relatively low resolution of the EM map provides a rather hazy and ambiguous picture of the Tf/TfR interaction. After the crystal structure of apoTf became available (74) and employing the modeled structure using the structures of iron bound human N-lobe Tf and diferric hen ovoTf, the computational structure models of apoTf/TfR and Fe_2Tf/TfR complexes were generated by Yamamura group in 2009 (75). These models eliminate the 9 Å conformational change of Tf upon complexation and are consistent with the available mutagenesis experiments (66,67). Moreover, these models suggest that the

residue Arg651 in TfR is a hot spot for Tf/TfR binding, which can interact with the residue Glu385 in both apoTf and Fe_2Tf.

In combination with previous structures of the free TfR, the TfR/HFE complex (76) and the EM model of Tf/TfR complex, a most recently published crystal structure of the Fe_NTf/TfR complex (PDB: 3S9N) at a high resolution of 3.22 Å (Figure 1-5B) (65) reveals various aspects of the intramolecular movements in TfR as a result of Tf binding and the interactions between the N-lobe and C1-subdomain of Tf and TfR that allow for the cellular uptake of Tf and affect iron release from Tf in the presence of TfR. Three primary interaction motifs are involved here (Figure 1-5C-D). 1) The N1 subdomain of Tf contacts the bottom region of the helical domain of TfR by a salt bridge between Arg50 2) Two loops within the N2 subdomain of Tf, the PRKP loop (residues [142-145]) and the loop [154-167], make contacts with the N-terminal of TfR. Three residues in the PRKP loop, Pro142, Lys144, and Pro145, participate in high affinity receptor binding (67). 3) The C1 subdomain of Tf forms a large interaction surface with the helical domain of TfR through Tf Asp356-TfR Arg651 salt bridge, and side chain interactions between a number of charged Tf residues (Arg352, Glu357, Glu367 and Glu385) and TfR (77). Although no experimental evidence was provided that the C2 subdomain of Tf is involved in binding to TfR (65), it may stabilize binding of the iron-loaded C-lobe of Tf in the Tf/TfR complex, as the evidence of mutation of Lys511 in the C2 subdomain, which does not contact with TfR, can affect the receptor binding (32). Additionally, conformational changes at the TfR dimer interface that induced by Tf binding, priming TfR to undergo pH-induced movements that affect the Tf/TfR binding. The mechanisms

of iron release from each lobe of Tf in the presence of TfR are different: binding of His349 to TfR is critical for stimulating iron release from the C lobe, whereas binding with TfR may limit access to a kinetically significant anion binding site in the N2 subdomain (78) that hinders iron release from the N lobe.

Although this high-resolution crystal structure of the Fe_NTf/TfR complex allows a more accurate description of the specific interactions between the two binding partners at neutral pH, it remains hypothetical how the internal motions relate to changes of TfR binding preferences throughout endocytosis. Understanding of the Tf/TfR pathway could further allow us to understand molecular mechanisms governing Tf/TfR interaction and garner important knowledge needed for the rational design of Tf conjugates in drug delivery strategies to maximize the use of this system.

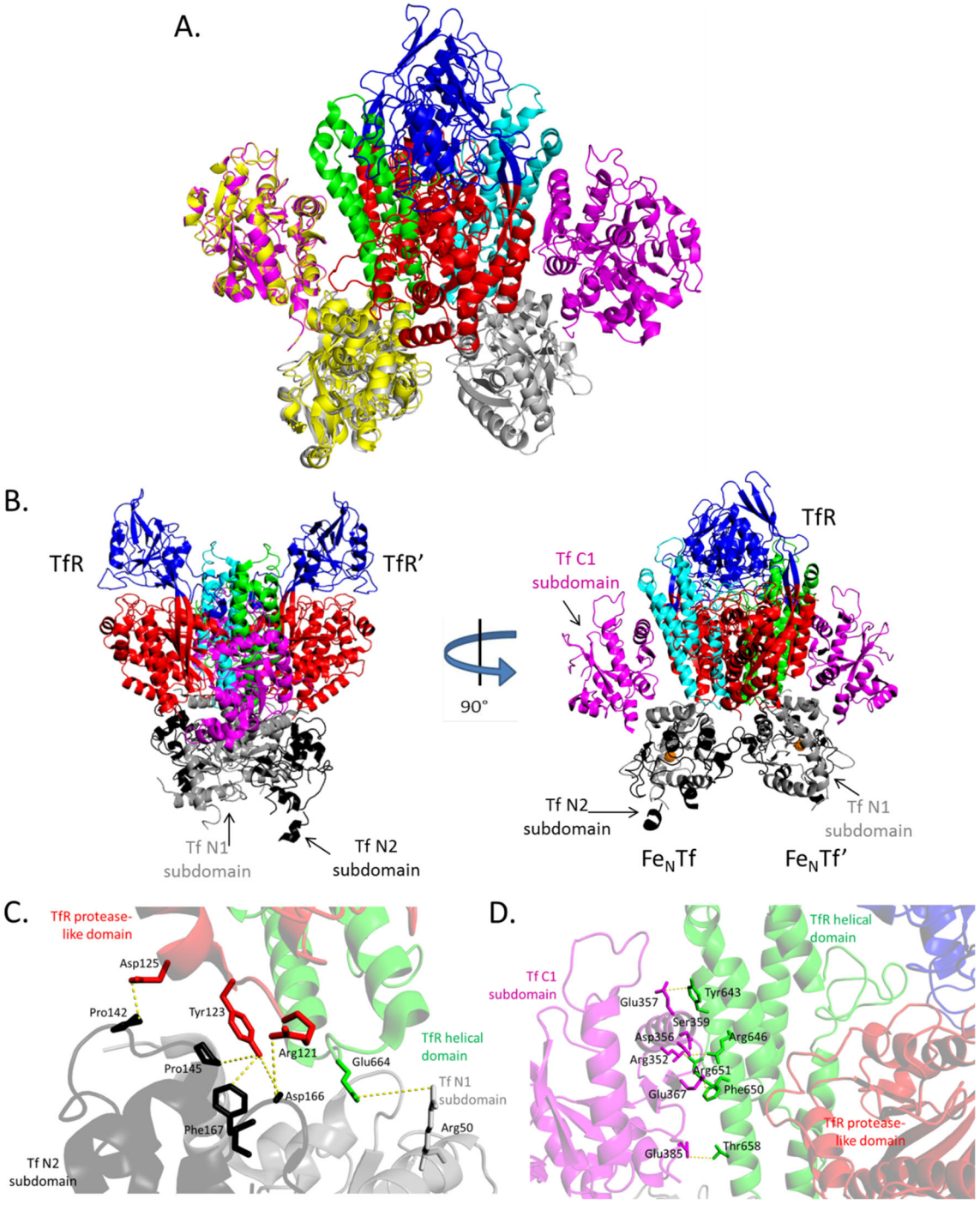

Figure 1-5 The structures of Tf/TfR complexes. (A) The overlay structures of the cryo-EM model of Fe_2Tf/TfR (PDB: 1SUV) and the rabbit Fe_2Tf (yellow, PDB: 1JNF), showing the ~9 Å shift between the N- and C-lobe of Tf. (B) The crystal structure of Fe_NTf/TfR complex (PDB: 3S9N). The primary interaction motifs of Tf N-lobe/TfR and Tf C1/TfR in Fe_NTf/TfR complex (PDB: 3S9N) are shown in panel (C) and (D), respectively. The TfR homodimer is colored according to the domains: the apical domain is blue, the protease-like domain is red, and the two monomers of the helical domain are green and cyan, respectively. The

N- and C-lobe of Tf molecule in Fe_2Tf/TfR in panel (A) are colored in white and magenta, respectively. The Fe_NTf molecules in panels (B), (C) and (D) are colored according to subdomains: N1 is gray, N2 is black, and C1 is magenta. The Fe^{3+} bound to each N-lobe of Tf in panel (B) is shown as the orange dot.

1.1.5 TfR and its Homologous Proteins

There are at least seven different homologous proteins in the TfR family in primates, including TfR1, TfR2, glutamate carboxypeptidase II or prostate-specific membrane antigen (GCP2 or PSMA), N-acetylated α-linked acidic dipeptidase-like protein (NAALADase), N-acetylated α-linked acidic dipeptidase 2 (NAALAD2), prostate-specific membrane antigen-like protein or glutamate carboxypeptidase III (PSMAL or GCPIII), and N-acetylated α-linked acidic dipeptidase-like protein 2 (NAALADase2). In general, the TfR family members can be divided into two subfamilies based on their functions: receptors and enzymes. However, of these homologs, only hTfR1, hPSMA and NAALADase have the published structures so far and the functions of some members remain uncertain (79). TfR2 is also a receptor protein, which is expressed in the liver and erythroid cells, participating in modulating hepcidin expression. Mutations to TfR2 result in type 3 hemochromatosis (80). It has 66% similarity to the extracellular domain of TfR1, but 30% lower binding affinity for Tf (81). The differences in the helical domain between the two TfRs, as well as the C-terminus, together with the apical domain arm junction (residue 306-330 in TfR1) account for the different Tf binding rates (82). Other than TfR, the best-studied member in this family is PSMA which is primarily functioned as an enzyme. It is weakly expressed in normal prostate tissue, but the amount is markedly increased in prostate cancer cells due to the regulation of androgen (83). In addition,

PSMA is also highly expressed in other cancers, more specifically in the tumor-associated neovasculature (84). Therefore, it has been used as a prostate cancer cell-surface biomarker and a target for imaging the neovasculature of tumors. PSMA acts as a glutamate carboxypeptidase with two separate catalytic functions: folate hydrolase (in the proximal renal tubules and duodenum) and NAALDase (in the brain), resulting in the release of glutamate from the enzyme substrates (85,86).

A structure-based alignment of TfR1 and PSMA reveals certain common features: a short N-terminal cytoplasmic tail, a single hydrophobic transmembrane domain, and a large extracellular domain (Figure 1-4A) (79). A novel MXXXL motif in the cytoplasmic tail in PSMA mediates its internalization via clathrin-dependent endocytosis (87). As shown in Figure 1-6, the extracellular domain of both proteins has three structurally diverse domains: an apical domain, a protease or protease-like domain, and a helical domain. The extracellular domain of PSMA shows structural homology to TfR1 (26% sequence identity, 46% similarity, and 14% gaps) (88), while PSMA has a more compact dimer interface and an enzymatically active site. The helical domain of TfR is the primary site for Tf and HFE interaction and dimer contacts. In contrast, the residues in the helical domain of PSMA involved in Tf and HFE binding are nonconservatively substituted (88), resulting in no Tf or HEF binding ability. The helical domain in PSMA only involves in forming the dimer interface and the substrate-binding cavity. The apical domain of TfR is equivalent to the protease-associated domain, a homology domain that can be found in the non-catalytic part of several families of the subtilases and zinc-containing metalloproteases, inserted within a loop of the peptidase domain of family M8/M33

zinc peptidases (89,90). The function of the apical domain may relate to mediate substrate determination of peptidases or form protein–protein interactions (89). In PSMA, the apical domain contains the binding site of the J591 antibody (91), but the function in TfR is unclear. The currently available models of Tf/TfR suggest that this domain does not participate in Tf binding. Some studies have shown that the apical domain of TfR may participate in some viruses (e.g., arenaviruses (92) and canine and feline parvoviruses (93)) and ferritin (94) binding, evolved to not interfere with Tf binding. The protease-like domain in TfR is closely related to that of carboxy- or aminopeptidase family and it is highly conserved in TfR/PSMA family (53% identical to TfR2 (79)) and 29% identical to PSMA (88)). Unlike TfR, the protease domain of PSMA contains a binuclear zinc site, catalytic residues, and a proposed substrate-binding arginine patch (88). The active site and the substrate-binding cavity in PSMA are formed with a contribution of all three domains. The two Zn atoms, a catalytic water (or OH^-), and their coordinating residues (histidine and glutamate/aspartate) in the active site are highly conserved between PSMA orthologs and related Zn-dependent exopeptidases (for example, *Streptomyces griseus* aminopeptidase (Sgap), *Aeromonas proteolytica* aminopeptidase (AAP), peptidases V and T (PepV and PepT), and carboxypeptidase G2 (CPG2)) (88). In TfR, four out of the five presumed Zn-binding ligands (His553, His377, Glu425, and Asp387, with the sole exception of Asp453 in PSMA) in the protease-like domain are missing, and TfR lacks the protease activity. The substrate-binding cavity is undisputedly one of the most important portions in PSMA which is shaped by Phe209, Arg210, Asn257, Glu424, Glu425, Gly427, Leu428, Gly518, Tyr552, Lys699, Tyr700, and

an arginine-rich patch (Arg-210, -463, -534, and -536) (88,95). A beta-hairpin, residues 692-704 in PSMA termed the glutarate sensor (red arrow in Figure 1-6B), which is reported to be important for its substrate recognition and/or binding (95), contains insertions in PSMA (relative to TfR) and exhibits unique seconder structure element in PSMA which is not present in TfR. This beta-hairpin connects the helical domain to the rest of PSMA, but it is much shorter in TfR and unable to reach into the substrate-binding cavity in PSMA.

Since the protein function is directly related to its 3D structure, any change to a protein at any structural level, including slight changes in the folding and shape of a protein, may render it nonfunctional. PSMA, function as an enzyme, the specific shape and configuration allows the formation of active site and substrate-binding cavity. In TfR, the missing of the Zn-binding ligands and the different shape of the substrate-binding cavity lead to the loss of the enzyme function. Instead, the residues in TfR involved in Tf and HFE binding, as well as TfR/TfR dimerization, are nonconservatively substituted in PSMA. We argue that TfR function had to co-evolve with that of Tf (MTf (melanotransferrin)/Tf split), likely before the true vertebrates arose (Figure 1-7) (50,79), and the sequences/structures divergent from PSMA and were kept in TfR are responsible for its new function (including the pH-dependent preference for apo and holo forms of Tf).

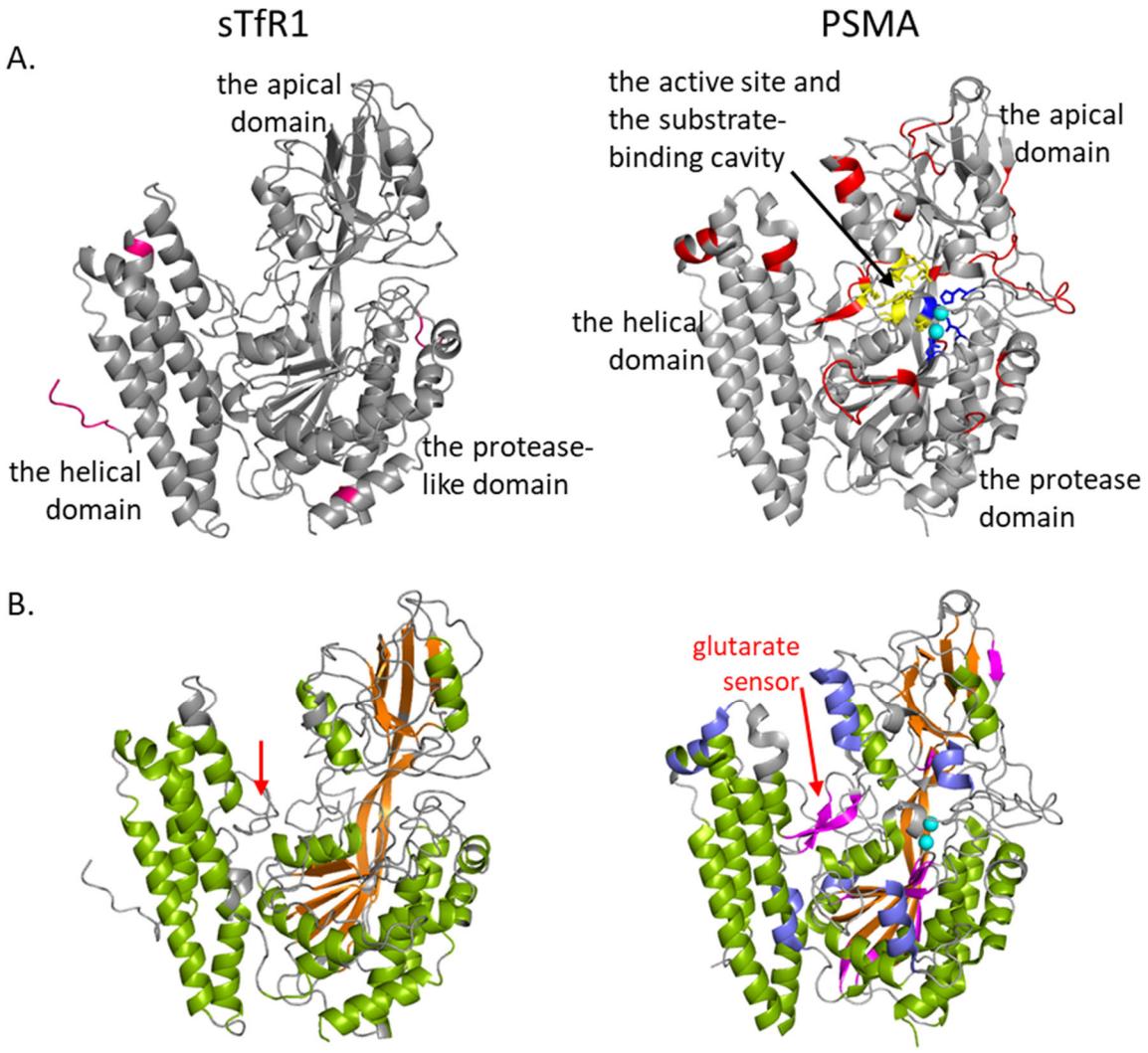

Figure 1-6 The structural alignment of sTfR1 (PDB: 1CX8) (left) and PSMA (PDB: 2OOT) (right) highlighting the insertions (A) and structure comparison (B). (A) The insertions in TfR (relative to PSMA) are colored in pink, and the insertions in PSMA (relative to TfR) are colored in red. (B) The helices and β-strands that common to both TfR and PSMA are colored in green and orange, respectively. The helices and β-strand that unique to PSMA are colored in slate and magentas, respectively. The two zine atoms in PSMA are highlighted in cyan dots and the zinc binding sites are shown in blue in panel A. The residues formed the substrate-binding cavity are highlighted in yellow. The red arrow in panel B is pointed to the glutarate sensor in PSMA, and the analogous region in sTfR1 is also pointed.

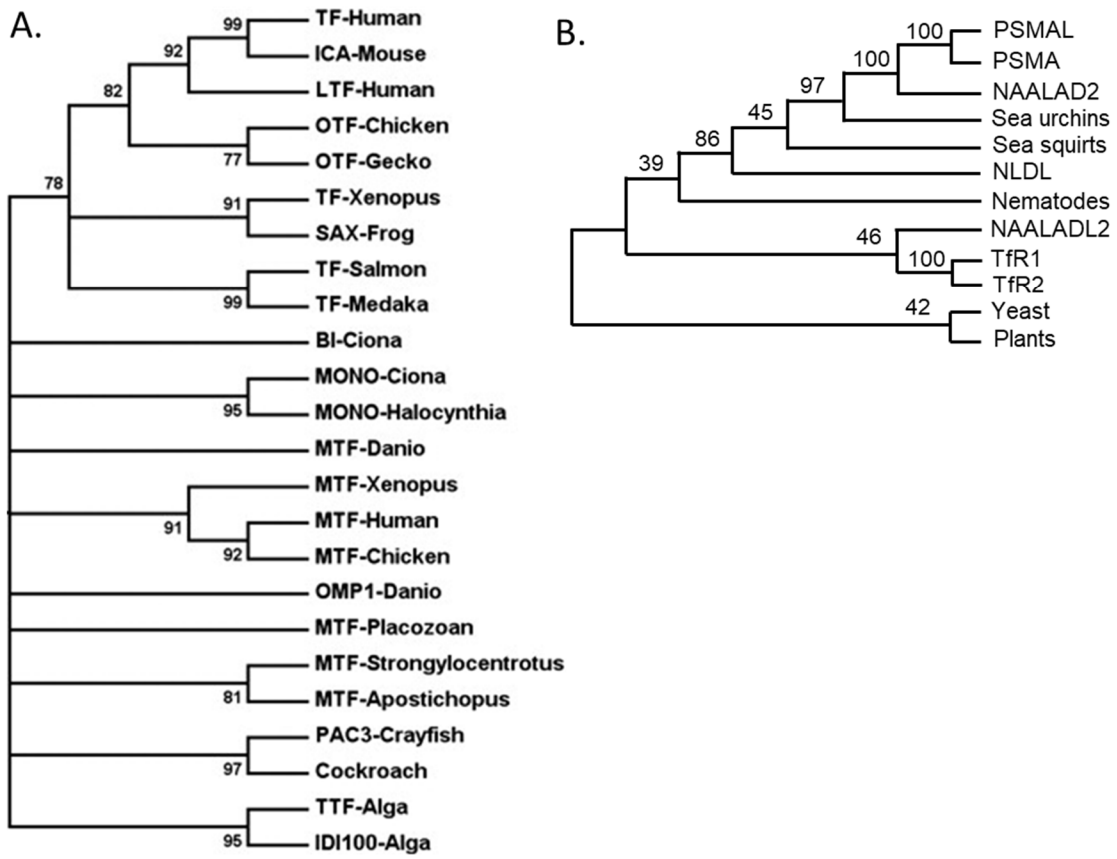

Figure 1-7 Relative evolutionary relationships among Tf family members (A) and TfR/PSMA family (B). Numbers on the branch represent the percentage of 1000 for Tf family and 2500 replicates for TfR/PSMA family in which each cluster was formed. Tree B was produced using one representative from each major group of sequences. Figure A and B are reproduced from reference (50) and (79), respectively. ICA: inhibitor of carbonic anhydrase. LTF: lactoferrin. OTF: ovotransferrin. SAX: saxiphilin. BI: ciona Tf2. MONO: ciona Tf1. OMP1: otolith matrix protein 1. PAC3: pacifastin 3. TTF: triplicated transferrins.

1.2 Mass Spectrometry as a Tool to Study Protein Structure and Function

1.2.1 Contributions of Mass Spectrometry to Structural Proteomics

The term ‘proteome’ was first used in 1995, to describe the entire complement of protein (96). The derived word ‘proteomics’, which is used quite commonly, deals with the large-scale study of protein properties, especially their structures, functions, and control of biological processes (97,98). This field is a collection of various techniques,

including protein separation, identification, quantification, and analysis. In the post-genomic era, mass spectrometry (MS) has increasingly become the method of choice for protein bioinformatics analysis because of its high throughput in analyzing the protein primary sequence, post-translational modifications, and protein-protein interactions. MS-based methods are also being developed to determine both higher order structure and the dynamics of proteins as well as protein complexes, which successfully complement other biophysical techniques, including X-ray crystallography and nuclear magnetic resonance (NMR) spectroscopy. In the recent revolution, the combination of MS to other methods, such as hydrogen/deuterium exchange (HDX), cross-linking, ion mobility, limited proteolysis, and chemical modification has led to a new field of structural proteomics. Each of these can provide unique characters for studying protein structure.

1.2.2 Direct Electrospray Ionization Mass Spectrometry (ESI MS) Analysis of Protein and Protein/Ligand Binding

ESI MS works as an ionization technique allowing protein ions to be extracted directly from the solution. It can be performed under gentle conditions and applied to a wide range of analytes, especially for macromolecules as it is able to overcome the propensity of these molecules to fragment when desorbed and/or ionized. A high electric field of 3-4 kV is applied to the tip of the capillary, which is situated in the ion source of the mass spectrometer. In this strong electric field, the sample emerging from the tip is dispersed into an aerosol of highly charged droplets by a co-axially introduced

nitrogen, flowing around the outside of the capillary. The charged droplets diminish in size and increase in surface charge density by solvent evaporation, via a warm flow of nitrogen passing across the front of the ion source. Finally, charged sample ions, free from the solvent, are released from the droplets and pass through a sampling cone into the analyzer of the mass spectrometer. ESI typically produces multiply charged ions with a statistical distribution which effectively extending the mass range of the analytes from kDa to MDa, and the extent of this multiple charging is determined by the physical dimensions of the protein in solution (99). The number of charges for a denatured protein (unfolded form) is greater than the native protein (folded from). By analyzing the charge-state distribution of protein ions in ESI MS, the integrity of the higher order structure can be assessed.

Since the early 1990s, ESI MS has emerged as a versatile tool to study the nature of the noncovalent protein/protein, protein/small molecule, and protein/DNA complexes. It is a sufficiently soft ionization method, which allows noncovalent biological complexes to be transferred intact from the solution into the gas phase under appropriate instrumental conditions, and the observation of the complex in the gas phase can indicate its interactions in solution. However, it should be noted that since the hydrophobic interactions are weakened in solution compared with the hydrogen bonds between water molecules (100), the protein/ligand complexes formed mainly through the hydrophobic interactions are actually forced by the hydrophobic effect. Thus, those complexes are prone to be dissociated when transfer from the solution into the gas phase and, in this case, the observation in the gas phase does not correlate

binding properties in solution. Conversely, electrostatic interactions and hydrogen bonds are stronger in the gas phase than in the solution (100). So protein/ligand complexes formed mainly through these forces can be retained in the gas phase.

Moreover, this technique measures the mass-to-charge ratio (*m/z*) with high mass accuracy which can be used to directly determine the binding stoichiometry of protein/ligand complexes based on their masses. One example is that ESI MS can be used to probe the interactions of Tf with metals (for example, Fe^{3+} and In^{3+}) and synergistic anions by monitoring the compositions of the metal-protein complexes and their large-scale conformational dynamics (58,101,102). The former approach can be done by analyzing the mass of the protein ions, and the latter is performed by analyzing the different charge state distributions.

Another advantage of the direct ESI MS assay is that it can combine with liquid chromatography and additional MS-based methods to further select and analyze the complexes. Furthermore, a nanospray adaptation of ESI, nanoESI, can extend the application of ESI MS to larger protein assemblies, such as oligosaccharides and glycoproteins. It can significantly drop the amount of sample, increase the sensitivity and efficiency, has better tolerance to salts and more efficient desolvation (103).

1.2.3 The Studies of Protein Conformation and Dynamics by Hydrogen/Deuterium Exchange Mass Spectrometry (HDX MS)

In solution, protein molecules are not static, but rather are in the equilibrium of interconverting states. Protein conformation and dynamics can be probed with various

techniques, such as X-ray crystallography and high-resolution NMR. Although in many cases these techniques can provide detailed structural information of the proteins or protein complexes, their inherent limitations make the application for analyzing the biopharmaceutical products impractical. For example, X-ray crystallography requires the protein to be crystallized prior to analysis, which makes it impossible to carry out the direct examination of the protein conformation under certain relevant productions or physiological conditions. Although high-resolution NMR reveals the solution structure of a molecule without crystallization, which is useful for the study of partially folded or unfolded proteins that are difficult to crystallize, it is still restricted the physical size of the protein systems (in general within 25 kDa).

During the past two decades, HDX in solution combined with ESI MS has become a powerful tool to explore both protein conformation and dynamics under various conditions (104-108), as well as the protein/ligand interactions (109) and protein folding (110) by obtaining deuterium content across the polypeptide backbone at either peptide or protein level. The high sensitivity and mass accuracy make MS an ideal technique for monitoring a 1 Da mass shift between hydrogen and deuterium. When performing HDX MS, it measures the sum of all populations of molecules or peptide segments in the sample solution. Each isotope cluster in the mass spectrum is reported as the shape, the width, and the isotopic distribution. Any unusual information can indicate interesting protein dynamics, conformational heterogeneity, and interconverting states (111). This technique is reliable, sensitive and is capable of visualizing various states of protein systems without crystallization.

The rate of HDX is based on the solvent accessibility and hydrogen bonding of the backbone segments. In a folded protein, protons that are buried in the protein interior or are involved in the formation of hydrogen bonds on the secondary structure (α-helices and β-sheets) are not able to exchange or exchange quite slowly unless they become exposed to the solvent by a conformational change (112-114). Besides these, several other factors, such as pH, temperature, side-chain, and isotope effects, can also contribute to the HDX protection (115). Although the hydrogen atoms on the polar and charged side chains are frequently exchanged very fast since they are exposed to the solvent, the contribution of labile side chain hydrogen atoms to the overall exchange rate can be easily eliminated during the digestion and LC separation by lowering the solution pH to 2.5-3 as well as the temperature to 0-4°C, which result in a very slow exchange rate for the backbone amide hydrogen atoms (average exchange rate 10^{-4} s^{-1}) (109,116,117), except for the N-terminal residue (exchange rates >10 s^{-1}) (118). Since HDX measurement focuses on the exchange of the backbone amide hydrogen atoms, it allows the measurement to achieve a single residue level resolution (with the exception of proline).

The kinetics measured in HDX depends on both protein dynamics and intrinsic amide hydrogen exchange rates. The mathematical formalism used to describe protein hydrogen exchange as a two-step process was introduced by Hvidt and Nielsen several decades ago (119):

$$\text{NH (closed)} \underset{k_{cl}}{\overset{k_{op}}{\rightleftharpoons}} \text{NH (open)} \xrightarrow{k_{int}} \text{ND (open)} \rightleftharpoons \text{ND (closed)} \qquad (1)$$

where k_{op} and k_{cl} are the rate constants for the opening (unfolding) and closing (refolding) steps that expose/protect a particular amide hydrogen to/from exchange with the solvent and k_{int} is the rate constant for the intrinsic exchange reaction of the exposed hydrogen. In general, the protected state represents the native state, whereas the unprotected state describes a fully unfolded (random coil) state, a partially unfolded (intermediated) state, or a structural fluctuation within a native conformation which transiently exposes a protected amide hydrogen to solvent without large-scale structure loss. In most HDX studies, the observed rate constant for the exchange process, k_{HDX}, is given by

$$k_{HDX} = \frac{k_{op} k_{int}}{k_{cl} + k_{int}} \tag{2}$$

Two distinct exchange regimes are commonly identified in HDX measurements, named EX1 ($k_{int} >> k_{cl}$) (Figure 1-8B) and EX2 ($k_{int} << k_{cl}$) (Figure 1-8A). HDX measurements under native or near-native conditions usually follow the EX2 kinetics (107,120), which amide hydrogen atoms are exposed briefly in solution through fast local conformational fluctuations. As a result, HDX under these conditions does not provide any kinetic rate information at which conformational fluctuations occur but yields thermodynamic information. Instead, nonnative HDX reactions favor the EX1 regime, where k_{cl} is decreased under denaturing conditions or k_{int} is increased at high pH conditions. Proton exchange occurs upon the first unfolding event, therefore this HDX behavior can reflect the kinetic information of the unfolding event. Alternatively, a bimodal behavior may also be observed in the intermediate EX1/EX2 exchange regime where the values of k_{int}

and k_{cl} are comparable ($k_{int} \approx k_{cl}$) (Figure 1-8C). The exposure time in the competent state is long enough for one or more protons to exchange during each unfolding event (the fast exchanging species) but too short for the entire set of all protons to exchange at once. When HDX reactions follow EX1 or EX1/EX2 exchange regime, a distinction among various conformations of protein coexist in the solution at equilibrium. As a result, these types of spectra exhibit very convoluted exchange patterns as the form of bi- or multi-modal isotopic distributions of protein ions which can reveal two or more distinct conformational states (121) or conformational heterogeneity in a sample (122,123). In principle, isolating each individual sub-distribution corresponding to a specific conformer prior to fragmentation allows multiple conformers to be detected separately.

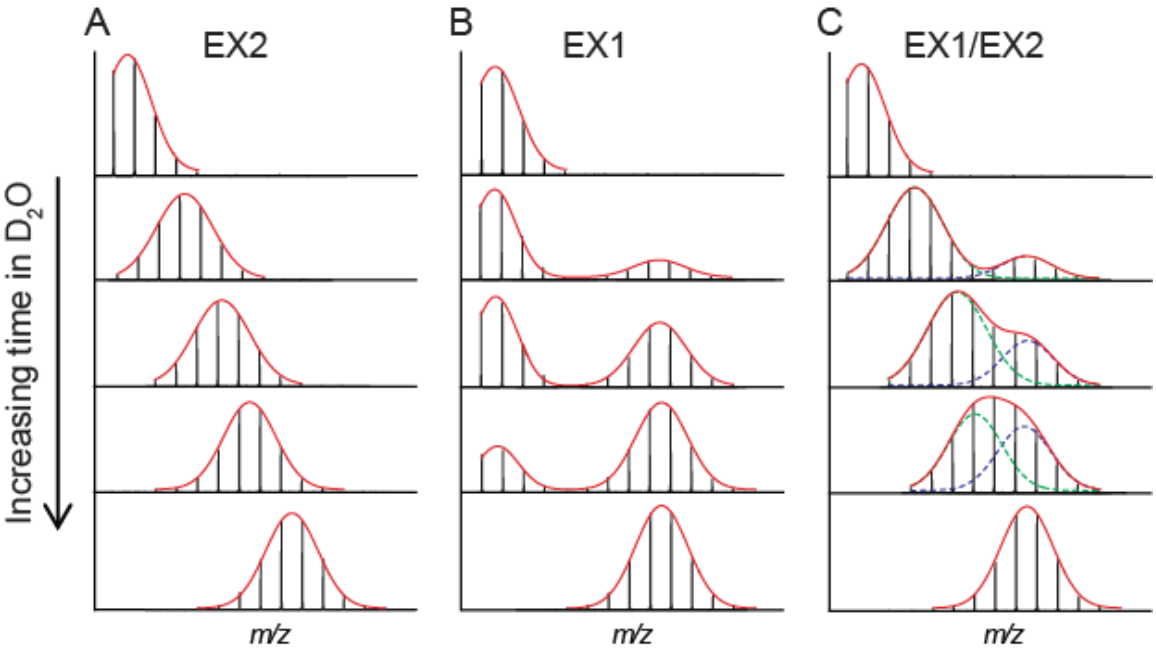

Figure 1-8 Simulated HDX patterns for a two-state system carried out under the conditions corresponding to (A) EX2, (B) EX1 and (C) the intermediate EX1/EX2 exchange regime.

1.2.4 Inductively Coupled Plasma Mass Spectrometry (ICP MS) Based Methods for Protein Quantitation

The accurate quantitation of the proteins is one of the essential prerequisites for protein studies in multiple research topics. Several different techniques for the protein quantitation have been suggested during the recent years, most of them are based on the stable isotope labeling combined with mass spectrometry (ESI MS or matrix-assisted laser desorption/ionization mass spectrometry (MALDI MS)) (124). However, these methods require a reference standard and specific labeling reagents, and the obtained signal intensity in MS is ambiguous due to the diverse ionization efficiencies of different proteins or peptides (97). In recent years, ICP MS has emerged as an attractive and complementary approach to ESI MS and MALDI MS for protein quantitation. It is a sensitive elemental detection technique in metallomics studies for measuring metal- and metalloid-containing compounds and their interactions within biological systems (125). Comparing with other methods, ICP MS has several unique characteristics. 1) It uses a high temperature (6,000-10,000 K) argon plasma as the ion source which can readily break all chemical bonds in the sample and to generate positively isotopic charged ions. As a result, 2) the response of an element in ICP MS is irrespective of its compound structure or matrix effects. More importantly, 3) the limits of detection in the absence of interferences from ubiquitous metals and plasma-related ions can be achieved at low fmol level (126,127). Besides, 4) ICP MS can combine with various separation methods, such as gas chromatography, liquid chromatography, and capillary electrophoresis. All these characteristics are propitious for ICP MS to be an ideal method

for protein quantitation with high accuracy and low detection limit. Unfortunately, not all elements can be detected by ICP MS. Many abundant elements, such as hydrogen, carbon, and oxygen, most gaseous elements, and the elements without naturally occurring isotopes, are hard to be ionized in ICP due to their high first ionization potentials. In addition, there exist many polyatomic interferences in ICP MS that are formed from precursors, such as the sample matrix, the reagents used in sample preparation, argon plasma gas, and the entrained atmospheric gas. Such polyatomic interferences are $^{40}Ar^{16}O^{+}$ on ^{56}Fe, $^{14}N^{16}O^{1}H^{+}$ on ^{31}P, and $^{16}O_2{}^{+}$ on ^{32}S. There are several approaches can be used to overcome such polyatomic interferences: selecting an interference-free isotope for analysis, using the correction equations, and using a technique termed collision/reaction cell which is used to promote reactive and non-reactive collisions that are responsible for polyatomic interference reduction in a gas filled multipole located in front of the mass analyzer (128,129).

1.2.5 Imaging Mass Spectrometry of Biological Tissues

Biological imaging MS is one of the most important bioanalytical techniques which are currently used for mapping the spatial distributions of multiple compounds and molecules in investigated tissues in the fields of analytical and biomedical research, providing a new tool for clarifying and understanding the molecular complexities of cells and tissues.

MALDI MS is one of the popular imaging MS techniques for peptides, large biomolecules, metabolites, and drugs (130-134). This technique can be used to identify

phosphorylation sites in proteins, but it cannot provide direct quantitative determinations of phosphorus and metals in biological samples. Another commonly used MS imaging technique is secondary ion mass spectrometry (SIMS), which can produce images of the distribution of elements, isotopes, nanoparticles and small molecules in tissues with a high spatial resolution (achieving submicrometer level) (135-137), but analyzing for large proteins still remains a challenge (138). It uses high energy primary ions (such as Ar^+, Ga^+, Bi^{3+} with primary ion energies of several keV) to strike the sample surface, which sputter both neutral and charged secondary species from the sample. However, the excessively hard ionization can also lead to severe in-source fragmentation (139). Up to six orders of magnitude of the inherent matrix effects can significantly affect the quantification of the images (140,141). Besides MALDI and SIMS, a new category of methods, ambient ionization, such as desorption electrospray ionization (16,142) and matrix-assisted laser desorption electrospray ionization (MALDESI) (143), has been also employed for imaging with little or no need for sample preparation (144). However, precisely because lacking sample preparation and enrichment, the intrinsic poor sensitivity for ionization of peptides and proteins comparing to MALDI can be particularly problematic in experiments.

Due to the serious quantitative problems of the above methods, an alternative approach, laser ablation inductively coupled plasma mass spectrometry (LA-ICP MS), has been established as a powerful imaging MS technique that can be used directly to quantitatively analyze the distributions of elements and isotopes at the trace and the ultratrace concentration level in microtome thin tissue sections (optimum at 20-30 μm

thickness) of biological matrices (140,145,146). LA-ICP MS was initially established for analyzing the elemental and isotope compositions in geological and archeological samples from the 1980s (147,148) and was later applied to describe the trace elemental distributions in biological tissues (149,150). It is a fast and high sample throughput technique with minimal sample preparation and high sensitivity, accuracy, and precision (145). The principal schematic of elemental imaging LA-ICP MS is illustrated in Figure 1-9. A laser beam is focused onto the surface of the thin tissue slice and scanned line by line. The sample is ablated, gasified, and then carried by the carrier gas (He and/or Ar) into ICP MS for ionization and detection.

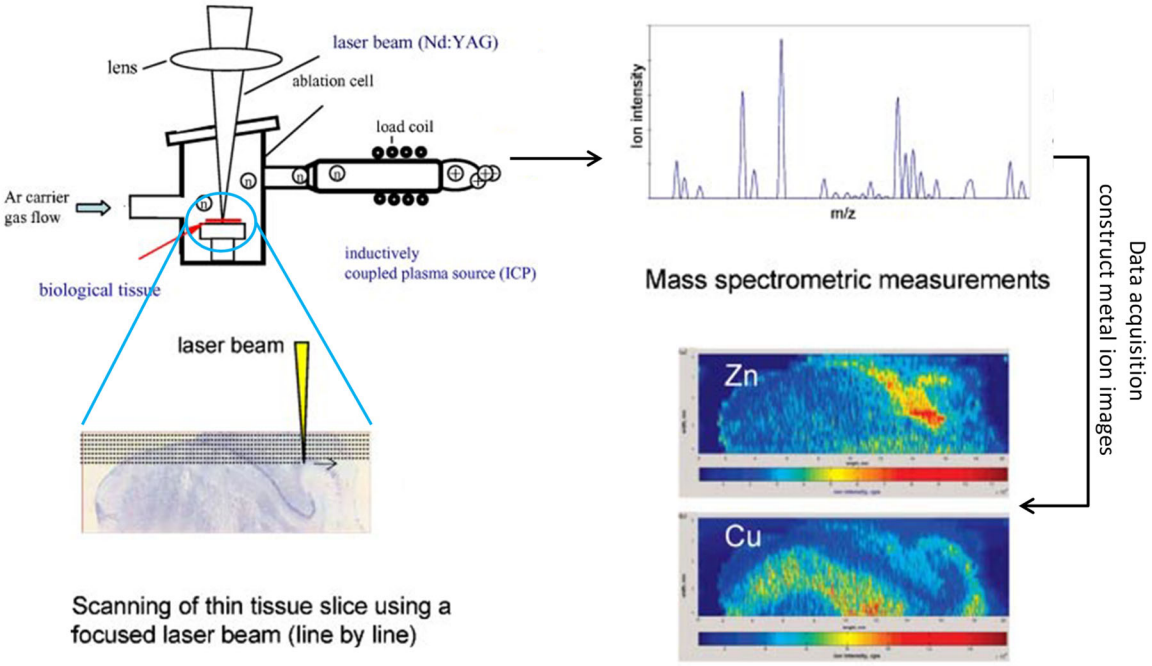

Figure 1-9 Principles of imaging MS technique by LA-ICP MS. A thin biological tissue section is ablated by a focused laser beam in the laser ablation chamber. Then the ablated material is analyzed by ICP MS, and metal ion images are constructed. Reproduced from reference (145).

1.3 Aims and Outlines of the Dissertation

TfR-mediated endocytosis has been explored as an efficient pathway for therapeutic molecules and protein delivery. It is clear that successful implementation of such strategy will critically depend on:

- Aim 1: Detailed understanding of the binding mechanism of multiple forms of Tf/TfR at both neutral and acidic pH and the role of TfR participating in iron release from Tf
- Aim 2: Develop sensitive and reliable assays that would monitor the biodistribution of exogenous Tf and Tf-based drugs in tissues and reliable measurements of their levels in blood and other biological fluids

TfR is unusual in that its binding preferences are tuned by pH, with the holoTf being strongly favored at neutral pH and the apoTf favored at endosomal pH. Although the crystal structures of apoTf (74), Fe_2Tf (151), TfR (63), and TfR coupled with the HFE protein (76) and Fe_NTf (65) have been determined for some time, they mainly focus on the TfR behaviors at neutral pH and the structures of free TfR and it coupled with Fe_2Tf and apoTf at acidic pH remain elusive and evade many crystallographic efforts (Figure 1-10A). Moreover, a single, static picture is far from enough to understand the whole picture of TfR-mediated endocytosis. To address these issues and achieve the Aim 1, MS coupled with HDX was used as a tool in this work to investigate the structural changes and conformational dynamics of TfR binding with different forms of Tf under different conditions that mimic various stages encountered during endocytosis and a proposed

mechanism of Tf/TfR interaction throughout the endocytotic cycle was described in CHAPTER 2.

To achieve the Aim 2, metal labeling combined with ICP MS detection (Figure 1-10B) was developed and validated for detection/quantitation of exogenous Tf in biological samples (CHAPTER 3). We take advantage of the two metal binding sites in Tf, by which a constant metal to protein ratio (2:1) can be achieved, and the ability of Tf to bind a wide range of other metals (gallium and indium). In addition to the iron binding site, we also explore the utility of the His-tag, a histidine-rich segment of the recombinant Tf as a potential site for nickel tagging. This study demonstrated the feasibility of using indium as a potential tracer of exogenous Tf and using ICP MS method to quantitate In_2Tf in biological samples and image it in organ cross-sections.

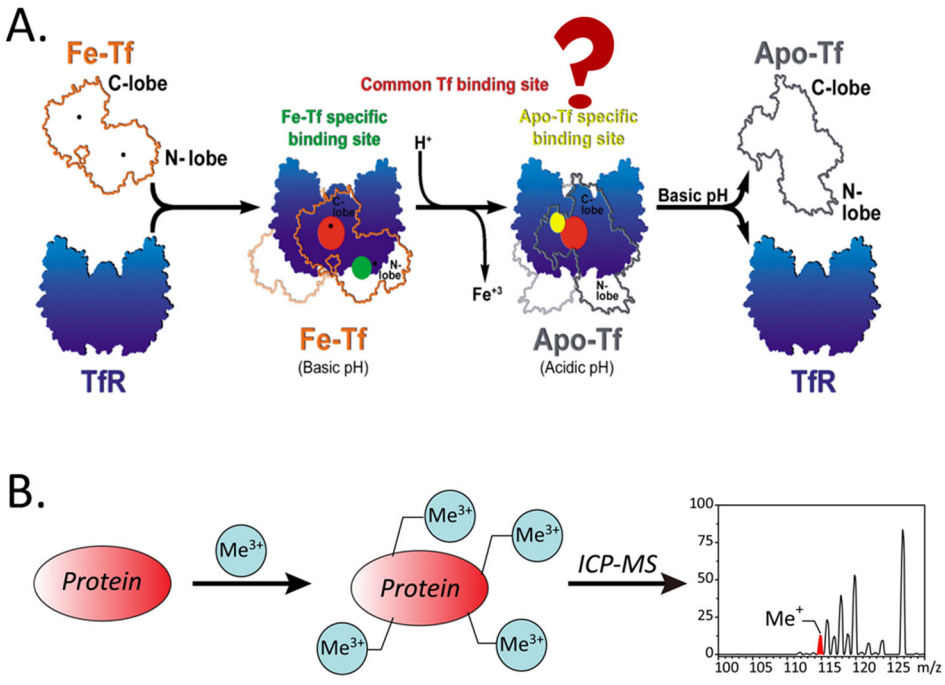

Figure 1-10 Schematic diagram of (A) Tf/TfR binding mechanism and (B) the process of metal labeling and ICP MS detection. The panel (A) is from Reference (66).

CHAPTER 2

TRANSFERRIN RECEPTOR CONFORMATIONAL DYNAMICS AND INTERACTIONS WITH TRANSFERRIN STUDIED BY HYDROGEN/DEUTERIUM EXCHANGE MASS SPECTROMETRY

2.1 Project Goals

TfR, as a carrier protein for Tf, has different Tf binding affinities at different pH levels, with high holoTf binding affinity at neutral pH and high apoTf binding affinity at endosomal pH. Thus, the pH sensitivity of the interactions of holo- and apoTf with TfR are critical to the receptor-mediated endocytosis. In this chapter, we use HDX MS as a tool to investigate the conformational dynamics changes of TfR in different Tf/TfR models to explore the detailed molecular mechanism of Tf/TfR interactions throughout the endocytic cycle and the role of TfR participating in iron release in the endosome. In the present work, following major questions have been addressed:

- How does the conformation of TfR change when it binds to holoTf at pH 7.5?

  Comparison of HDX data of TfR in the absence and the presence of holoTf at pH 7.5 is used to evaluate the conformational change within TfR as a result of Tf binding. It is expected that significant differences will be observed in/near the crystallographically identified Tf/TfR interface regions (the helical domain and the N-terminus of TfR), while extra protection afforded by Tf to TfR could provide a means to localize regions within TfR, which are affected indirectly by the binding, are also essential to the binding of Tf.

- Are there any specific conformational transitions occur within TfR at different pH levels which modulate its ability to bind holo- and apo-forms of Tf?

We compare the HDX data of TfR at pH 7.5 and 5.5 (“neutral” and “acidic” state of TfR, respectively). Any changes of the backbone protection pattern of TfR upon acidification could help to characterize the pH-induced conformational change of TfR that primarily affects TfR binding selectivity by pH.

- What’s the mechanism of environmental regulation of the receptor binding selectivity: How TfR help iron release from Tf and do not allow apoTf release from TfR at pH 5.5? Why apo Tf dissociate from TfR at pH 7.5?

  This is achieved by using HDX MS to characterize the Tf/TfR binding interface on the holoTf/TfR and apoTf/TfR complexes at both pH 7.5 and 5.5. It is expected that the different forms of Tf have site-specific interaction regions on TfR. The analysis at pH 5.5 correspond to the binding interface between the “acidic” state of TfR and the closed and open conformation of Tf, respectively, that account for its role in participating iron release and attribute to apoTf binding, while the analysis at pH 7.5 correspond to the binding interface between the “neutral” state of TfR and the closed and open conformation of Tf, respectively, that response to its high holoTf binding affinity and the dissociation of apoTf. The combination of the information of the conformations of “neutral” and “acidic” state of TfR and the site-specific Tf/TfR binding interfaces at neutral and acidic pH could lead to a better understanding of the molecular mechanism of modulation of TfR binding selectivity by pH.

In addition to process the HDX data, we extend our exploration for the structure/function of TfR to the molecular evolution of the TfR/PSMA family. The distant relatives of TfR are proteases (such as PSMA). Despite having strikingly similar 3D

structures (Figure 1-6), TfR and PSMA interact with their partner proteins in a very different fashion. We argue that the TfR segments showing significant divergence from PSMA are likely to harbor structural elements that are responsible for its new receptor function, including the pH-dependent preference for different forms of Tf, or the loss of the enzyme function. Once the new receptor function was acquired, it was conserved and should prevent further mutations within the relevant region. To achieve this, we apply the sequence-structure homology approach between PSMA and TfR to identify important segments within TfR and compare with the HDX data help to answer the above questions.

2.2 Materials and Methods

2.2.1 Protein Materials

To mimic the receptor-mediated endocytosis, several protein samples were used in this work: free TfR (N251D) (the sequence can be found in Figure 2-2), Fe_2Tf/TfR and apoTf/TfR complexes at pH 7.5, as well as free TfR (N251D), Fe_2Tf*/TfR (K206E/R632ATf/TfR) and apoTf/TfR complexes at pH 5.5. The apo-form of Tf was produced by washing the nonglycosylated Fe_2Tf with 1 mM EDTA in 3% (v/v) CH_3CO_2H, followed by buffer exchange to 150 mM ammonium acetate, pH 7.5. A mutant Tf molecule, K206E/R632ATf (Fe_2Tf*), in which iron is locked into each of the two homologous lobes of Tf by reducing the iron release rates by 2-4 orders of magnitude compared to the wild-type Tf (45,61), was used to bind with TfR at pH 5.5. The Fe_2Tf/TfR,

Fe_2Tf*/TfR and apoTf/TfR complexes were prepared by incubating molar excess Fe_2Tf, Fe_2Tf* and apoTf with TfR at pH 7.5 and 5.5, respectively, for 30 minutes.

All protein samples listed above were generously provided by Professor Anne B. Mason (University of Vermont, College of Medicine).

2.2.2 Protein Purification

TfR was first mixed and incubated with molar excess Fe_2Tf, Fe_2Tf* and apoTf in 150 mM ammonium acetate at pH 7.5 and 5.5, respectively. All free TfR and the Tf/TfR complexes were then purified by size-exclusion chromatography (SEC) with a mobile phase of 150 mM ammonium acetate at the corresponding pH values. SEC purification was carried out using Agilent 1100 HPLC (Agilent Technologies, Santa Clara, CA) equipped with GE Healthcare, Superose 12 column (30 cm ×10 mm) at a flow rate of 0.45 mL/min. The elution profiles were recorded by following the 280 nm absorbance. The free TfR, as well as the Tf/TfR complexes fractions (highlighted in the boxes in Figure 2-1A-C), were collected and characterized by native nano-ESI MS (Figure 2-1E). The SEC fraction of each sample was concentrated a day before the HDX experiment using centrifugal membrane filters with a molecular weight cutoff of 30,000 (Amicon, Millipore) to the final concentration about 12 μM (about 1.8 mg/mL for TfR and 3.7 mg/mL for the Tf/TfR complexes).

Since apoTf weakly binds to TfR at neutral pH, to estimate the dissociation of the apoTf/TfR complex under the HDX experimental condition, the SEC purified fraction of apoTf/TfR at pH 7.5 (the fraction highlighted in the black box in Figure 2-1C) was

concentrated to about 3.7 mg/mL and diluted ten-fold with 150 mM ammonium acetate, pH 7.5, then reinjected into SEC column. The SEC profile of the reinjected apoTf/TfR complex was shown in Figure 2-1D.

2.2.3 Peptide-Resolved HDX Measurements

H/D exchange was initiated by diluting the pre-concentrated SEC purified protein solutions ten-fold into a D_2O-containing buffer at 25°C to final concentration about 1.2 µM. At designated times (30 seconds, 2 minutes and 10 minutes), an equal volume of quench solution (6 M guanidine HCl, 250 mM tris(2-carboxyethyl)phosphine HCl, 0.1% formic acid) was added and rapidly mixed, yielding pH 2.5. The quenched protein solution was immediately digested online using Waters Enzymate™ BEH Pepsin Column (2.1 x 30 mm, 5 µm) using 0.1% formic acid in water at 100 µL/min. All peptides were collected and desalted in an inline peptide trap for 4.5 minutes and then were resolved by a Waters C18 column using a linear gradient of 5-35% 0.1% formic acid in acetonitrile over 7 minutes at 40 µL/min. Sample preparation for HDX experiments was performed by a LEAP autosampler PAL (LEAP Technologies, Carrboro, NC). The LC/MS measurements were performed on an ACQUITY UPLC system combined with a Synapt® G2-Si mass spectrometer (Waters Corporation, Milford, MA) acquiring in MS^E mode.

To account for back-exchange, experiments with fully deuterated control (the endpoint) were performed. The endpoint sample was treated in a different way. A certain amount of SEC-purified TfR was first digested offline using custom prepared pepsin beads (POROS) in 0.1% formic acid in water at 100 µL/min. After lyophilizing, the

powder of TfR peptides was dissolved in a deuterated solvent (150 mM ammonium acetate in 90%/10% D_2O/H_2O) and was equilibrated at 25°C for 30 minutes as fully exchanged peptides. Following the quench step, the deuterated peptide solution was manually injected into the ACQUITY UPLC, trapped, except the online immobilized pepsin column, and analyzed by LC/MS by using the same protocol as described above for the HDX experiments.

2.2.4 HDX Data Analysis and the Calculation of the Threshold of Significant Difference

The MS^E data for undeuterated TfR were searched against the input sequence of TfR (N251D) to generate the list of peptides using ProteinLynx Global SERVER (PLGS; Waters). Peptides identified by PLGS were further filtered and analyzed using the DynamX HDX Data Analysis Software (Waters) with minimum products per amino acid 0.3, max sequence length 20 amino acids. The deuterium exchanged peptide was assigned based on the same retention time and theoretical *m/z* value by comparison to the unexchanged peptide. The number of deuterium uptake (#D in Da) for each peptide was calculated by the DynamX algorithm. The percentage of deuterium uptake level (HDX%) for each peptide was calculated as follows: $HDX\% = (m_t - m_0)/(m_{EP} - m_0) \times 100\%$, with m_t, the centroid mass at incubation time t; m_0, the centroid mass of the undeuterated control; and m_{EP}, the centroid mass of the endpoint control.

To evaluate the differential HD exchange among different samples and avoid any arbitrary comparisons (such as visual comparisons based on the heat maps, or using absolute differences between HD exchange rates on the butterfly or difference plots), a

two-tailed student's t-test evaluation was used in this work to statistically identify if a peptide exhibiting a significant difference in structural dynamics or not at each exchange time point between different samples with the threshold of significance setting to 95% confidence interval ($P \leq 0.05$), as described by Houde, et al. (152). Specifically, the simple average of all individual standard deviation (SD) values of the difference in deuterium uptake level between two states ($\Delta D_{i,t}$) from triplicate analyses was used to compute the standard error of the mean (SEM) for any mean $\Delta D_{i,t}$ value. Then multiplied the SEM value by the appropriate two-tailed student's t-table value for the 95% confidence interval (for n=3, degrees of freedom is 2, the t-value is 4.303), given an estimated 95% confidence interval value for any mean $\Delta D_{i,t}$ value that was calculated from triplicate analyses, which if exceeded would statistically be considered as a significant difference in deuterium uptake level.

2.2.5 pH Dependence of Amide Hydrogen Exchange Rate

While the comparison of the deuterium exchange levels at different pH levels is not straightforward, the pH of the HDX reaction is logarithmically correlated with the exchange rate due to the different intrinsic exchange rates (k_{int}) of each backbone amides, where k_{int} is strong pH-dependent and sensitive to neighboring side chains (153-155). Lowering the pH from 7.5 to 5.5 decreases the overall intrinsic exchange rate k_{int} of amide protons of TfR by a factor of 55 (calculated according to previously defined nearest neighbor effects (154,155) using the online Excel spreadsheet at http://hx2.med.upenn.edu/download.html). In order to get a meaningful comparison at

different pH levels, we deconvolved the pH effect by converting the on-exchange times at low pH condition into those at high pH condition to offset the difference in k_{int} values, as we compared local protection patterns obtained following 10 minutes of exchange at pH 5.5 with those recorded following 30 seconds of exchange at pH 7.5.

2.3 Results and Discussion

2.3.1 Protein Purification and Initial Characterization of the Tf/TfR Complexes

The Tf/TfR complexes used in this work were prepared by incubating molar excess Tf with TfR under each condition. In order to remove the excess Tf added during protein preparation, improve the sensitivity and minimize the complexity of the MS and HDX MS analysis, all free TfR and Tf/TfR complexes used in the HDX experiment were firstly purified by SEC. The collected SEC fractions of each sample (highlighted in the boxes in Figure 2-1A-C) were characterized by native ESI MS. As shown in Figure 2-1E, the purified TfR (the red trace) is homogeneous and Tf effectively binds TfR to form a stable Tf/TfR complex with 2:1 stoichiometry (the black trace) without any contamination of excess Tf or 1:1 protein-receptor complex.

Our MS data confirm the presence of the apoTf_2TfR complex at pH 7.5 (Figure 2-1E), which is consistent with the previous study that apoTf can form relatively stable complexes with TfR at neutral and mildly basic pH with the same stoichiometry as the complexes formed by holoTf (44). However, the binding affinity of apoTf and TfR at neutral pH is relatively low, with the k_d value at 10^{-7} M level, about 30 times lower than the k_d value of holoTf/TfR (66-69). It should be noticed that the weak interaction could

cause a fast dissociation of the analyte back into solution. Since in the HDX experiment, the concentrated protein sample has to be initially diluted ten-fold into an aqueous buffer containing deuterium, the weak interaction makes it possible for a large fraction of the apoTf/TfR complex to dissociate upon dilution. Therefore, it is necessary to check the composition in the suspect apoTf/TfR solution at neutral pH. This was done by collecting the SEC fraction of the apoTf/TfR complex (highlighted in the black box in Figure 2-1C) at pH 7.5, following the concentration and dilution processes that simulate the deuterium exchange experimental conditions, and then rechromatographing on SEC. As shown in Figure 2-1D, the later elution peak (at 11.2 min) in the reinjected chromatogram of the collected apoTf/TfR fraction, with the same elution time as Tf (the blue dotted line), indicates the presence of the free apoTf, about 23% of the apoTf_2TfR complex (calculated by the SEC peak area of each species) dissociated at pH 7.5 during the dilution process. The weak binding affinity and the quick dissociation of the apoTf/TfR complex at pH 7.5 make it difficult to purify the apoTf_2TfR complex without interference from the free protein and/or the apoTf_1TfR complex. However, even in this relatively unfavorable condition, the major component in the solution, the apoTf_2TfR complex, can still keep at around 77% which is competent in the use of HDX measurement.

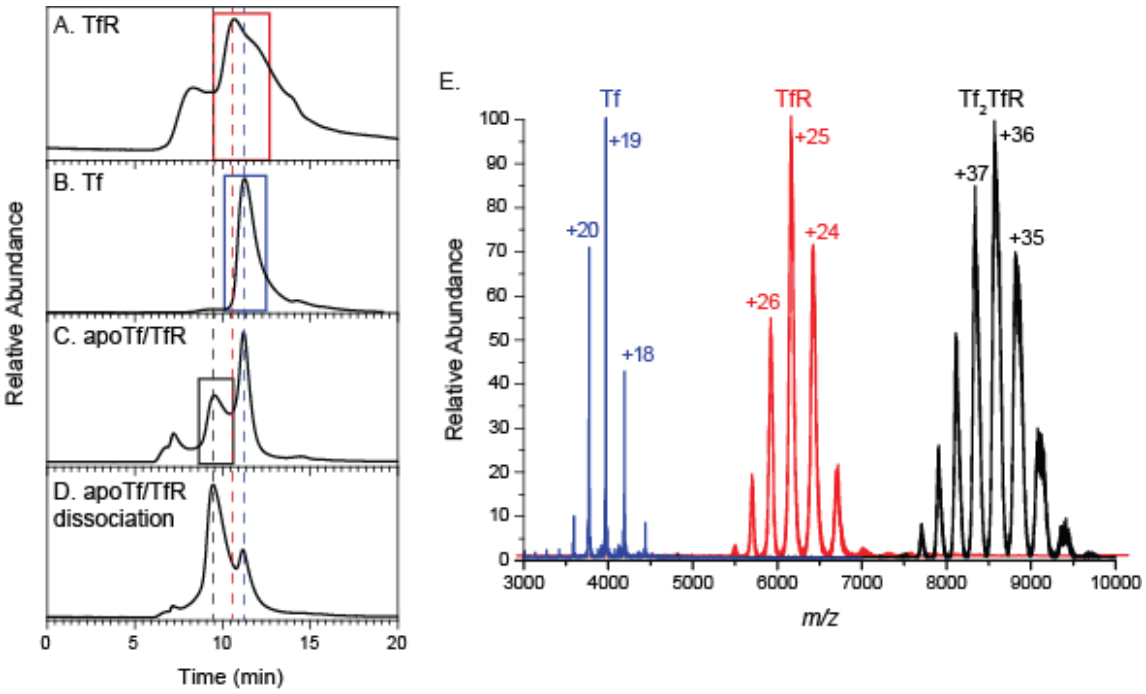

Figure 2-1 SEC of TfR (A), apoTf (B) and the product of incubating TfR with molar excess of apoTf (C) at neutral pH. The black, red, blue dotted lines in panel A-D represent the elution time of Tf/TfR complex, TfR and Tf, respectively. Dissociation of the apoTf/TfR complex at neutral pH was investigated by reinjecting the highlighted apoTf/TfR SEC fraction in panel C. The SEC of the reinjected apoTf/TfR fraction was shown in panel D, where the later elution peak with the same elution time as Tf indicates the presence of the free protein at pH 7.5. Colored boxes in panels A-C indicate the SEC fractions collected for each sample which were characterized by native ESI MS in panel E and used in the following HDX experiments.

2.3.2 Peptide Mapping and Sequence Coverage of TfR under HDX MS Condition

Overall, 83 of the most abundant peptide fragments of TfR which are found in all TfR and Tf/TfR complexes with 81% sequence coverage (Figure 2-2), including most of the residues playing important roles in Tf binding and some of the residues located at the TfR/TfR dimer interface region, were used to characterize the local HDX protection patterns of TfR in this work to identify changes in conformational dynamics within TfR throughout endocytosis, with the aim of characterizing the binding mechanism of multiple forms of Tf/TfR at both neutral and acidic pH levels. The majority of the missing

sequence is due to the presence of the N-linked glycosylations at Asn317 and Asn727 that may enhance enzyme resistance by reducing accessibility of pepsin to peptic cleavage sites (156). Additionally, pepsin cleavage specificity also impacts the sequence coverage of TfR, as the presence of His, Lys, Arg and Pro in the P1 position strongly disfavors pepsin activity. Pepsin also discriminates against Pro in the P2, P2' and P3' positions, as well as His, Lys and Arg in P3 position (157). (The P1-P1' is the peptide bond where the enzyme cleavage occurs. Amino acid residues are designated P1, P2, P3, etc. and P1', P2', P3', etc. in the N- and C-terminal directions from the cleaved bond, respectively.) The low cleavage probability of pepsin at these sites could produce larger peptides that are rich in Pro, His, Lys or Arg. Since our limitation of the max sequence length is 20 amino acids, the low cleavage probability of pepsin could cause sequence missing for the Pro/His/Lys/Arg-enriched sequences, such as the N-terminus and amino acids [684-701].

2.3.3 Conformational Changes within TfR as a Result of Tf Binding at Neutral pH

2.3.3.1 Overall Conformational Signatures of TfR in Tf Binding

Evolution of the deuterium content of TfR reveals a wide range of protection levels across the protein sequence (Figure 2-2, Figure 2-3A-C and Figure 2-4). Overall, the protease-like domain, consisting of seven β-sheets in the center mixing with ten flanking α-helices, appeared to be more stable in HDX than the other two domains in the free receptor. This should be not surprising since the folded conformation of the protease-like domain can restrict the solvent accessibility and the enhanced intrachain

hydrogen bonds of the α-helix and β-sheet structural elements can also contribute to the HDX protection (158,159).

Once holoTf bonded to the receptor, TfR became less flexible, as most of the regions gained protection and kept protected during the time course (Figure 2-2 and Figure 2-3), which reflects that binding with Tf can stabilize TfR. It should not surprise that significant differences in HDX kinetics upon Tf binding were observed in/near the crystallographically identified Tf/TfR interface regions (the N-terminus and the helical domain of TfR), the kinetics of deuterium uptake of some regions in the protease-like and the apical domains were also decelerated in its complex form, with the apical domain which is far from the Tf binding interface had the least effect on Tf binding comparing with the other two domains. HDX data provide a means to localize several segments that are affected indirectly by the binding, indicating the apparent dynamic conformational changes within TfR are essential to the binding of Tf.

Deuterium uptake profiles for most peptide segments revealed a single isotopic distribution that increased in mass over the time course, suggesting that these regions display the more common EX2 kinetic behavior. Interestingly, several peptide segments located at the protease-like and the apical domains exhibited bimodal isotopic distributions in the free TfR and/or Tf/TfR complexes (highlighted in yellow in Figure 2-2). Two of these, [506-522] and [523-537] in the protease-like domain, are closed to the Tf binding site, while others are located at the edge of the interdomain cleft formed by the three domains (Figure 2-5A). The observation of the bimodal isotopic distributions in HDX, which arises from the EX1 kinetic behavior or the heterogeneous conformational

populations of the protein, can provide unprecedented insights into protein conformational dynamics that cannot be characterized by static crystal structures or other solution spectroscopy. Such understanding could support the functionally-relevant features of the protein. The detailed discussions about the bimodal peptides are presented in CHAPTER 2.3.3.3, 2.3.3.4 and 2.3.3.5.

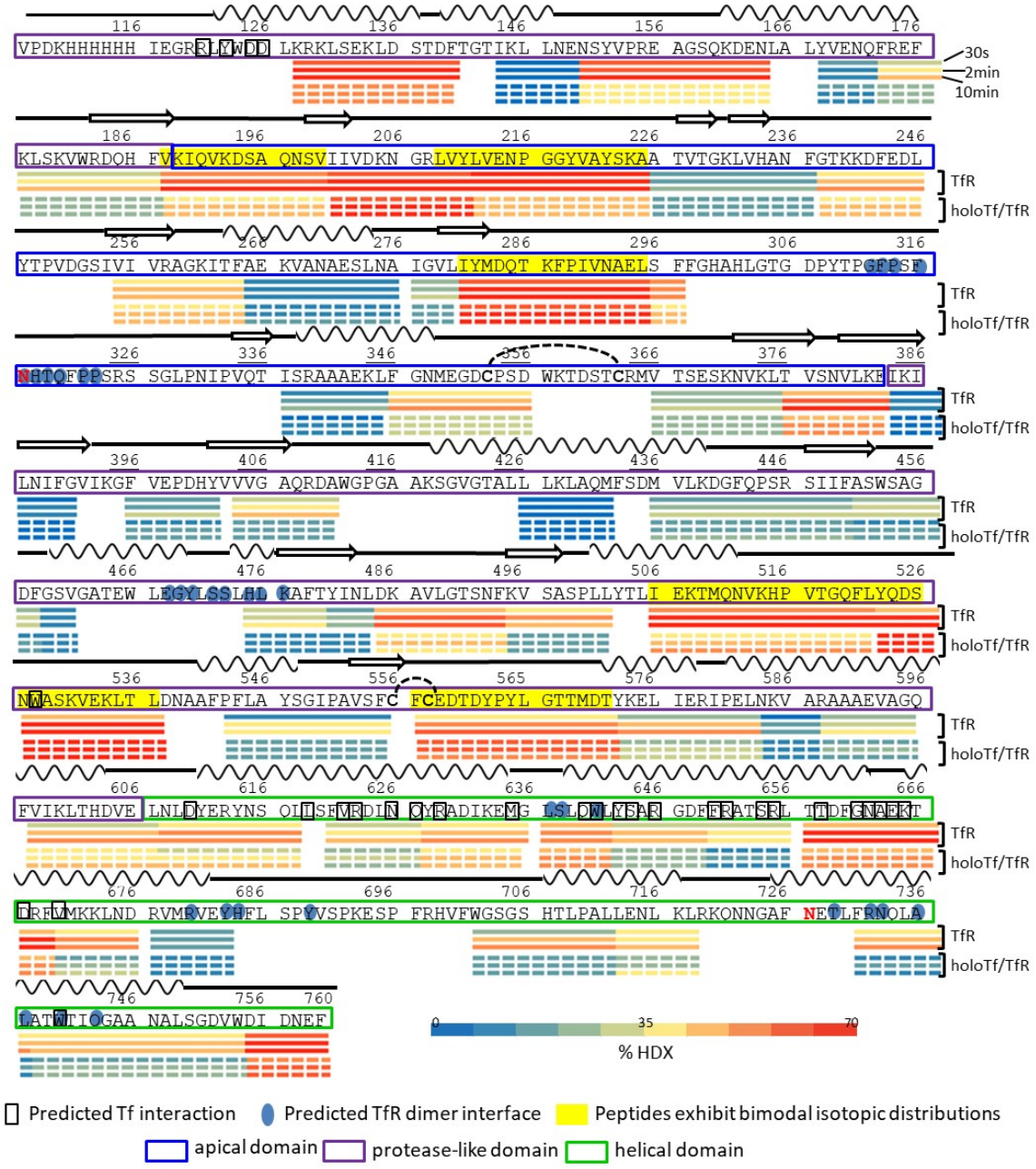

Figure 2-2 Heat map of TfR in the absence (solid lines) and the presence (dashed lines) of holoTf at pH 7.5. The level of deuterium incorporation (%HDX) for each time point (from top to bottom: 30 seconds, 2 minutes, and 10 minutes) is rendered in colored horizontal layers for each peptide. Secondary structure is indicated above the sequence. The locations of the predicted Tf interaction sites and the TfR dimer interface based on the crystal structure of Fe_NTf/TfR (PDB: 3S9N) are highlighted by a black box and a blue oval, respectively. The protease-like domain, apical domain and helical domain are highlighted in purple, dark blue and green boxes in the sequence, respectively. The N-linked glycosylation sites (Asn317 and Asn727) are highlighted in red in the sequence.

The peptides exhibited bimodal isotopic distributions in the free TfR and/or Tf/TfR complexes are highlighted in yellow in the sequence.

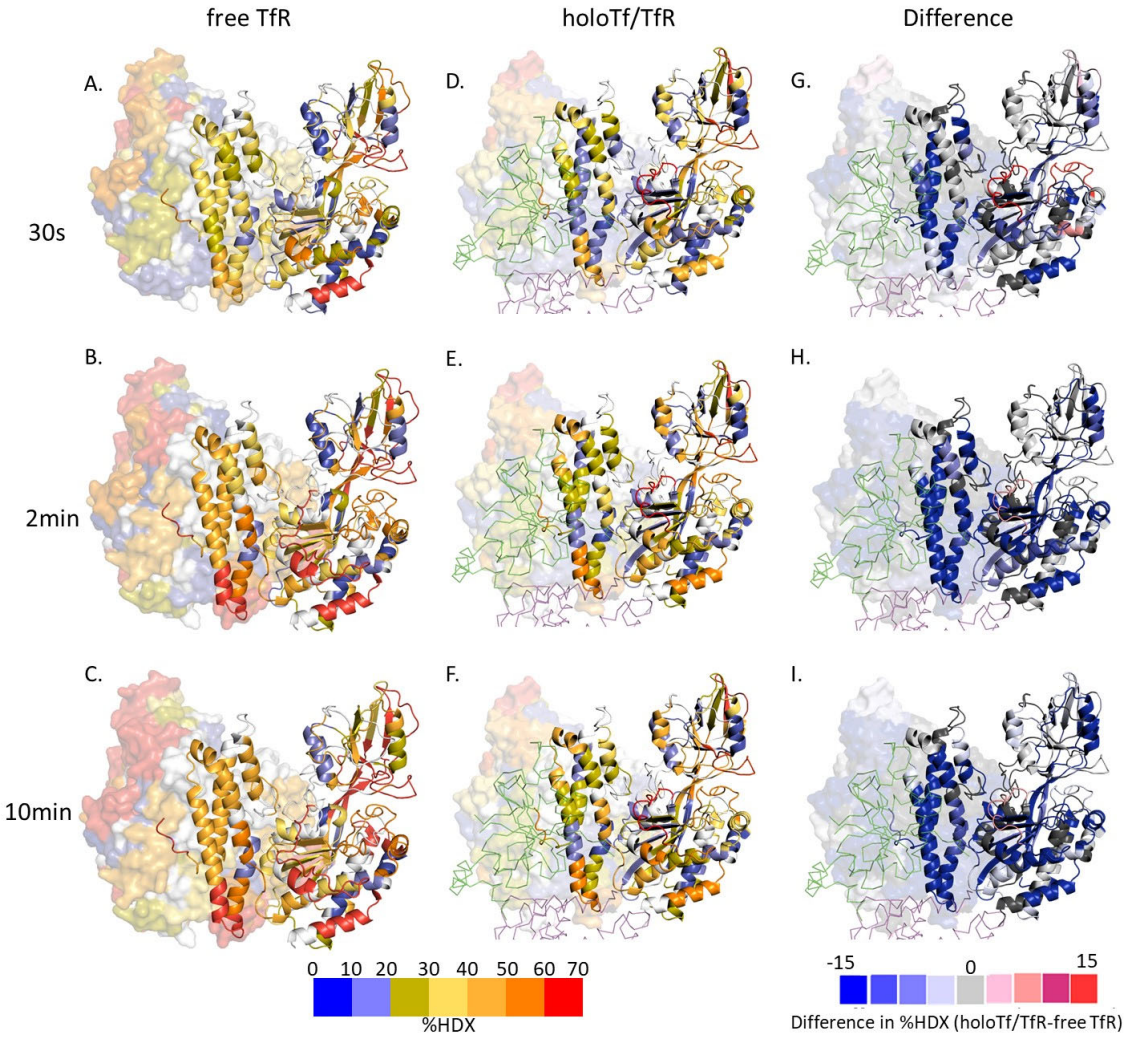

Figure 2-3 Mapping of HDX protection data on the crystal structure of the free TfR (PDB: 1CX8) (A-C) and the holoTf/TfR complex (PDB: 3S9N) (D-F) following 30 seconds (top row), 2 minutes (middle row) and 10 minutes (bottom row) of deuterium exchange at pH 7.5. Color coding reflects the protection of segments from highly protected (blue) to highly flexible (red). The differences in the percentage of exchange (complex – free receptor) are also shown in G-I, following the same exchange time course. Residues not observed are colored in white in structure A-F and in black in structure G-I. The N-lobe of Tf is colored in pink and the C1 subdomain of Tf is colored in green. One monomer of TfR is shown in cartoon, while the other is shown as surface.

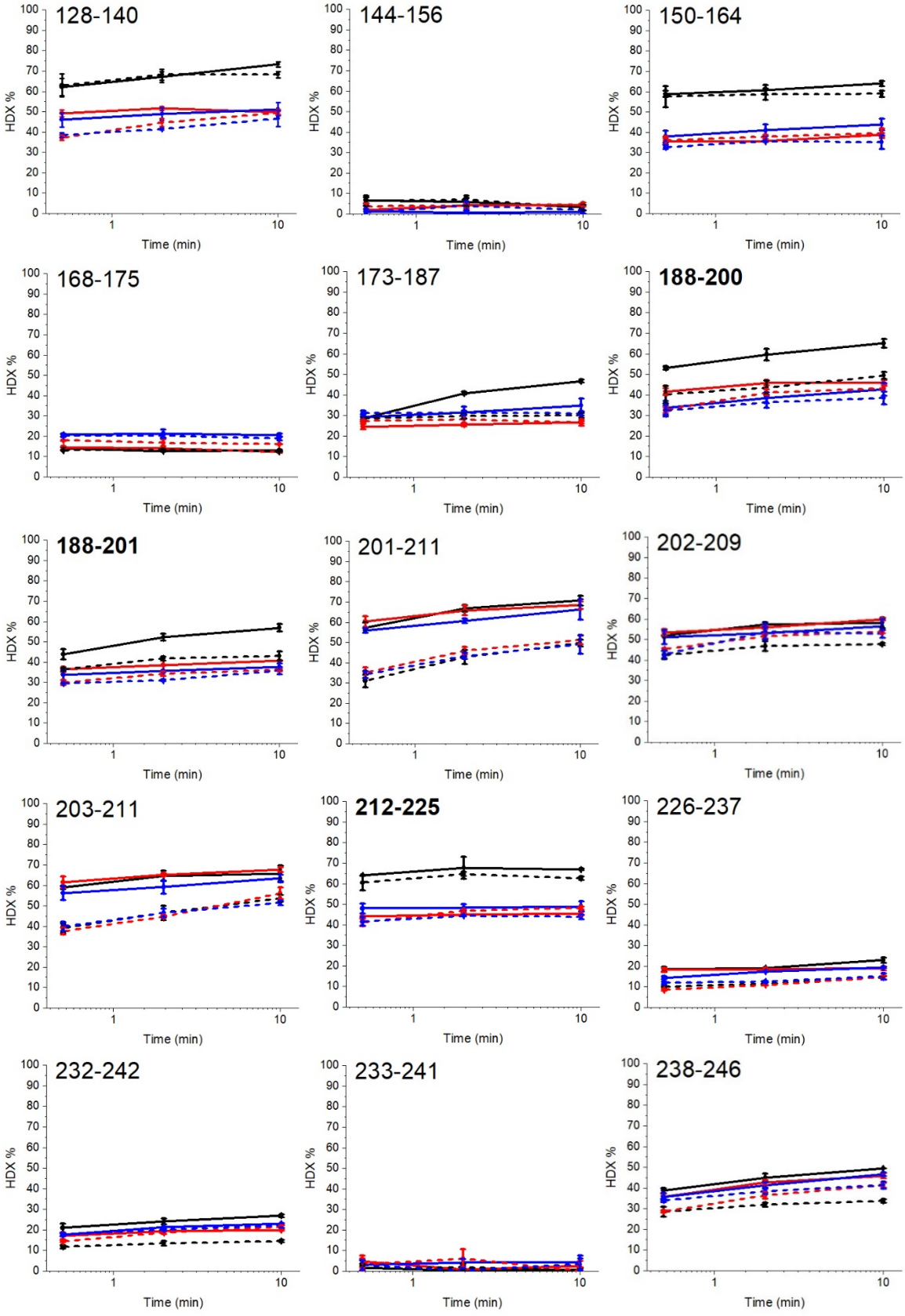
128-140
144-156
150-164
168-175
173-187
188-200
188-201
201-211
202-209
203-211
212-225
226-237
232-242
233-241
238-246
HDX %
Time (min)

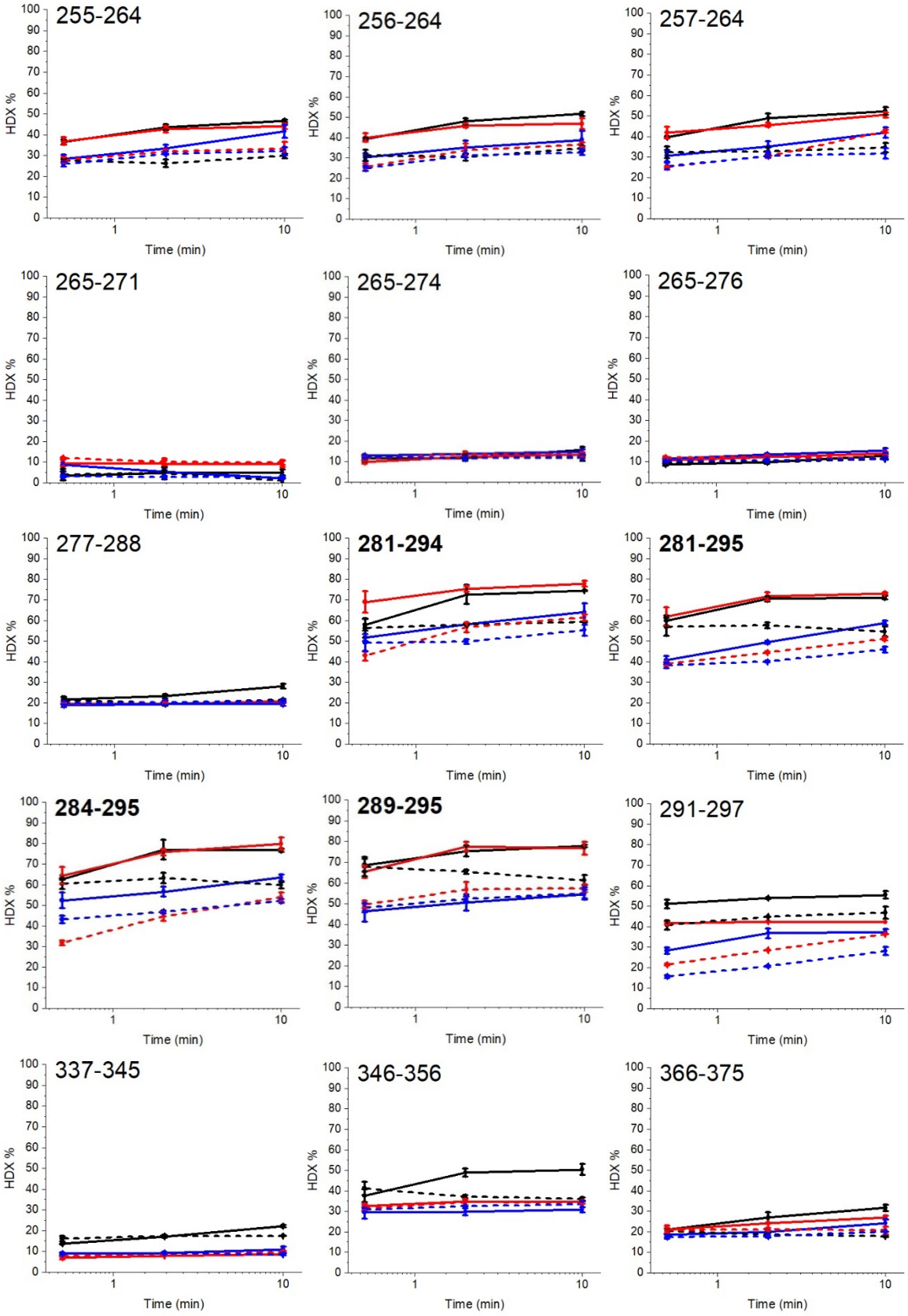
255-264
256-264
257-264
265-271
265-274
265-276
277-288
281-294
281-295
284-295
289-295
291-297
337-345
346-356
366-375
HDX %
Time (min)

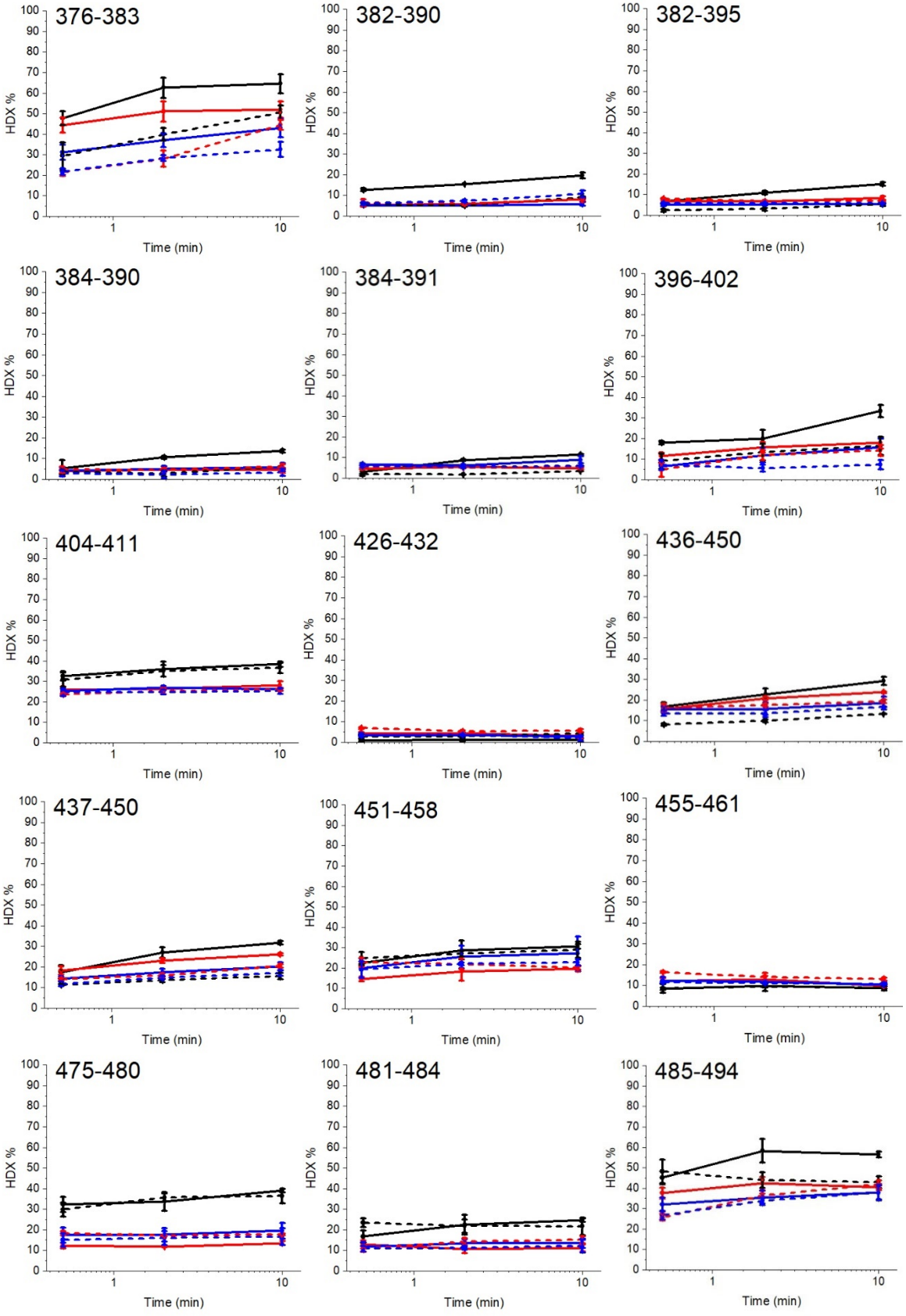
376-383
382-390
382-395
384-390
384-391
396-402
404-411
426-432
436-450
437-450
451-458
455-461
475-480
481-484
485-494
HDX %
Time (min)

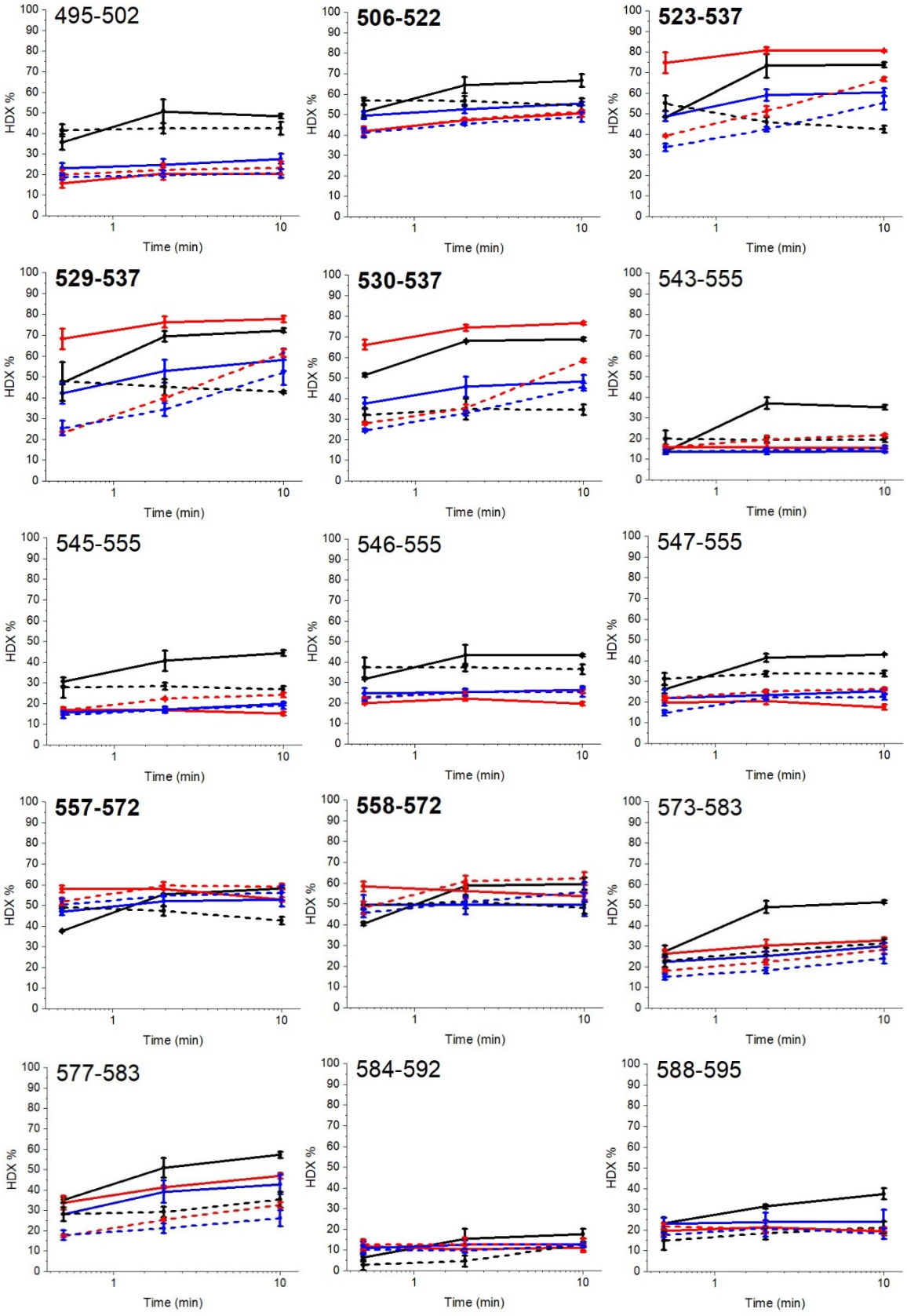
495-502
506-522
523-537
529-537
530-537
543-555
545-555
546-555
547-555
557-572
558-572
573-583
577-583
584-592
588-595
HDX %
Time (min)

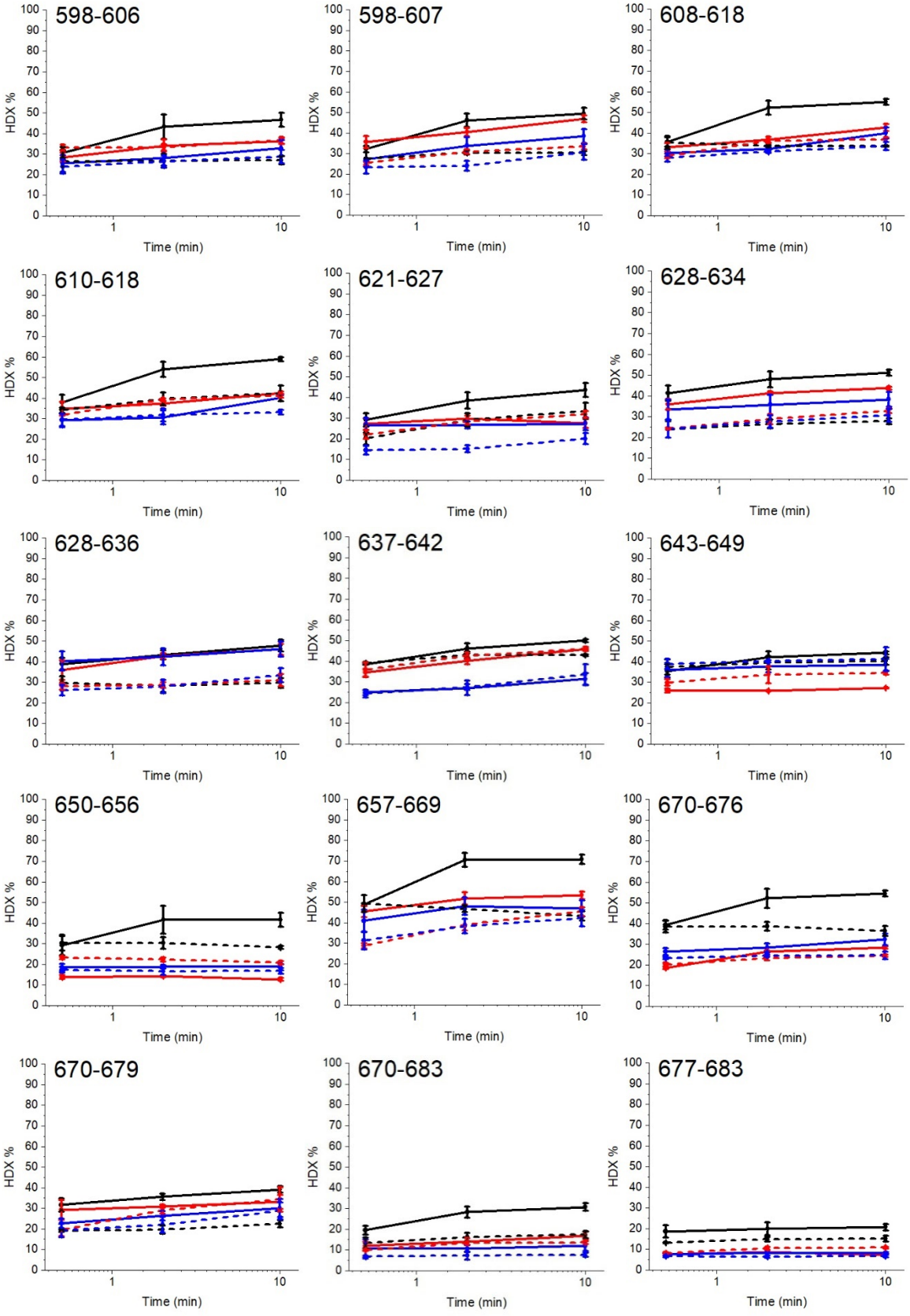
598-606
598-607
608-618
610-618
621-627
628-634
628-636
637-642
643-649
650-656
657-669
670-676
670-679
670-683
677-683
HDX %
Time (min)

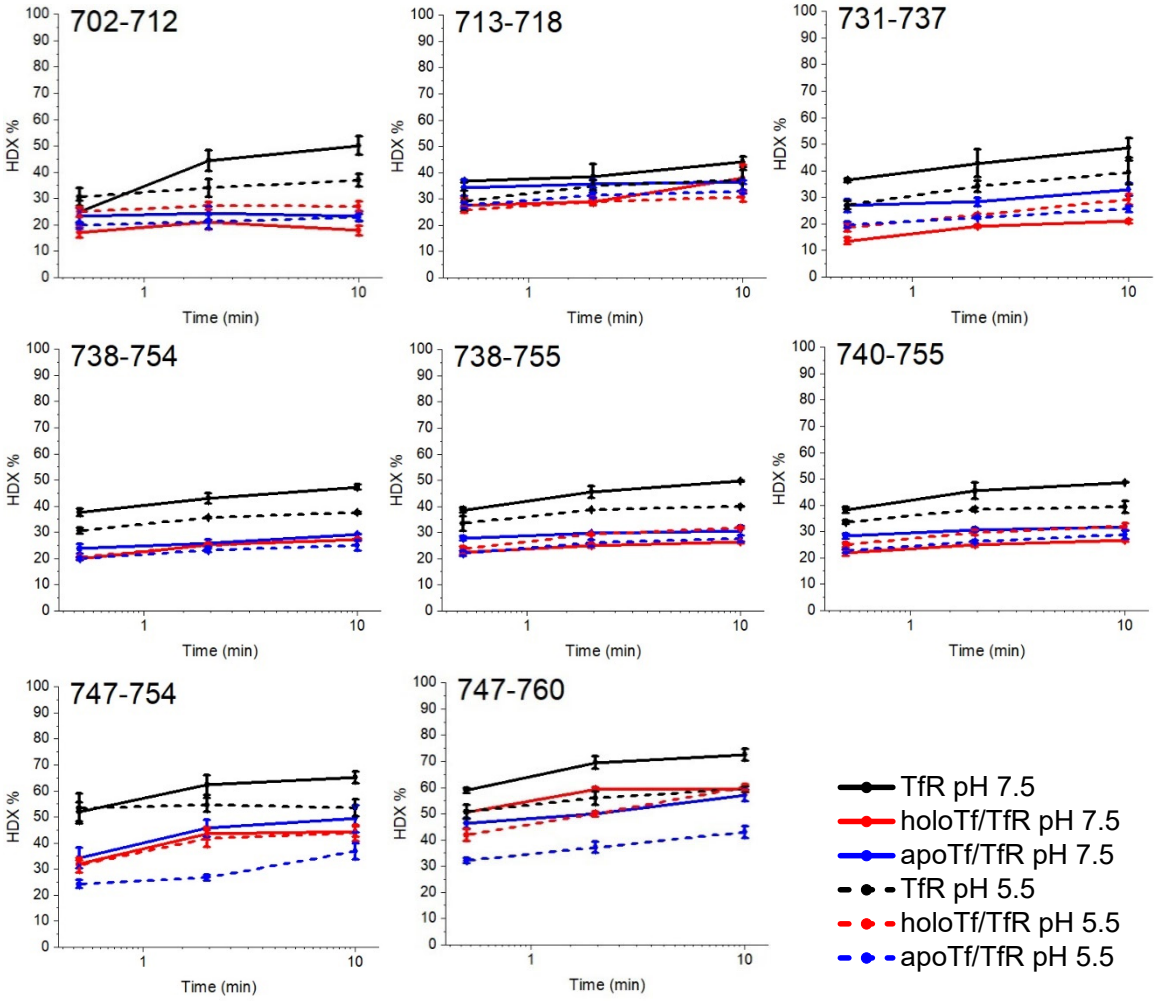

Figure 2-4 Deuterium uptake plots for all observable peptides of TfR in the free TfR (black), holoTf/TfR (red) and apoTf/TfR complex (blue) at pH 7.5 (solid lines) and 5.5 (dashed lines). Error bars represent standard deviation values from three individual experiments. The bold peptides display bimodal isotopic distributions in free TfR and/or Tf/TfR complexes.

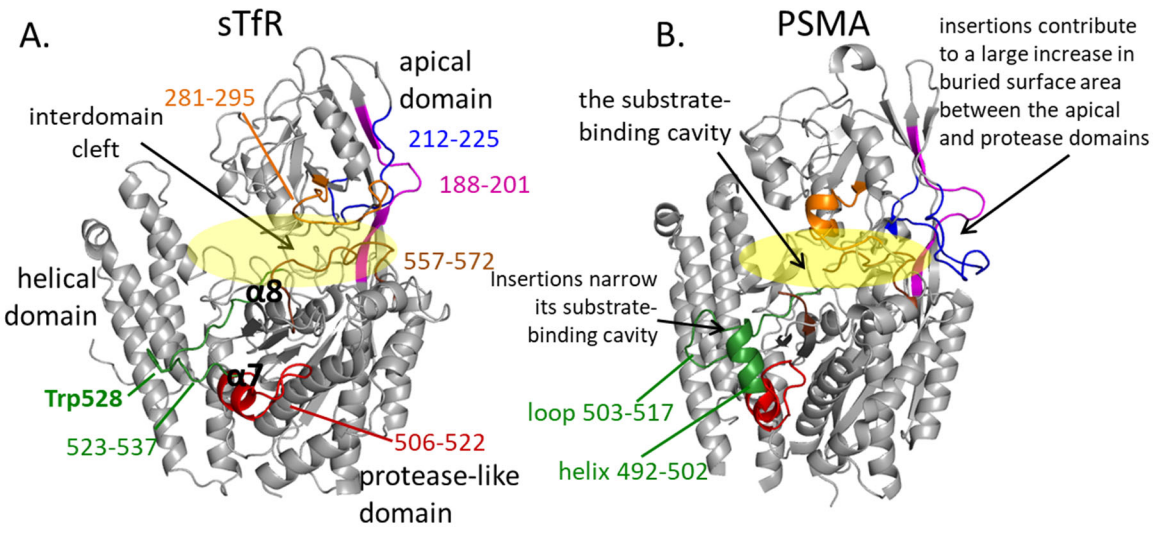

Figure 2-5 Structure alignment of (A) TfR (PDB: 1CX8) and (B) PSMA (PDB: 2OOT) showing the positions of the peptides exhibit bimodal isotopic distributions in TfR. The peptides are labeled and colored accordingly. The interdomain cleft in TfR and the substrate-binding cavity in PSMA are highlighted in yellow.

2.3.3.2 Conformational Changes at the TfR/TfR Dimer Interface

The ectodomain of TfR is a noncovalent homodimer that the helical domains from each monomer make contacts with each of the three domains within the other monomer, contributing substantially to the extensive dimer contact regions. Four representative peptide segments located at the receptor dimer interface region, the segment (*ii*) [475-480], (*iii*) [670-676], (*iv*) [677-683] and (*v*) [731-737] as shown in Figure 2-6, were selected to investigate the structural dynamic changes. Upon holoTf binding, all above peptides gained protection obviously (with the threshold of significance for exchanging 30 sec, 2 min and 10 min is ±9%, ±10% and ±7%, respectively (see Method 2.2.4 for the calculation of the threshold of significance)). Unlike the other three peptide segments (*ii*, *iii* and *v*), the peptide segment (*iv*) [677-683] was highly protected even in the free TfR (only ~20% backbone amide hydrogens exchanged to deuterium after 10

minutes of the exchange reaction). This is likely because this segment is located deeply in the dimer interface that limits the solvent accessibility (Figure 2-6A) (the average relative SASA (solvent accessible surface area, ranging from 0 to 100%) for this segment in the free TfR is about 7.1%, computed using the online ASAView server http://ccbb.jnu.ac.in/shandar/servers/asaview/ (160)). In contrast, the peptide segment (*i*) [437-350] located at the bottom of the protease-like domain, not at the TfR/TfR dimer interface region, exhibited a similar exchange behavior in free TfR and the Tf/TfR complex (the difference in HDX% for the segment (*i*) at each time point is -1%, 4% and 6%, comparing with the threshold of significance ±9%, ±10% and ±7%, respectively). The decrease in deuterium uptake level in the presence of Tf observing for the peptides located at the TfR/TfR dimer interface region suggests a conformational change occurs at the dimer interface upon Tf binding that brings the two TfR monomers close to each other to restrict solvent access. This observation agrees with the changes observed in HFE/TfR (76) and Fe_NTf/TfR (65).

Previous studies (65,76) also suggested the endosomal pH could trigger a chain reaction that causes a pH-induced movement at the TfR/TfR dimer interface, altering Tf binding. To further evaluate the pH effect at the TfR/TfR dimer interface region, we examined the deuterium exchange patterns for these representative peptides at different pH levels (pH 7.5 exchanging for 30 seconds vs. pH 5.5 exchanging for 10 minutes to offset the intrinsic hydrogen exchange rate). As shown in Figure 2-6D-E, all of these peptide segments exhibited very similar exchange behaviors in the free TfR, as

well as in the holoTf/TfR complex, at different pH levels, suggesting the pH change has minor to no effect on the local conformation at the TfR/TfR dimer interface region.

In summary, obvious protections from exchange were observed for several peptide segments at the TfR/TfR dimer interface region upon Tf binding at neutral pH which is due to the decrease of solvent accessibility, but no difference in protection under different pH conditions. Given these data and the available crystal structures of TfR, HFE/TfR and Fe_NTf/TfR, it is reasonable to suggest that binding with holoTf at pH 7.5 causes a local conformational change at the TfR/TfR dimer interface that brings the two TfR monomers into proximate. Then the two monomers maintain their relative position in the holoTf/TfR complex when lowering the pH to 5.5.

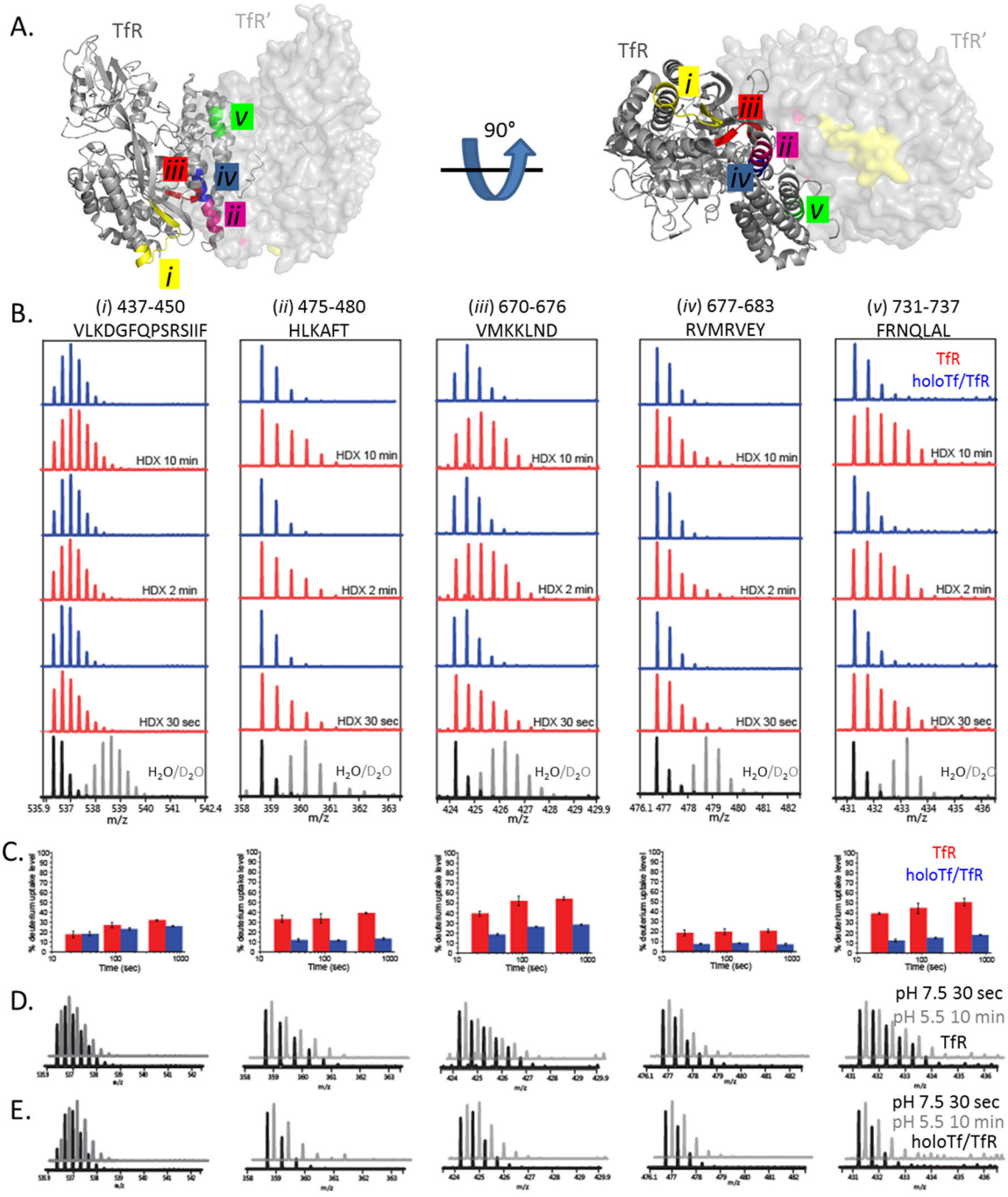

Figure 2-6 HDX data of the representative peptide segments at the TfR/TfR dimer interface. (A) TfR crystal structure (PDB: 1CX8) highlighting the locations of the five representative peptide segments. One TfR monomer is depicted in cartoon, while the other one is shown as surface. (B) The mass spectra extracted for the five representative peptide segments from TfR (red) and the holoTf/TfR complex (blue) at pH 7.5. The non-exchanged control and the fully deuterated spectra for each peptide are colored in black and gray at the bottom, respectively. (C) The deuterium uptake bar graph calculated from the panel (B) as the percentage of deuterium uptake level *versus* the exchange

time for the five representative peptide segments from TfR (red) and holoTf/TfR complex (blue) at pH 7.5. The error bars represent the SD over three independent runs. (D-E) Comparison of the deuterium uptake levels of the five representative peptide segments from TfR (D) and holoTf/TfR complex (E) at pH 7.5 exchanging for 30 seconds (black) and at pH 5.5 exchanging for 10 minutes (gray).

2.3.3.3 Local Structural Dynamics of TfR in the Protease-Like Domain

The conformational flexibility of TfR in the absence and the presence of Tf was examined, revealing the protease-like domain of TfR was relatively stable, especially for the regions buried inside in the protease-like domain (Figure 2-2 and Figure 2-3). While, the N-terminal α-helix, peptide segment [128-140], exchanged rapidly even in the free TfR, as its deuterium uptake level reached to 61% by exchanging for 30 seconds (the deuterium uptake levels for the helices in the helical domain ranged from 19% to 49% by exchanging for 30 seconds) (Figure 2-3A and Figure 2-4), and was protected in the holoTf/TfR complex (the difference in HDX% is 12% with the threshold of significance is ±9%), suggesting this N-terminal helix might be not rigid and nearly unstructured in the free TfR, but be stabilized by Tf binding. The N-terminus of this helix contains several contacts (Leu122, Tyr123, Trp124, and Asp125) with the N2 subdomain of Tf (65). Although the HDX data for these N-terminal contacts were missing, we predicted they were protected upon Tf binding, and the protection extended into the rest of the helix.

Another notable change of the deuterium uptake pattern in the protease-like domain of TfR was observed for two adjacent peptide segments, [523-537] and [506-522] (Figure 2-5A). The mass spectra recorded for both peptide segments displayed multimodal exchange patterns in the free protein and Tf-bound forms (Figure 2-7),

suggesting the presence of the local conformational heterogeneity within this region in solution.

The segment [523-537] is located between the helix α7 and α8 of the protease-like domain and does not show any secondary structure (63), and the segment [506-522] is derived from the helix α7 and connected to the segment [523-537] (Figure 2-5A). As shown in Figure 2-7A, the peptide segment [523-537] populated two conformations in the free receptor, one was nearly fully exchanged and the other was almost fully protected. When holoTf bound to the receptor at pH 7.5, the higher *m/z* population became and remained constant as the major component in the holoTf/TfR complex, indicating a local unfolding event occurred within this region upon Tf binding as early as 30 seconds of the exchange to give a state that underwent fast H/D exchange. This highly flexible conformation, which often leads to high binding specificity (161), contributes to stabilizing the holoTf/TfR complex at neutral pH by lowering the energy barrier in Tf binding due to the increasing entropy at the binding transition states with flexibility (161). Interestingly, detailed inspection of the mass spectra for this segment in holoTf/TfR and apoTf/TfR at pH 5.5 revealed a unique trimodal isotopic distribution at 2 minutes of the exchange but not at the shorter or longer exchange time points nor in the free TfR, suggesting the presence of a transient partially unfolded intermediate in the Tf/TfR complex formations in solution (the population described in the green curve in Figure 2-7A). Moreover, this intermediate was the major component in the holoTf/TfR, but as equal to the other two components in the apoTf/TfR. The difference observed here suggests this region may participate in stimulating iron release in the endosome.

Two overlapping peptide segments in this region, [529-537] and [530-537], also exhibited bimodal isotopic distributions in the free TfR and Tf/TfR complexes at pH 7.5, as those observed in the peptide segment [523-537] (Figure 2-7B-C). While within each peptide segment, it exhibited similar HDX profiles between the holo- and apoTf/TfR complexes at pH 5.5 and there is no sign of the partially unfolded intermediate as observed in the segment [523-537]. Since these three overlapping peptide segments align at the C-terminus and the partially unfolded intermediate was only observed in the segment [527-537], but not [529-537] nor [530-537], it is reasonable to propose that the transient partially unfolding event at pH 5.5 was occurred within the region [523-528] that participating in stimulating iron release from Tf in the endosome. Investigating the structure of Fe_NTf/TfR, the region [523-528] does not make any direct contact with iron-loaded Tf but it is located in proximity to the bridge between the N- and C-lobe of Tf (residues 332–340) (65,162) (Figure 2-8). At acidic pH, we suggest the conformational change of this region influences the bridge in Tf by forming a new cation-π interaction through Trp528 in TfR with Lys340 in Tf, resulting in movement of the bridge to accommodate Tf clefts opening. Indeed, the positions of the bridge in the structures of apoTf and Fe_NTf/TfR are different, implying that the loss of iron from the N-lobe accompanies the movement of the bridge (65).

The segment [506-522] also exhibited clear two isotopic distributions in the free receptor (Figure 2-7D) which were probably due to its conformational heterogeneity, the presence of the different ensembles (helix-loop), and the contribution of the flexible loop. It is interesting to note that in the free TfR at pH 7.5, the low *m/z* population

shifted to higher *m/z* range at 2 minutes of exchange but shifted back at 10 minutes of exchange, suggesting a transient unfolding/folding transition occurs within this region, which is probably caused by the helix-coil transitions that typically for helical edges (163). This change was not observed in the free TfR at pH 5.5 which could be due to the low intrinsic exchange rate at the lower pH level. Once Tf was bound to TfR, the low *m/z* population shifted to higher *m/z* as early as 30 seconds of exchange and it became and remained as the major component, suggesting binding to Tf could induce the local unfolding event. Moreover, the HDX profiles look similar in the different forms of the Tf/TfR complex at pH 5.5, indicating this region does not involve in iron release process. Although based on our current understanding, there is no evidence indicating that any residue within the segment [506-522] is involved in Tf binding, the allosteric effect by protein binding could also cause the non-interfacial sites to undergo a different HD exchange behavior (164). The conformational change of this segment upon Tf binding could be induced by the allosteric transition through its adjacent loop [523-537].

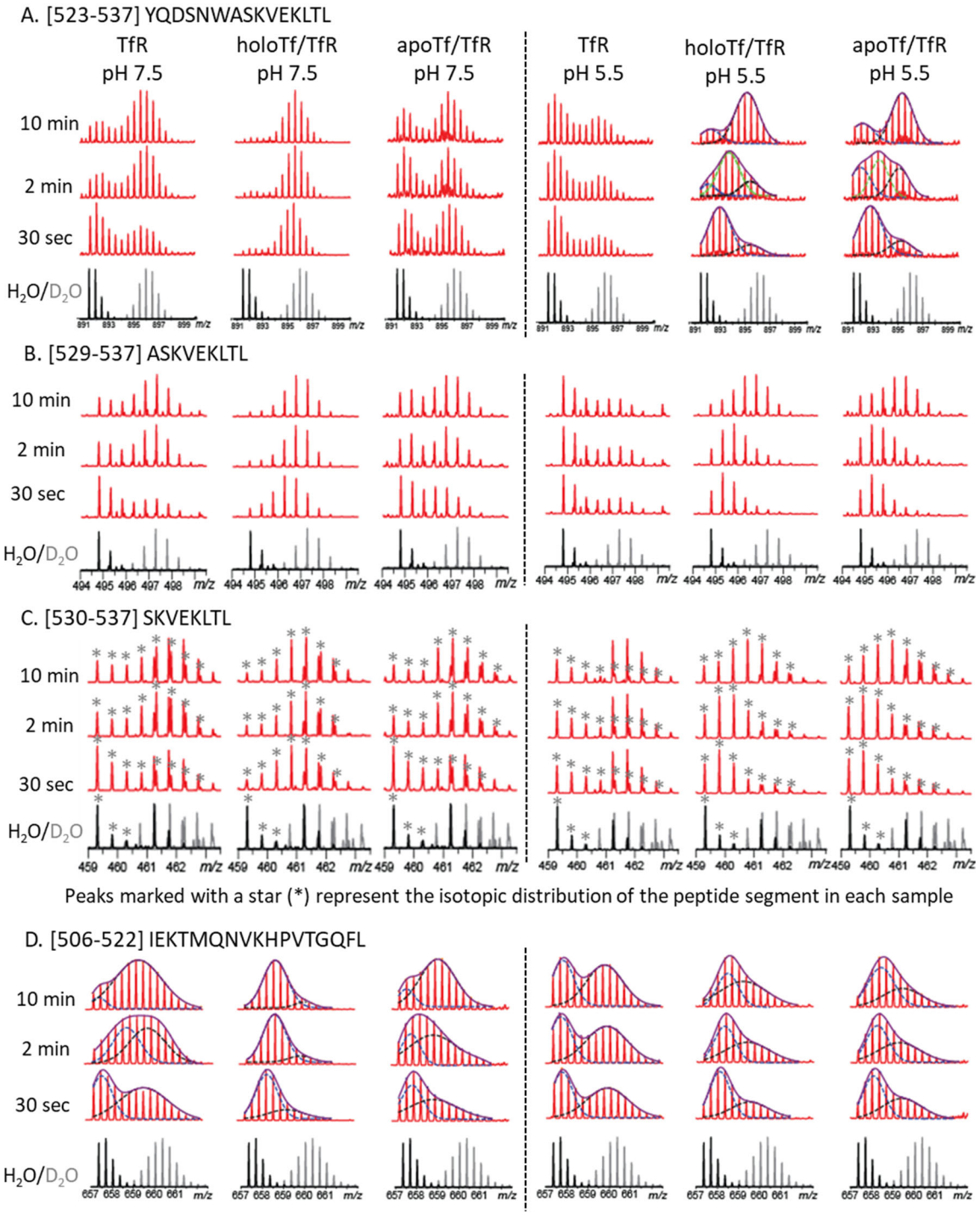

Figure 2-7 The *m/z* spectra of TfR peptic segment (A) [523-537], (B) [529-537], (C) [530-537] and (D) [506-522] in the absence and the presence of the binding partner at different pH levels. The spectra of the peptide segment [523-537] in Tf/TfR complexes at pH 5.5 after 2 minutes of the exchange were fitted to a trimodal distribution (population 1: blue curves; population 2: green curves; population 3: black curves). The non-exchanged control (black trace, labeled as H_2O) and the fully deuterated spectra (gray trace, labeled as D_2O) are shown at the bottom.

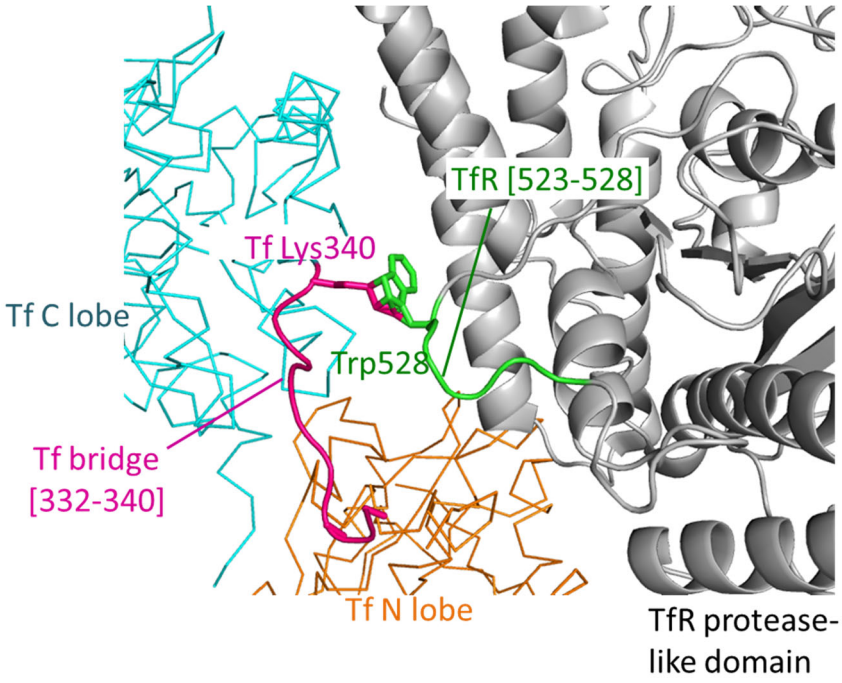

Figure 2-8 Structure of Fe_2Tf/TfR (PDB: 1SUV) showing the locations of the region [523-528] in TfR (PDB: 3S9N) (green) and the bridge between the N- and C lobe of Tf ([332-340] (magentas). The suggested interaction Lys340 - Trp528 at acidic pH is illustrated.

2.3.3.4 Binding to Tf Stabilize the TfR Apical Domain

TfR consists of three domains: a protease-like domain, an apical domain, and a helical domain. There is also an interdomain cleft formed by the portions of the three domains (Figure 2-9A). Careful examination of the HDX profiles revealed clear bimodal isotopic distributions for several noncontiguous peptide segments located at the edge of the cleft (Figure 2-9A), [188-201], [212-225], [281-295] and [557-572], in the free TfR as early as exposing to the deuterated buffer for 30 seconds (Figure 2-10A-C and Figure 2-11). Interestingly, in the Tf/TfR complexes, these peptides exhibited a single isotopic distribution that shifted to the relative high *m/z* range as early as 30 seconds of the exchange, except for that in the apoTf/TfR at pH 7.5. In the apoTf/TfR complex at pH

7.5, these peptides exhibited bimodal isotopic distributions, which could be due to the weak apoTf binding affinity and the rapid dissociation under the relatively unfavorable condition (the SEC data indicated about 23% apoTf/TfR was dissociated at pH 7.5 under the HDX experimental condition (Figure 2-1C-D)). In contrast to the above peptide segments located at the cleft region, a loop segment [346-356], for example, located at the opposite position of the interdomain cleft in the apical domain (Figure 2-9A) exhibited single isotope distribution in all free receptor and the complex forms, and the presence or the absence of Tf did not influence its deuterium uptake level obviously (Figure 2-10D). Notably, unlike other reported bimodal patterns, which are induced by ligand binding (165,166), the above peptide segments exhibited bimodal isotopic distributions in the absence of the binding partner but single isotopic distribution in the complexes. Given their close spatial proximity to one another and location at the interdomain cleft, we suggest the observed bimodal isotopic distributions could result from the heterogeneous conformations of TfR in solution and Tf binding could induce the local conformational fluctuations at the interdomain cleft region that transit the slow exchanging conformation into the fast exchanging conformation.

In TfR, the apical domain forms a lid structure that covers the interdomain cleft. It flexibly connects with the protease-like domain by two β strands which act as a hinge, allowing small rotation of one domain relative to the other (63). Based on the different conformations observed for the peptide segments located at the interdomain cleft region in HDX and the flexibility of the apical domain, we propose that the interdomain cleft in TfR appears to have different 3D shapes in solution based on the different

positions of the apical domain: the Position I and II as shown in Figure 2-9B which represents a relatively closed and an open state, respectively. For the peptide segments display bimodal isotopic distributions, the species representing the fraction of the slow exchanging, solvent-restricted population correspond to the Position I (closed), whereas the species representing the fraction of fast exchanging, solvent-accessible population correspond to the Position II (open). In the free TfR, the two different conformational structures coexist in equilibrium in solution. Binding with Tf causes a shift of the species to fast exchange, suggesting the conformation of the cleft is stabilized into a relatively open position (the Position II). At acidic pH, the single high *m/z* species observed in HDX in the Tf/TfR complexes indicate the interdomain cleft maintains this conformation through the endocytic cycle until the complex returns back to the cell surface. In the apoTf/TfR complex at pH 7.5, the weak binding affinity of apoTf makes the apical domain flexible again and the interdomain cleft more favorable at the closed position, as the larger percent of the low *m/z* population in apoTf/TfR complex comparing with those in TfR at pH 7.5.

Previous studies (65,72,75) suggested the Tf binding sites on TfR are on the helical domain and the N-terminus of the protease-like domain which are distant from the interdomain cleft ((Figure 2-9A). Clearly, these changes in the conformation of the interdomain cleft upon Tf binding are not induced by direct protein-protein interaction, allosteric effects must attribute to it. Investigating the structures of free TfR and TfR bound to Tf, a disordered loop in the apical domain (residues 306-330) (Figure 2-12), involved in TfR dimerization and Tf binding, rotates towards the Tf binding site when Tf

is present (65). We propose that Tf binding triggers a perturbation of the hydrogen-bonding network around the interdomain cleft through this disordered loop (His318 in TfR interacts with His349 in Tf) and that causes the conformational change of the apical domain. In addition, since the allosteric regulation generally alters the entropy and enthalpy and, therefore, regulates protein function (167), the conformational entropy changes due to the loss of the flexibility of the apical domain upon Tf binding could further enhance the strength of the interactions of TfR with Tf and stabilize the complex.

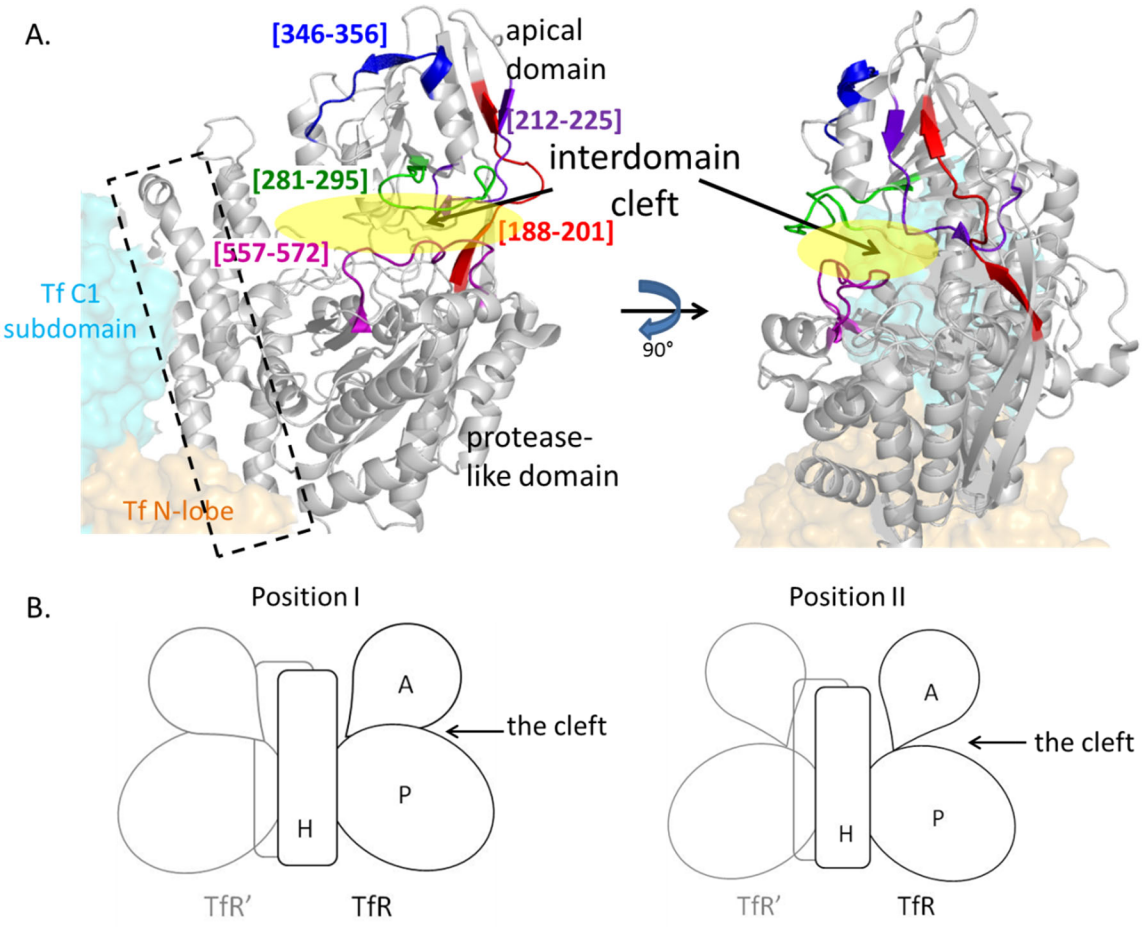

Figure 2-9 TfR interdomain cleft. (A) Locations of several peptide segments located at the interdomain cleft that exhibiting bimodal isotopic distribution. A control peptide segment [346-356] showing single isotopic distribution is highlighted in blue. TfR is colored in white, the C1-Tf subdomain is colored in cyan, and the N-lobe of Tf is colored in orange. The interdomain cleft is highlighted in yellow and the predicted Tf binding

region in TfR is highlighted in the black box. (B) Schematic diagram of the two relative positions of the apical domain of the free TfR that may coexist in the solution. H: the helical domain; A: the apical domain; P: the protease-like domain.

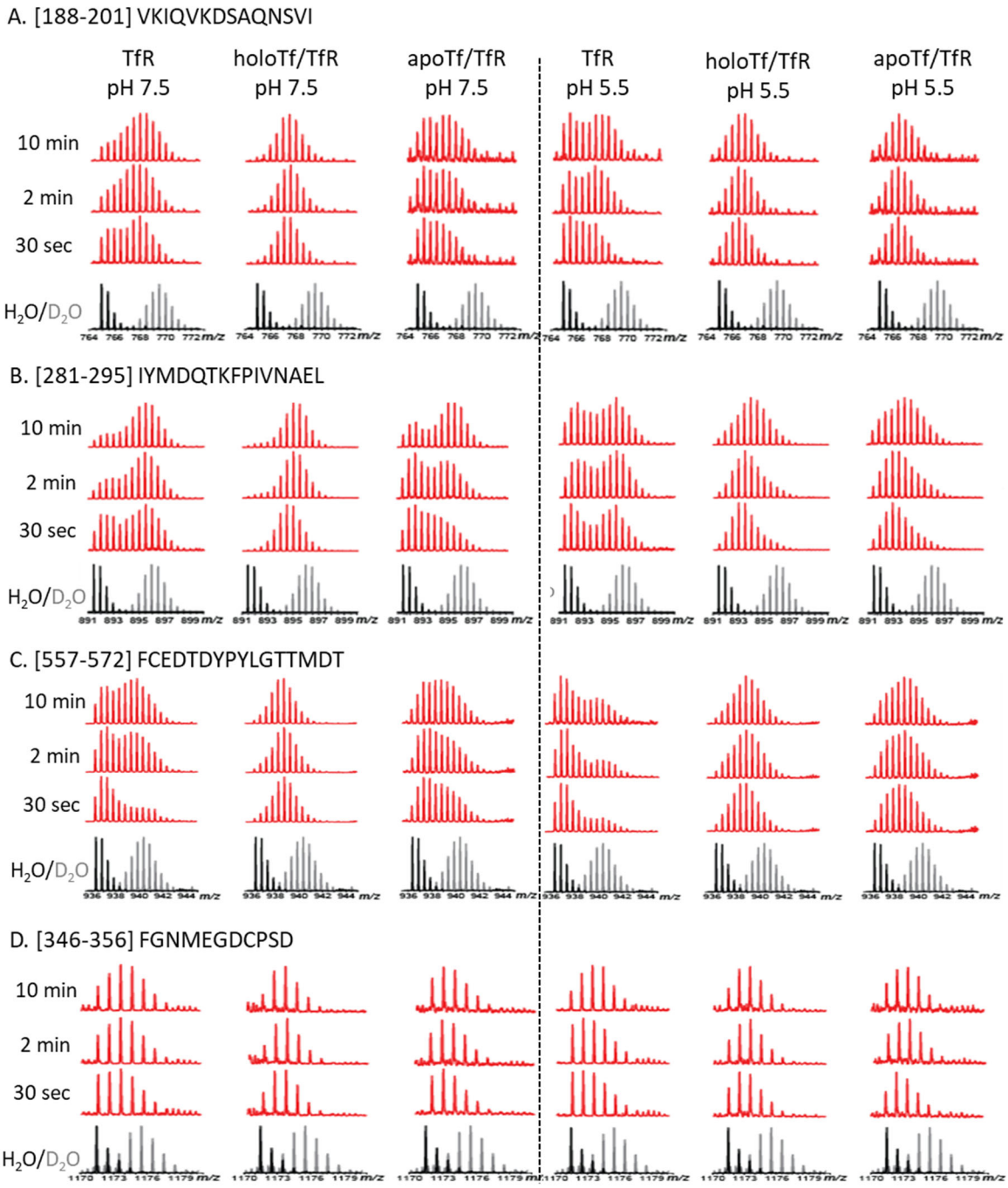

Figure 2-10 The *m/z* spectra of the peptic segment (A) [188-201], (B) [281-295], (C) [557-572], and (D) [346-356] in the absence and the presence of the binding partner at different pH values. The non-exchanged control (black trace, labeled as H_2O) and the fully deuterated spectra (gray trace, labeled as D_2O) are shown at the bottom.

- [188-200] VKIQVKDSAQNSV

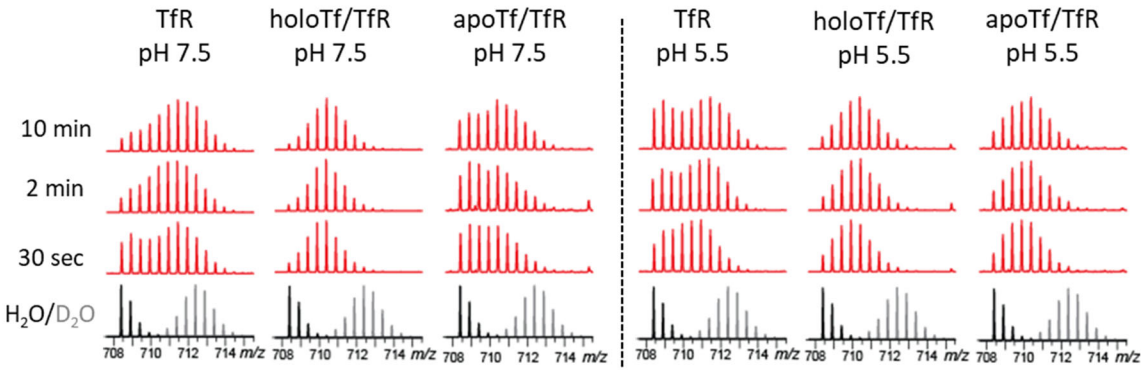

- [212-225] LVENPGGYVAYSKA

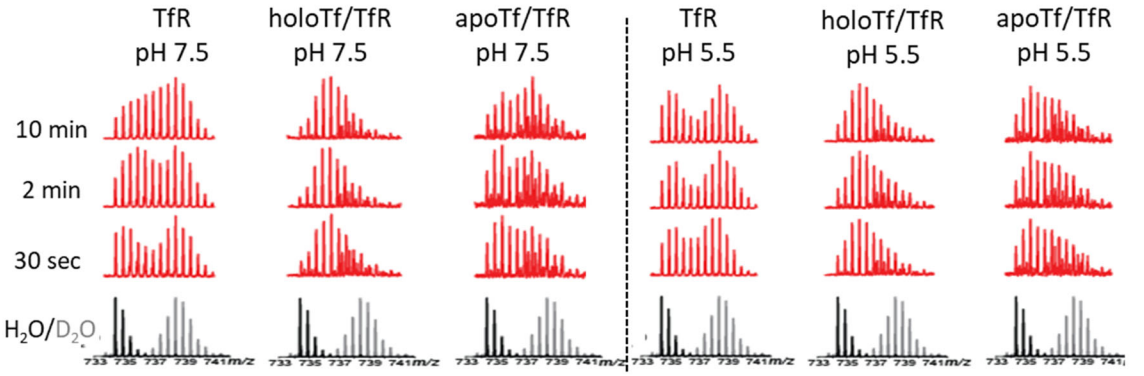

- [281-294] IYMDQTKFPIVNAE

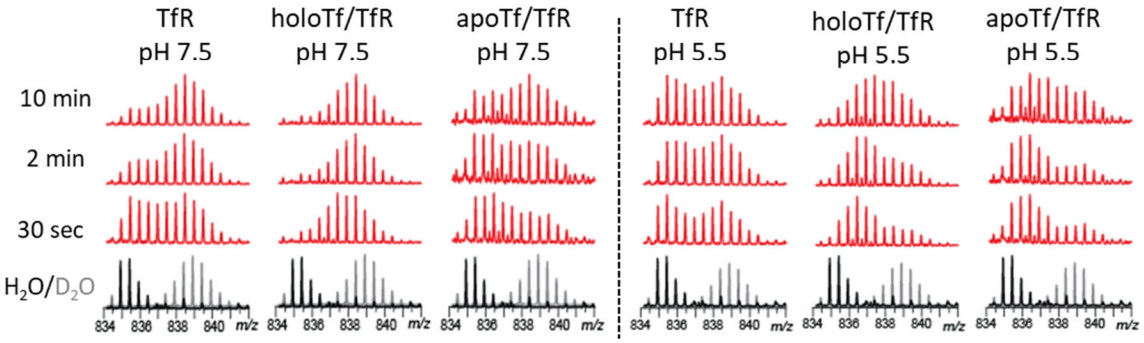

- [284-295] DQTKFPIVNAEL

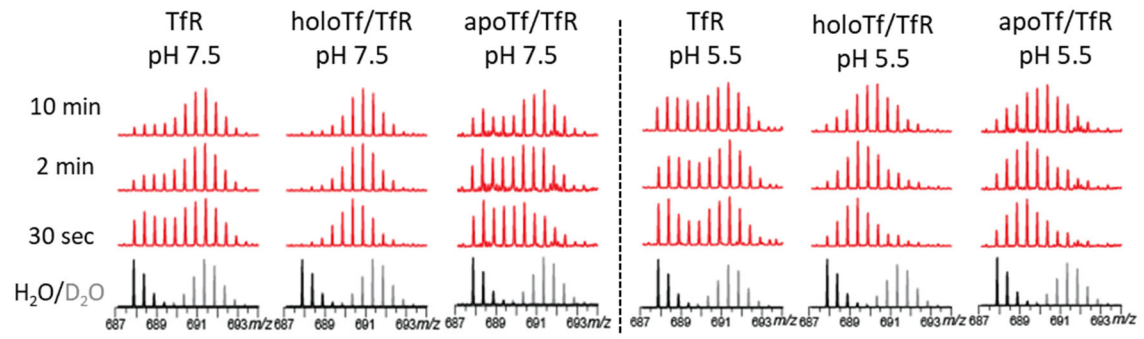

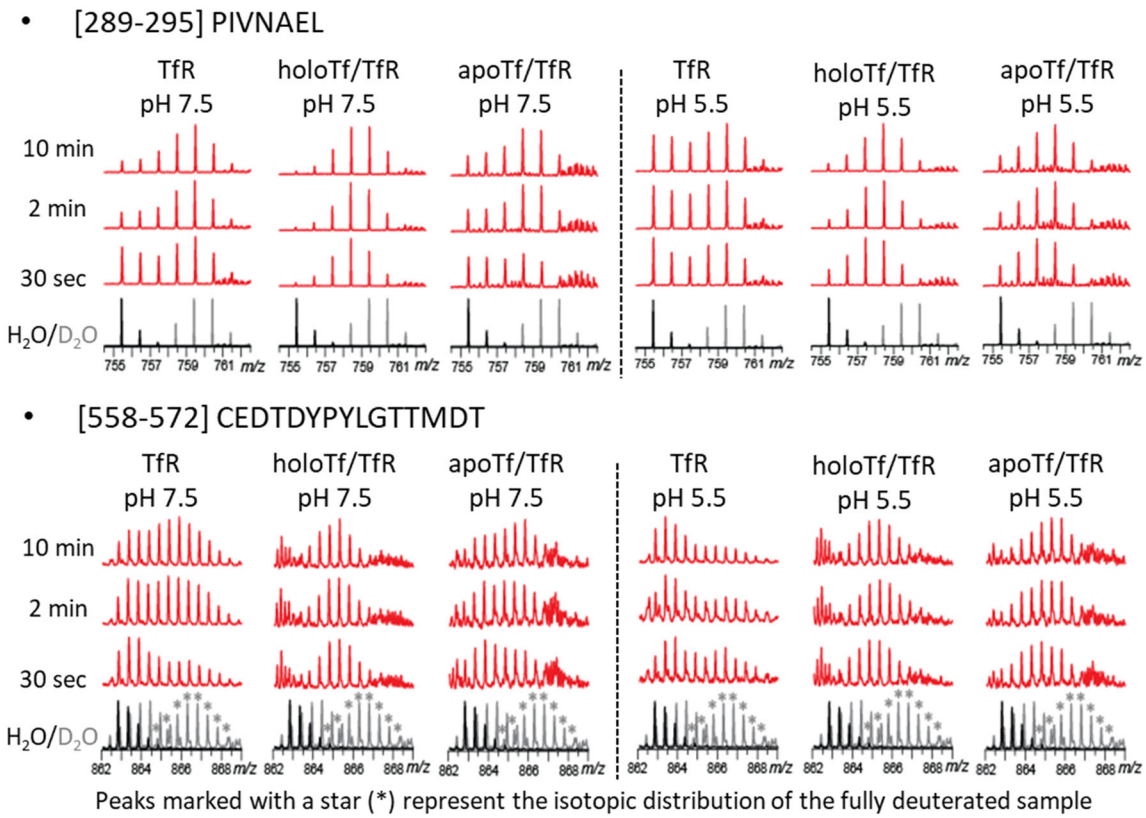

Figure 2-11 The *m/z* spectra of several overlapping peptic segments located at the edge of the interdomain cleft in the absence and the presence of the binding partner at different pH values. The non-exchanged control (black trace, labeled as H_2O) and the fully deuterated spectra (gray trace, labeled as D_2O) are shown at the bottom.

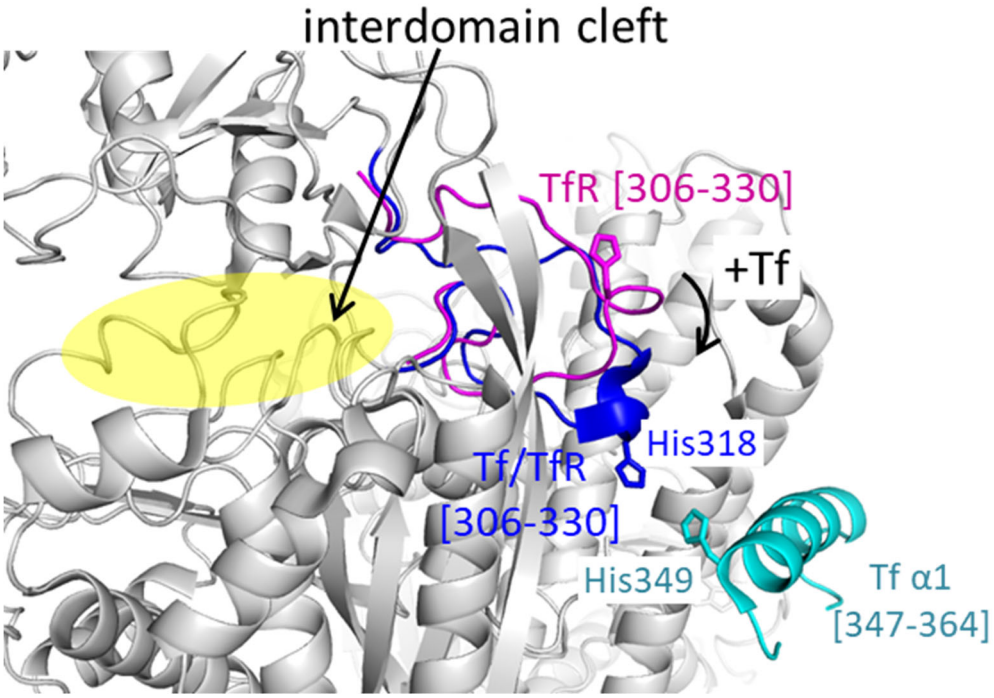

Figure 2-12 Structure of Tf/TfR showing the position of the disordered loop [306-330] in TfR (magentas) rotates towards the Tf binding site in the presence of Tf (blue). TfR is colored in white. The interdomain cleft is highlighted in yellow. The Tf molecule has been removed with the exception of the segment [347–364] (cyan).

2.3.3.5 Structural Comparison of TfR and PSMA

Despite TfR has a strikingly similar 3D structure to that of PSMA (Figure 2-5) (the structure of the protease-like domain, the apical domain, and the helical domain is 29%, 25%, and 23% identical to PSMA, respectively) (88), its function as a receptor rather than an enzyme. Since the function of a protein is directly dependent on its 3D structure, we propose the structural divergence of TfR/PSMA in molecular evolution is necessary for the evolution of new functions or the loss of former functions for TfR.

After aligning the sequences of TfR and PSMA (Figure 2-13), we found all TfR peptide segments exhibiting bimodal isotopic distributions in HDX have a small or large number of deletions compared with the analogous regions in PSMA. These regions are

conserved within each subfamily within vertebrates but variable between the TfR and PSMA subfamilies. In PSMA, these regions are involved in forming the substrate-binding cavity and the insertions contribute to a large increase in buried surface area between the apical and protease domains (about 2-fold larger than that in TfR (88)) and narrow its substrate-binding cavity (Figure 2-5). In TfR, the fact of the deletions at the edge of the cavity and the reduced area of the substrate-binding cavity could allow interferences with substrates access that leads to the loss of the enzyme function in molecular evolution. Comparing with PSMA, TfR has less interdomain contacts, making the apical domain more flexible in solution. This was demonstrated by the observation of the presence of the two different conformations in HDX for the segments located at the TfR interdomain cleft edge (CHAPTER 2.3.3.4). It is interesting to note that structural alignment analysis of the TfR region 506-537 shows the analogous region in PSMA has a unique short α-helix (PSMA residues 492-502) which is highly conserved within PSMA family but not present in TfR (Figure 2-5 and Figure 2-14). The loss of the short helix in TfR in the molecular evolution could increase the flexibility of this region (with large crystallographic b-factors in TfR) which could assume multiple conformations and induce the structural fluctuation due to the large inherent conformational entropy. We suggested at acidic pH the Trp528 in TfR could form a cation-π interaction with Lys340 in Tf that induce the movement of the bridge connecting the N- and C-lobe of Tf to accommodate Tf clefts open. Although the residue Trp528 is completely conserved in TfR and PSMA, it is involved in helix packing in PSMA (Figure 2-14), making it not easy to approach the binding partner.


188-201
TfR
PSMA
TfR Secondary Structure
PSMA Secondary Structure
TfR Conservation
PSMA Conservation
212-225
281-295
506-537
557-570
628-636
702-712
bimodal peptide

Figure 2-13 Sequence homology between TfR and PSMA subfamilies. The graph is generated using the online software Jalview (http://www.jalview.org/). The calculated quantitative alignment conservation annotation is measured as the number of conserved physico-chemical properties conserved for each column of the alignment (168). The residues which are completely conserved within each subfamily are highlighted in blue on the sequence. The peptide segments exhibited bimodal isotopic distributions in TfR are highlighted with red bars on the top of the sequence. The two peptide segments, [628-636] and [702-712], exhibited different protection patterns at different pH levels are highlighted in the black boxes.

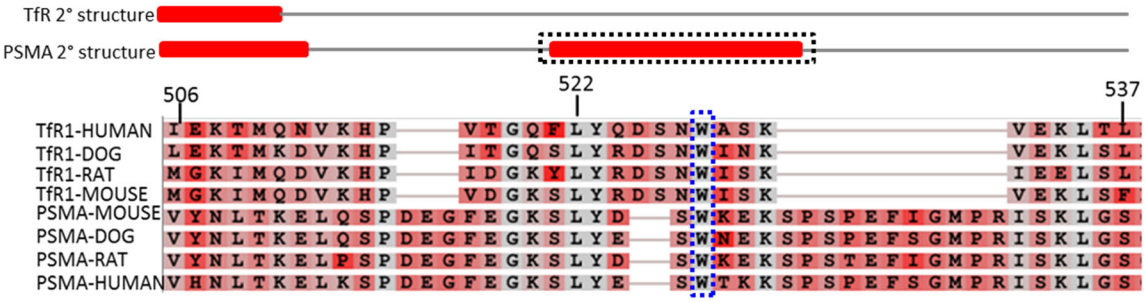

Figure 2-14 Partial sequence alignment conservation of amino acids 506-537 (numbering based on human TfR) in the protease-like domain of TfR/PSMA family. The unique α-helix (residues 492-502) in PSMA is highlighted in the black box. The TfR Trp528 is highlighted in the blue box. The diagram is generated using the BLASTP program (https://blast.ncbi.nlm.nih.gov/Blast.cgi).

2.3.4 pH-Induced Conformational Change within TfR

TfR has different binding affinities to holo- and apoTf at different pH levels. Thus, it is possible that TfR could undergo a pH-induced conformational change that is responsible for its different Tf binding properties. However, the lack of structural information of both free TfR and the Tf/TfR complexes at acidic pH greatly limits our understanding of the receptor binding mechanism. To get a detailed picture of how pH mediates the conformational change within TfR to impact Tf binding properties and the stabilities of different Tf/TfR complexes, we carefully examined the HDX data of TfR at different pH levels (pH 7.5 exchanging for 30 seconds (“neutral” state of TfR) vs. pH 5.5

exchanging for 10 minutes ("acidic" state of TfR) to offset the intrinsic exchange rate (see Materials and Methods 2.2.5)). Any change observed between the "neutral" and "acidic" states of TfR may be related to acid-driven structure change/realignment that impacts the stability of different Tf/TfR complexes in the endosome.

As shown in Figure 2-15A, TfR exhibited similar protection patterns at pH 7.5 and 5.5, with the exception of two regions in the helical domain, [628-636] and [702-712] (the differences in HDX% are 9.2% and -12.0%, respectively, with the threshold of significance is ±8.2%). The peptide segment [628-636], residing in the helix α2 and locating near both the TfR/TfR dimer interface and the Tf binding region, gained protection at pH 5.5 (Figure 2-15C). In contrast, the other peptide segment [702-712] tended to be more flexible at lower pH level (Figure 2-15D). It is a part of the loop (residues 685-710) that connects the helical domain to the rest of TfR (Figure 2-15B). Comparing the structures of TfR and PSMA, the analogous region of TfR segment [702-712] in PSMA has a six-amino acid insertion and shows as a beta-hairpin, termed the glutarate sensor, that is unique to PSMA (Figure 2-13 and Figure 2-15E). This region shows strong conservation among each subfamily but is family-distinctive (Figure 2-13). The role of this glutarate sensor in PSMA is for substrate recognition and/or binding (95) but unclear in TfR. In TfR, the loss of beta-strands makes this region unstructured. It is much shorter due to the deletions in TfR and unable to reach into the apical-protease domain interface, making the helical domain of TfR relatively flexible in solution. We suggest the conformational change of the segment [702-712] (as a part of the loop 685-710) in "acidic" state of TfR (became more flexible) is relevant vis-à-vis transduction of

conformational changes between/within the protein domains that trigger a rearrangement of the helical domain to dock apoTf at acidic pH. Specifically, lowering the pH to 5.5, the increase in flexibility of the segment [702-712] could be conveyed to the loop Arg719-Glu728 through the helix α5. The loop Arg719-Glu728 contains an *N*-glycosylation site on Asn727 which is critical for Tf binding and the correct transport of TfR back to the cell surface (169). Unfortunately, no data was collected for it which was probably due to the presence of glycosylation. It has been reported that the glycosylated form of protein is much less stable than the unglycosylated form as lowering the pH (170). We propose that changing the pH from neutral to acidic, the loop Arg719-Glu728 becomes slightly more flexible and expanded in solution. The loop Arg719-Glu728 interacts with the helix α2 through salt bridges between Asp631 and Glu634 in the helix α2 and Arg719 at neutral pH. At acidic pH, the movement of the loop Arg719-Glu728 could then form an additional salt bridge between Asp631 and Lys720 that stabilizes the helix α2 (Figure 2-15B). Due to the critical position of the helix α2 in the tertiary structure, connecting to both the helix α1 and α3 which have extensive interactions with Tf, the change at the helix α2 may play as a switch that affects the conformation/position of the rest of the helical domain (the helix α1 and/or α3) to make the apoTf binding more favorable at acidic pH.

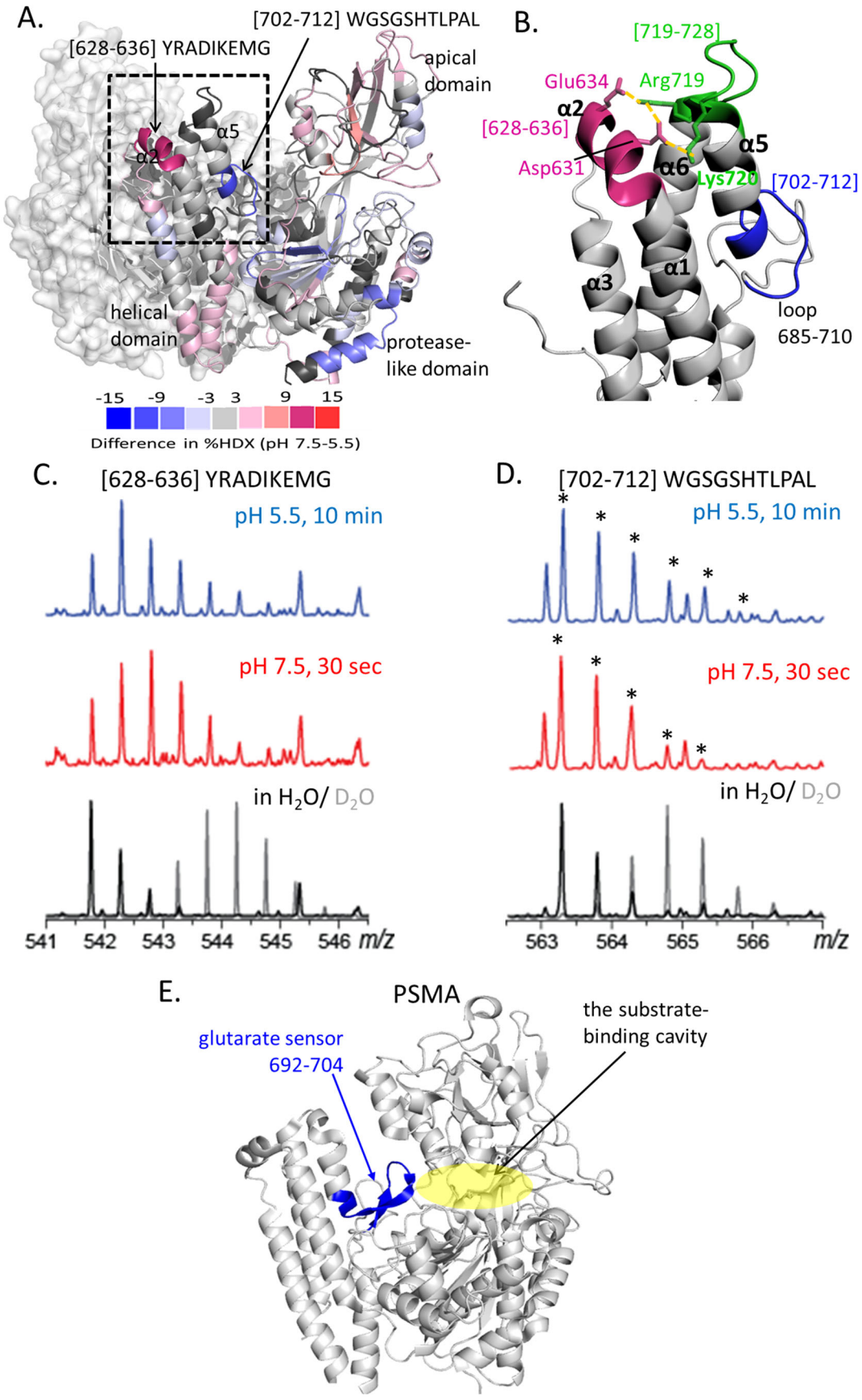
A.
[702-712] WGSGSHTLPAL
[628-636] YRADIKEMG
apical domain
α5
α2
helical domain
protease-like domain
-15 -9 -3 3 9 15
Difference in %HDX (pH 7.5-5.5)
B.
[719-728]
Glu634
Arg719
α2
[628-636]
α5
Asp631
α6
Lys720
[702-712]
α1
α3
loop 685-710
C.
[628-636] YRADIKEMG
pH 5.5, 10 min
pH 7.5, 30 sec
in H2O/ D2O
541 542 543 544 545 546 m/z
D.
[702-712] WGSGSHTLPAL
pH 5.5, 10 min
pH 7.5, 30 sec
in H2O/ D2O
563 564 565 566 m/z
E.
PSMA
glutarate sensor 692-704
the substrate-binding cavity

Figure 2-15 HDX comparison of TfR at different pH levels. (A) The deuterium uptake difference of TfR colored to the structure (PDB: 1CX8) obtained following 30 seconds of the exchange at pH 7.5 with those obtained following 10 minutes of the exchange at pH 5.5. Residues not observed in this work are colored in black. One TfR monomer is shown in cartoon, while the other monomer is shown as surface. (B) Zoom-in view of the area highlighted in panel (A). The suggested interactions between the helix α2 and the loop Arg719-Glu728 after a pH-induced conformational change are highlighted in yellow lines. The mass spectra of the peptide segment [628-636] and [702-712] in the free TfR at different pH levels are shown in (C) and (D), respectively. Peaks marked with a star (*) in panel (D) represent the signal of the peptide segment [702-712] exchanging in the deuterium-containing buffer at different pH levels. (E) The structure of PSMA (PDB: 2OOT) highlights the glutarate sensor.

2.3.5 Tf/TfR Binding Interfaces at Neutral and Acidic pH: Mechanism of Environmental Regulation of TfR Binding Selectivity

The binding affinities between TfR and Tfs are pH-sensitive, with the holoTf being strongly favored at neutral pH and the apoTf favored at acidic pH, and the presence of TfR can dramatically impact the iron release process from each lobe of Tf under acidic condition (171). It is believed that this is achieved through some yet unidentified adjustment of Tf/TfR binding interface in either Tf or TfR, or both (70,172,173). However, any solid proof of this conjecture is still lacking due to the unavailable crystal structure of either free TfR or the Tf/TfR complexes at acidic condition and the low resolution of the currently available crystal structure of Fe_2Tf/TfR complex at neutral pH (72). To test the hypothesis according to what conformational change within TfR that primarily affects the structure at the Tf/TfR interface region, makes the interaction with apoTf more favorable at acidic pH and holoTf more favorable at neutral pH and participates in the iron release in the endosome, we characterized the changes at the Tf/TfR binding interface at both neutral and acidic pH.

2.3.5.1 Characterizing Tf/TfR Binding Motif at Acidic pH and its Relation to Iron Release from Tf

In general, the difference in deuterium incorporation in TfR between the holo- and apoTf/TfR complexes at pH 5.5 (correspond to the state before and after iron release from Tf) was not significant, except for a few peptide segments in the helical domain of TfR (highlighted in the circles in Figure 2-16 with the threshold of significance is ±6.7% and the positions of these peptide segments are shown in Figure 2-17I), suggesting these segments are involved in control iron release from Tf. More importantly, all of them are located in/near the predicted Tf C1/TfR interface region based on the structure of Fe_NTf/TfR complex. Since the presence of TfR can accelerate iron release from the C-lobe of Tf and only the C1 subdomain interacts with TfR, the changes observed in HDX at the Tf C1/TfR interface region upon binding with different forms of Tf here could provide valuable structural information on the characterization of the specific binding sites between "acidic" state of TfR and the open and closed conformations of Tf, helping us better understand the mechanism of iron release process from the C-lobe of Tf in the presence of TfR.

Detailed comparisons of the deuterium uptake levels for the peptide segments at Tf C1/TfR interface region at pH 5.5 are shown in Figure 2-18. Extra protection afforded by apoTf to TfR was observed for two peptide segments, [621-627] and [637-642], residing in the helix α1 and α3, respectively, but not in the holoTf/TfR complex, suggesting these two segments contain contacts with apoTf but not with holoTf. The C-terminal peptide segment [747-760] was also protected in the apoTf/TfR complex,

compared to TfR alone. While in the holoTf/TfR complex, it was relatively protected initially (30 seconds), and then began approaching to the exchange level as that in the free TfR (became unprotected) during the time course, suggesting a weak binding at the TfR C-terminus in the holoTf/TfR complex. In comparison, the peptide segment [643-649] in the helix α3, contiguous with [637-642], exhibited similar protection levels in the free TfR and the apoTf/TfR complex but different protection levels between holo- and apoTf/TfR complexes, suggesting this segment might be involved in holoTf binding. In contrast, the peptide segment [628-636] in the helix α2 did not show any difference in all forms of the sample. Although the previous study (65) indicated the residue Arg629 in TfR interacts with Asn361 and Gly617 in Tf at neutral pH, conformational changes within TfR helix α2 (CHAPTER 2.3.4) and/or Tf in response to the changes of the surrounding environment cause these interactions no longer exist at acidic pH.

In summary, at pH 5.5, obvious protections were observed in the C-terminal region ([747-760]), as well as the segments [621-627] and [637-642] when TfR was bound to apoTf, while the segment [643-649] were only protected in the holoTf/TfR complex. These observations are consistent with the notion of both Trp641 and Phe760 in TfR are essential for apoTf binding at acidic pH which can form a hydrophobic patch on the outside edge of the helical domain and interact with His349 and His350 in Tf to stimulate iron release (70). However, after inspecting the crystal structure of Fe_NTf/TfR (PDB: 3S9N), the distances between the Trp641-Phe760 hydrophobic patch in TfR and His349 and His350 in Tf (about 6-13Å) are far more extended to form an interaction (Figure 2-19A). More likely, in order to build these interactions with apoTf at acidic pH, it

requires a larger conformational rearrangement in TfR and/or Tf. Specifically, at pH 7.5, the C-terminal segment interacts with His349 (and His350) in Tf through both hydrogen bonds and van der Waals (65). Once the holoTf/TfR complex enters the endosome, we suggest within TfR, the pH-induced conformational change at the helix α2 in the helical domain performs as a switch and triggers position shifts on the helix α1 and/or α3, as well as a possible compensatory movement by the helix α1 in the C1 subdomain of Tf (the red arrows in Figure 2-19B). The movements bring the TfR helix α3 close enough to Tf to form strong cation-π interactions between Trp641 and the C-terminus (Phe760) in TfR and the protonated His349 and His350 in Tf. In addition, these movements also convert the interactions of Asp356, Glu357 and Ser359 in the helix α1 of Tf with Arg651, Tyr643 and Arg646 in the TfR helix α3 into the new interactions with Arg623 and Asn626 in the TfR helix α1 to stabilize the apo- conformation.

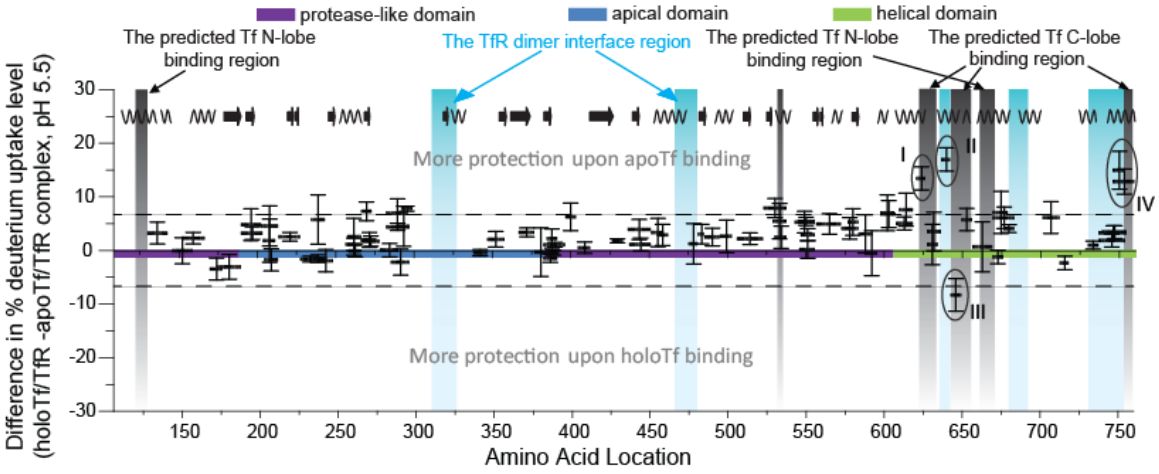

Figure 2-16 Plot of the different deuterium uptake levels following 2 minutes of the exchange between the holo- and apoTf/TfR complexes at pH 5.5. The dashed lines indicate the threshold of significant difference in HDX% (±6.7%). The peptic segments showing noticeable differences before and after iron release are highlighted (I: [621-627], II: [637-642], III: [643-649], and IV: [747-760]). The predicted Tf interaction regions and the TfR dimer interface regions (based on the crystal structure of Fe_NTf/TfR (PDB: 3S9N)) are highlighted in black and blue, respectively. The region of each domain is color

coded on the x-axis, purple for the protease-like domain, dark blue for the apical domain, and green for the helical domain, respectively.

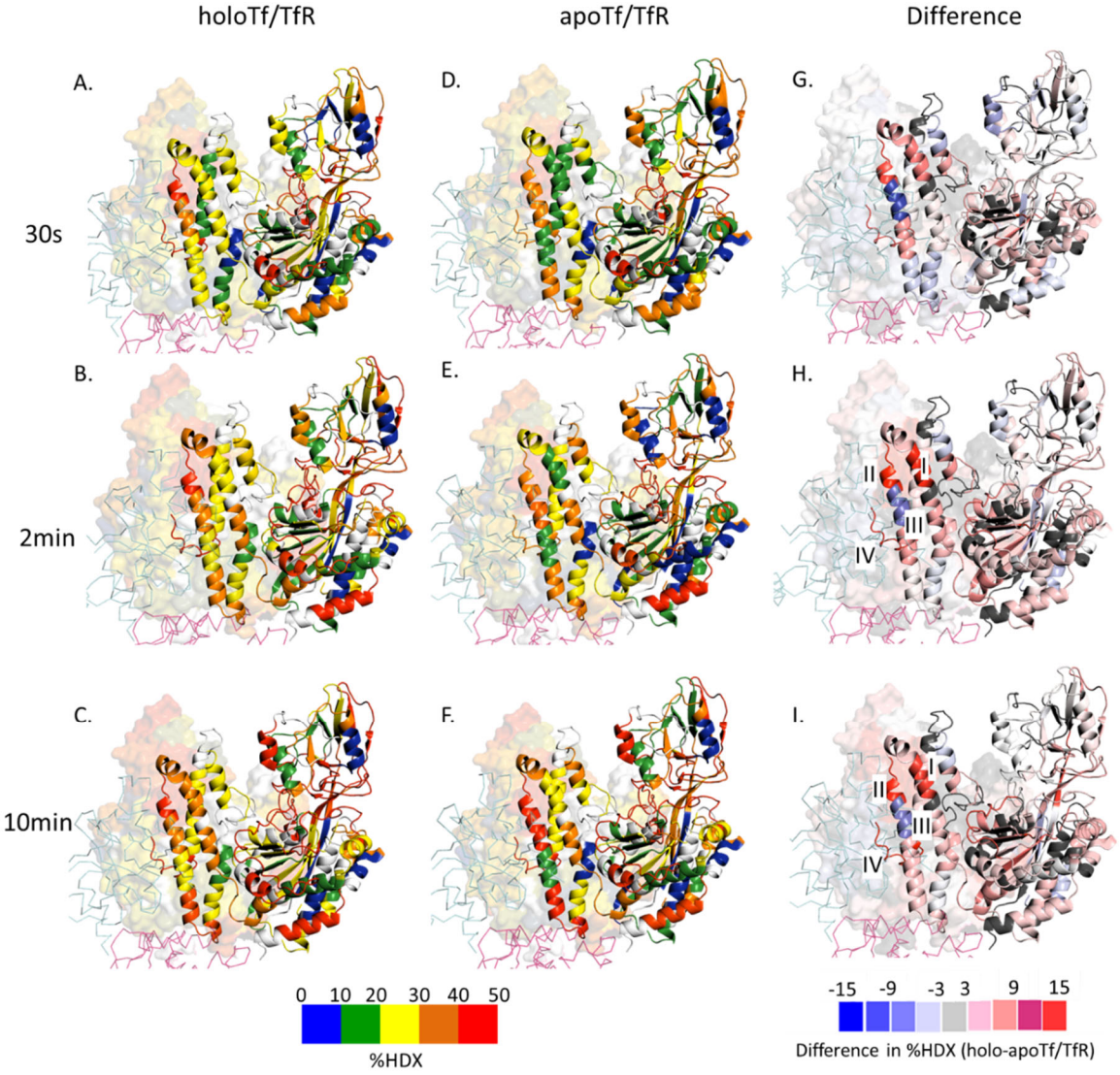

Figure 2-17 Mapping of HDX protection data on the crystal structure of holo- (A-C) and apoTf/TfR complex (D-F) following 30 seconds (top), 2 minutes (middle) and 10 minutes (bottom) of deuterium exchange at pH 5.5. Color coding reflects the protection of segments from highly protected (blue) to highly flexible (red). The differences in the percentage of exchange (holo –apo) are shown in G-I, following the same exchange time course. Residues not observed in this work are colored in white in structures A-F and are colored in black in structures G-I. The Tf is shown in ribbon with the N-lobe of Tf is colored in pink and the C1 subdomain of Tf is colored in cyan. One monomer in the homodimer of the Tf/TfR complex is shown in cartoon, while the other is shown as surface. The four segments (I: [621-627], II: [637-642], III: [643-649], and IV: [747-760])

showing noticeable differences before and after iron release are labeled in the panel I (with the threshold of significant difference in HDX% is ±6.7%).

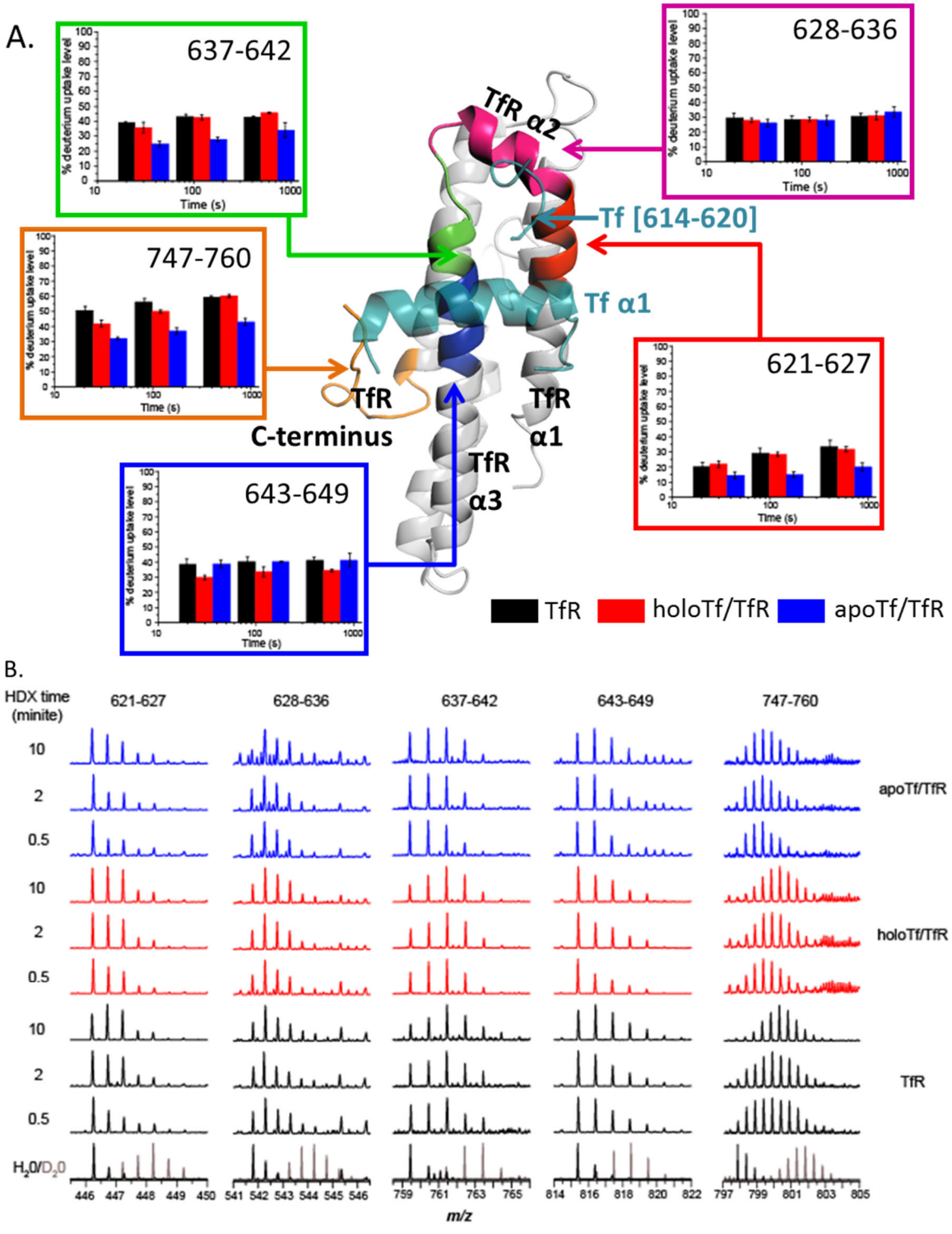

Figure 2-18 (A) The plots of deuterium uptake levels of the five peptide segments located at the Tf C1/TfR binding motif in the free TfR (black), as well as binding with

holoTf (red) and apoTf (blue) at pH 5.5. The Tf molecule has been removed with the exceptions of residues 347-366 (Tf α1) and 614-620 (cyan). The helical domain of TfR is colored in gray. (B) The *m/z* spectra of the five peptide segments in different forms of protein as described in panel (A). The non-exchanged control and the fully deuterated spectra for each peptide are colored in black and gray at the bottom, respectively.

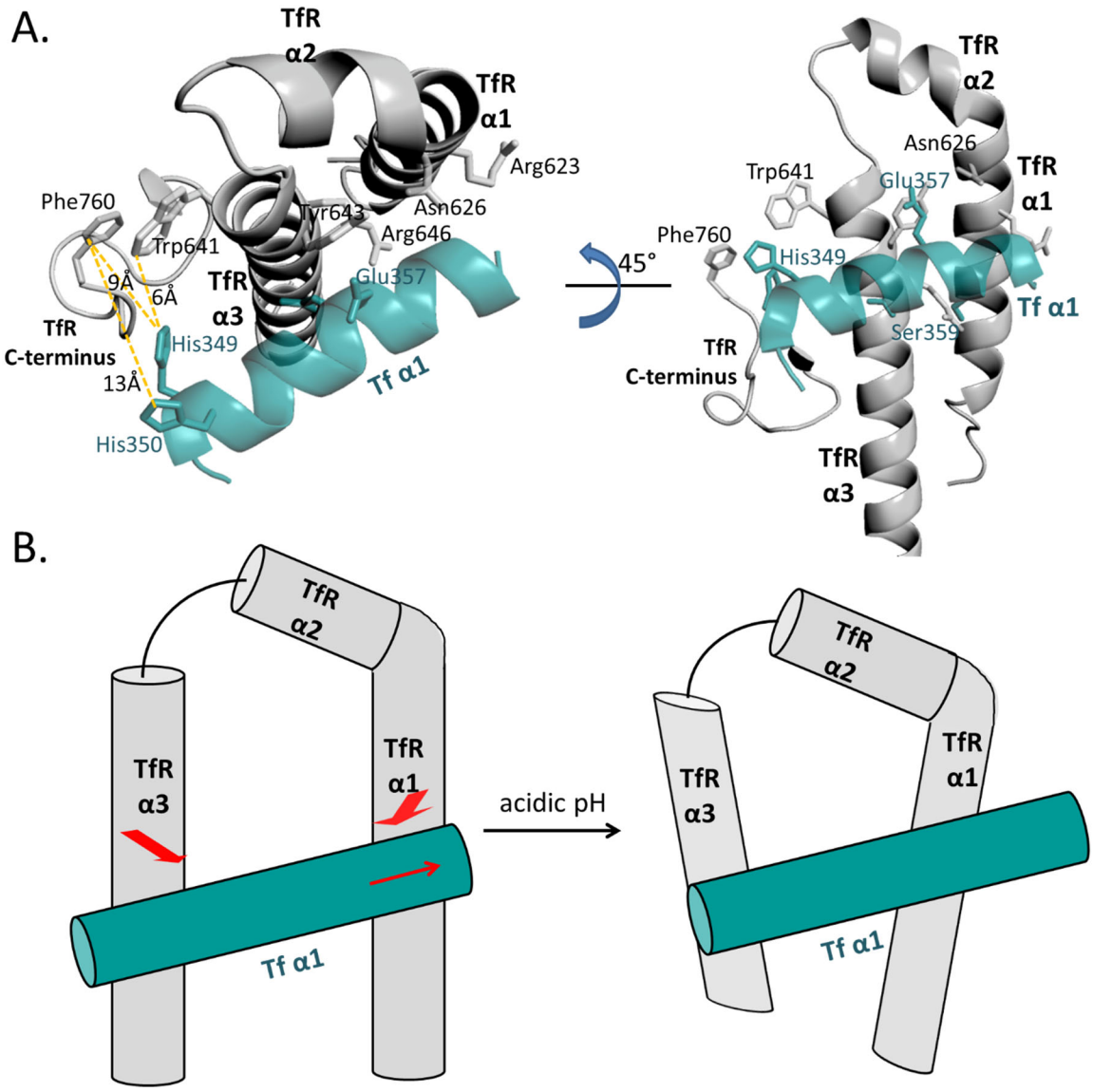

Figure 2-19 (A) Structure of the Tf C1/TfR binding motif in Fe_NTf/TfR (PDB: 3S9N) highlights the distances between the Trp641-Phe760 hydrophobic patch in TfR and His 349 and His350 in Fe_NTf (~6-13Å) at neutral pH by yellow dashed lines. Several residues at the interface of Tf C1/TfR are shown as sticks. (B) Schematic depicts the movements (red arrows) of the helical domain of TfR (gray) as well as the Tf helix α1 (cyan) in the endosomal pH which stabilize apoTf binding.

2.3.5.2 Tf/TfR Binding Motif at Neutral pH and its Relation to Tf Binding Affinity and Dissociation of apoTf from TfR

At neutral pH, TfR is able to weakly bind apoTf but apoTf dissociates more rapidly than holoTf. To characterize the changes within TfR that lead to its different Tf binding affinities and dissociation of apoTf from TfR, we compared the protection levels between holoTf/TfR and apoTf/TfR complexes at pH 7.5 (Figure 2-20). Obvious differences were observed at the Tf C1/TfR interface region in the helical domain, with the threshold of significance for exchanging 30 sec, 2 min and 10min is ±9.5%, ±7.9% and ±8.4%, respectively. Some peptide segments located at the protease-like and the apical domains, near/at the interdomain cleft region, also gained protection in the apoTf/TfR complex (colored in red in Figure 2-20G-I) due to the observations of the bimodal isotopic distributions (discussed in CHAPTER 2.3.3.3 and 2.3.3.4).

Figure 2-21 shows the comparison of the protection levels of the peptide segments located at the Tf C1/TfR interface region at pH 7.5 which correspond to the binding interface between “neutral” state of TfR and the open and closed conformations of Tf. The segment [637-642] in the TfR helix α3 was only protected in apoTf/TfR, whereas its neighboring segment [643-649] was only protected in holoTf/TfR. Both the C-terminus and the segment [621-627] in the TfR helix α1 gained protection in both holo- and apoTf/TfR complexes. Although both C-terminus and the segment [637-642] were still protected in the apoTf/TfR when increasing the pH from 5.5 to 7.5 (Figure 2-18 and Figure 2-21), we suggest the interactions between Trp641/Phe760 in TfR and His349/His350 in Tf weaken at pH 7.5 due to the deprotonation of His residues that

convert the strong cation-π interactions (between the protonated His and aromatic amino acids) to the weak π-π stacking interactions (between the neutral His and aromatic amino acids) (174), thus lead to the dissociation of apoTf from TfR at neutral pH. In addition, the segment [637-642] was only protected in the apoTf/TfR at both pH 7.5 and 5.5, not in holoTf/TfR (Figure 2-18 and Figure 2-21). We propose that the interaction between Trp641 in TfR and His349 in Tf is essential for apoTf binding and stabilizing the open conformation of the Tf C-lobe at both acidic and neutral pH. In contrast, the segment [643-649] was protected only in the holoTf/TfR at both pH 7.5 and 5.5 (Figure 2-18 and Figure 2-21). This segment contains the RGD binding sequence (Arg646-Gly647-Asp648) (175,176) which is conserved in TfR in mammals, birds, reptiles and amphibians (50). We suggest this RGD sequence in TfR is critical for holoTf binding, but not apoTf. At pH 7.5, comparing with the data at pH 5.5, extra protections in TfR upon holoTf binding were observed at the segment [621-627] and the C-terminus, which were contributed by the contacts between Val622, Arg623, Asn626, Glu759 in TfR and Val360, Val363 and Asn361, His349 in Tf, respectively. We propose these new contacts strengthen the interaction between TfR and holoTf and are responsible for its high holoTf binding affinity at neutral pH. In spite of the predict interactions of Arg629 in TfR with Asn361 and Gly617 in Tf in the Fe_NTf/TfR model (65), the segment [628-636] in the TfR helix α2 showed no change in protection in both complexes under experimental condition. These interactions in solution might be too weak to be captured by HDX.

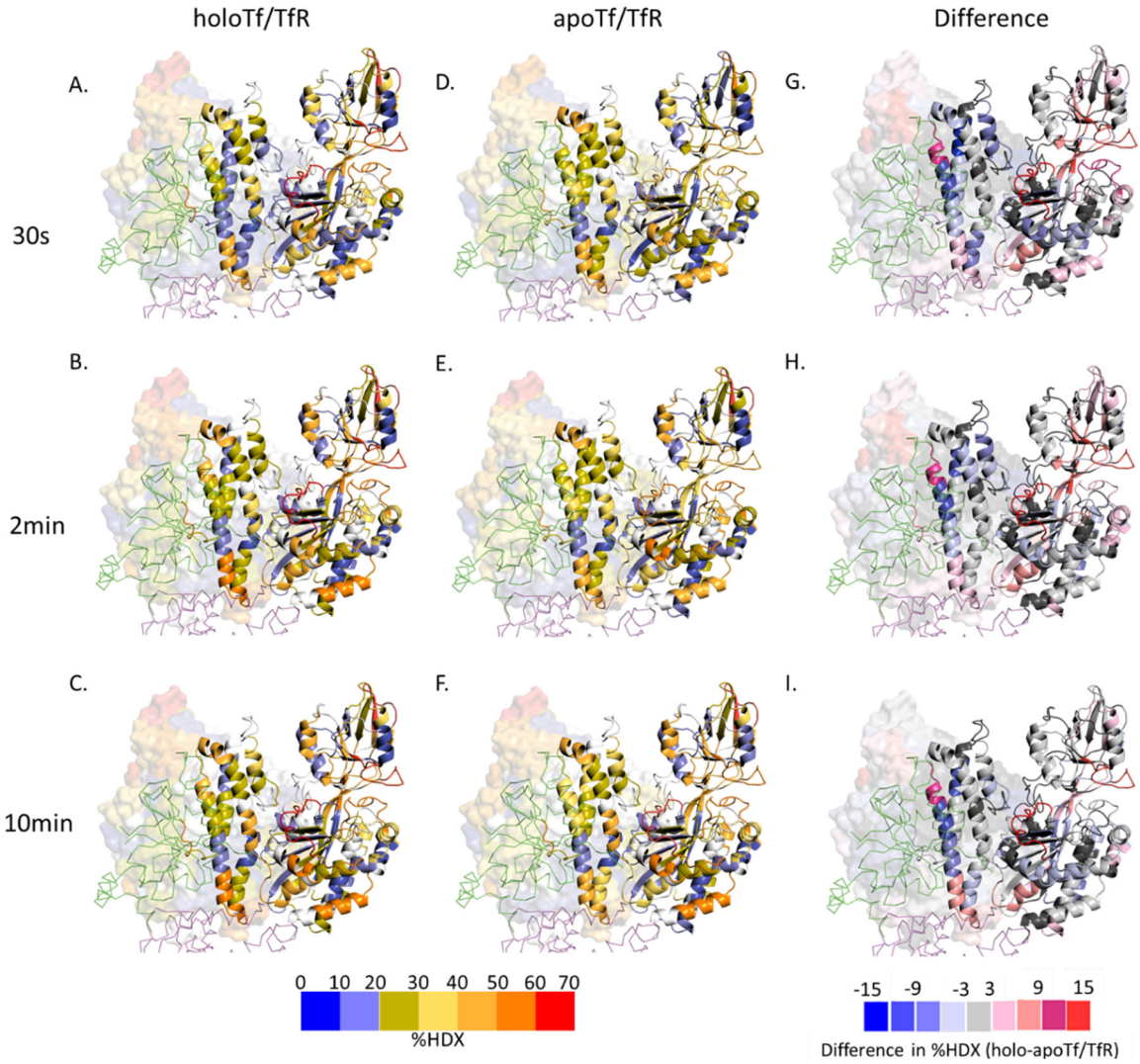

Figure 2-20 Mapping of HDX protection data on the crystal structure of holo- (A-C) and apoTf/TfR complex (D-F) following 30 seconds (top), 2 minutes (middle) and 10 minutes (bottom) of deuterium exchange at pH 7.5. Color coding reflects the protection of segments from highly protected (blue) to highly flexible (red). The differences in the percentage of exchange (holo –apo) are shown in G-I, following the same exchange time course. Residues not observed in this work are colored in white in structures A-F and are colored in black in structures G-I. The Tf is shown in ribbon with the N-lobe of Tf is colored in pink and the C1 subdomain of Tf is colored in cyan. One monomer in the homodimer of the Tf/TfR complex is shown in cartoon, while the other is shown as surface.

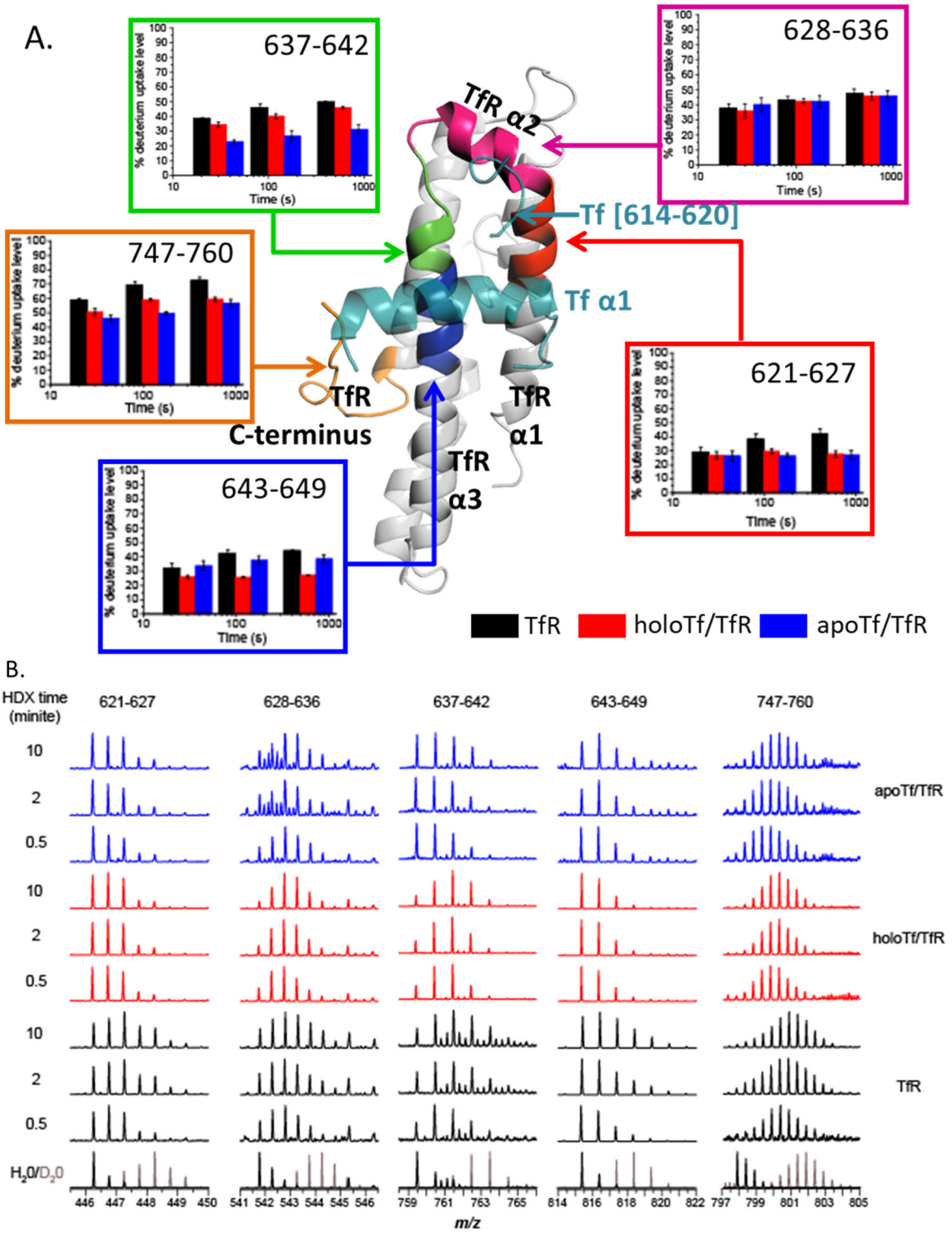

Figure 2-21 (A) The plots of deuterium uptake levels of the five peptide segments located at the Tf C1/TfR binding motif in the free TfR (black), as well as binding with holoTf (red) and apoTf (blue) at pH 7.5. The Tf molecule has been removed with the exceptions of residues 347-366 in Tf α1 and 614-620 (cyan). The helical domain of TfR is

colored in gray. (B) The *m/z* spectra of the five peptide segments in different forms of protein as described in panel (A). The non-exchanged control and the fully deuterated spectra for each peptide are colored in black and gray at the bottom, respectively.

2.4 Conclusion

Tf/TfR pathway is one of the primary routes for most mammalian cells to uptake circulating iron in plasma. Although the structure and dynamics of Tf and the roles of Tf in iron homeostasis are fairly well characterized (177-180), lacking the structures of TfR and Tf/TfR complexes, especially under the acidic condition, makes the studies of the Tf/TfR binding properties throughout receptor-mediated endocytosis even harder. In the present work, HDX MS is used to monitor the changes in conformational dynamics within TfR upon different forms of Tf binding at both pH 7.5 and 5.5. The proposed Tf/TfR binding mechanism is displayed in Figure 2-22. The changes in TfR afforded by Tf are of significance. Specifically, 1) several peptide segments located at the TfR/TfR dimer interface region gained protection upon holoTf binding at pH 7.5, indicating binding with holoTf results in a rotation at the TfR/TfR dimer interface that brings the two monomers into proximity contributes to the stabilization of the holoTf/TfR complex (Figure 2-22 I→II). 2) The observations of bimodal isotopic distributions of several peptide segments located at the interdomain cleft in the free TfR but not in Tf/TfR complexes suggest binding with Tf could induce the structural allosteric effect which reduces the flexibility of the apical domain of TfR in the Tf/TfR complex, making the interdomain cleft in a relatively open position (Figure 2-22 I→II). 3) The comparison between “neutral” and “acidic” states of TfR reveals the pH-induced conformational changes at the helical domain of TfR which are considered to be the key steps in Tf binding selectivity.

Lowering the pH to 5.5, the increase in flexibility of the loop 702-712 makes the helical domain relatively flexible in solution and the conformational change at the helix α2 (became more stable) plays as a switch that 4) triggers the position shifts on the helix α1 and α3 to stabilize the C-lobe of Tf in the open conformation by strengthening the apoTf binding through strong cation-π interactions (protonated His349/His350 in Tf with both the TfR C-terminus and Trp641 in the helix α3) and salt bridge or amide bridge interactions (Asp356 and Glu357 in Tf with Arg623 and Asn626 in TfR helix α1) (Figure 2-22 III). In addition, 5) the conformational change at Trp528 at pH 5.5 could influence the position of the bridge in Tf by forming a cation-π interaction with Lys340 in Tf whereby further accommodates Tf clefts opening (Figure 2-22 III). 6) By comparing HD exchange levels at the Tf C1/TfR interface region in different Tf/TfR complexes, we were able to capture conformational changes in TfR upon binding with different forms of Tf, allowing a detailed description of the site-specific interactions between TfR and the C-lobe of holo- and apoTf that account for its different Tf binding affinities. We propose the interaction between Trp641 in TfR and His349 in Tf is essential for apoTf binding and stabilizing the open conformation of the Tf C-lobe, while the RGD binding sequence (Arg646-Gly647-Asp648) in TfR is critical for holoTf binding. At pH 7.5, the interactions between Trp641/Phe760 in TfR and His349/His350 in Tf weaken due to the deprotonation of His, leading to the dissociation of apoTf from TfR. Extra protection in TfR upon holoTf binding observed at the segment [621-627] and the C-terminus contributes to its high holoTf binding affinity at neutral pH.

Altogether, our results extend the characterization of Tf/TfR interactions to both neutral and endosomal pH and provide, for the first time, the structural dynamics information of the Tf/TfR system under different conditions that mimic the stages encountered during endocytosis. Such a map greatly benefits our understanding of the molecular mechanism of modulation of TfR binding selectivity by pH and how TfR facilitates iron release from the C-lobe of Tf in the endosome, especially the structure information of neither free TfR nor the Tf/TfR complexes at acidic condition is available. Although this work is more focused on investigating the conformation and dynamics of TfR, following experiments are planned to characterize the changes on Tf in the different forms of Tf/TfR complex at neutral and acidic pH to better understand the Tf/TfR binding properties and the roles of iron release in the presence of TfR.

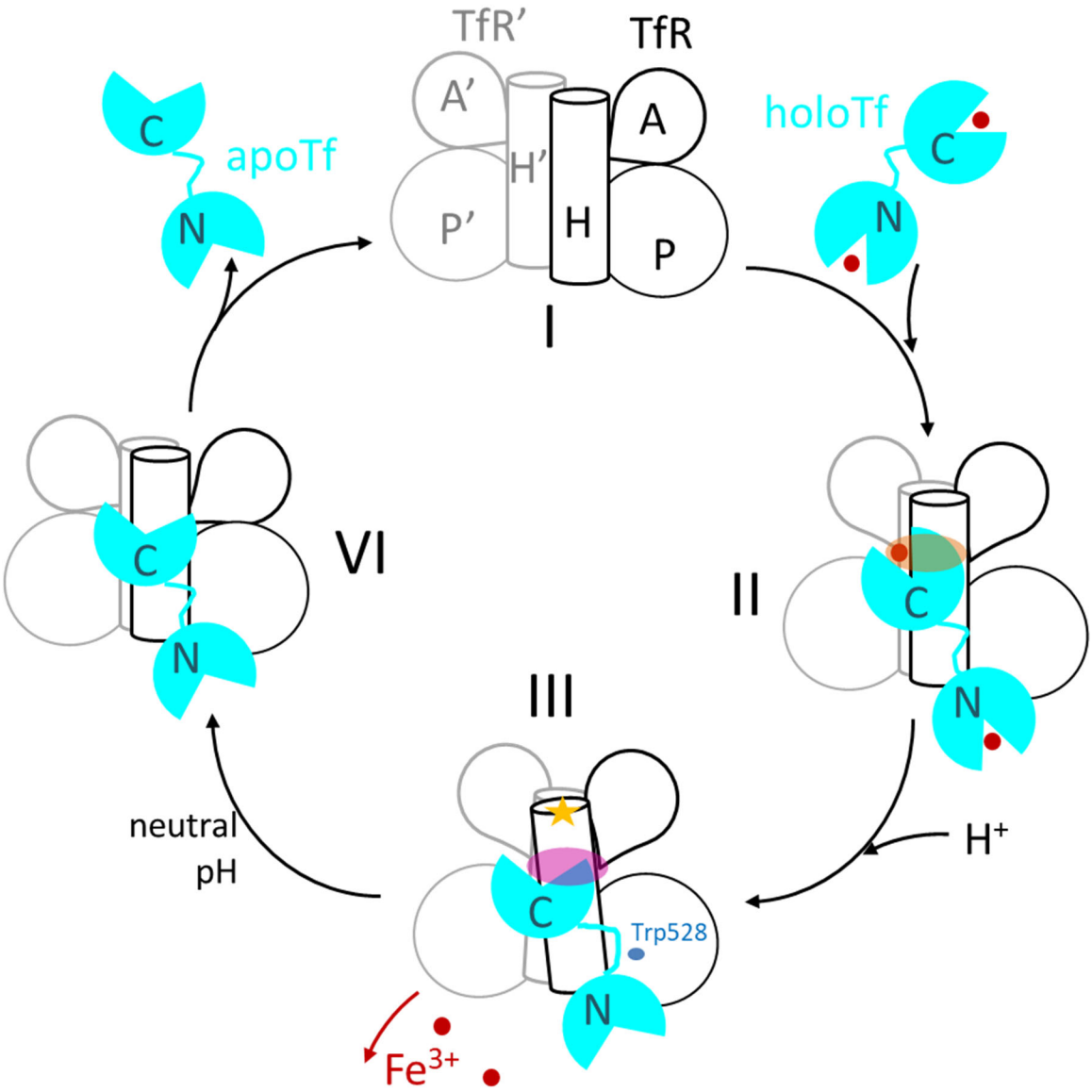

Figure 2-22 Schematic diagram illustrating the Tf/TfR interactions under different conditions. The specific binding site between "neutral" state of TfR and the C-lobe of holoTf at pH 7.5 is highlighted in orange in (II). The specific binding site between "acidic" state of TfR and the C-lobe of apoTf at pH 5.5 is highlighted in magenta in (III). The pH-induced conformational change at the helical domain of TfR is highlighted as star symbol in (III). H: TfR helical domain; A: TfR apical domain; P: TfR protease-like domain; C: Tf C-lobe; N: Tf N-lobe. Only one Tf molecule in Tf/TfR complex is shown in the schematic.

CHAPTER 3

EVALUATION OF NONFERROUS METALS AS POTENTIAL IN VIVO TRACERS OF TRANSFERRIN-BASED THERAPEUTICS

This chapter was published in *Journal of The American Society for Mass Spectrometry* 27(2) (2016): 211-219.

Abstract Transferrin (Tf) is a promising candidate for targeted drug delivery. While development of such products is impossible without the ability to monitor biodistribution of Tf-drug conjugates in tissues and reliable measurements of their levels in blood and other biological fluids, the presence of very abundant endogenous Tf presents a significant impediment to such efforts. Several noncognate metals have been evaluated in this work as possible tracers of exogenous transferrin in complex biological matrices using inductively coupled plasma mass spectrometry (ICP MS) as a detection tool. Placing Ni(II) on a His-tag of recombinant Tf resulted in formation of a marginally stable protein-metal complex, which readily transfers the metal to ubiquitous physiological scavengers, such as serum albumin. An alternative strategy targeted iron-binding pockets of Tf, where cognate Fe(III) was replaced by metal ions known to bind this protein. Both Ga(III) and In(III) were evaluated, with the latter being vastly superior as a tracer (stronger binding to Tf unaffected by the presence of metal scavengers and the retained ability to associate with Tf receptor). Spiking serum with indium-loaded Tf followed by ICP MS detection demonstrated that protein quantities as low as 0.04 nM can be readily detected in animal blood. Combining laser ablation with ICP MS detection allows distribution of exogenous Tf to be mapped within animal tissue cross-sections with spatial resolution exceeding 100 μm. The method can be readily extended to a

range of other therapeutics where metalloproteins are used as either carriers or payloads.

Keywords: ICP MS, Laser ablation, Tissue imaging, Targeted drug delivery, Stable isotopes

3.1 Introduction

A very large number of potent drug candidates showing superior characteristics *vis-à-vis* interactions with their intended therapeutic targets *in vitro* nonetheless fail clinical trials because of their inability to specifically target the intended site of action. Escalating the drug dosage remains a standard remedy for this problem, but therapeutically effective doses may (and frequently do) exceed safety limits and, in extreme cases, may be fatal for the host organism. More specific delivery can be achieved in some cases by taking advantage of certain anatomical features of the targeted sites (e.g., leaky vasculature and poor drainage in many tumors, which result in preferential retention of macromolecules via enhanced permeation and retention, EPR). The possibility to exploit the EPR phenomenon generated significant enthusiasm in the field of oncology (181) and has already led to the introduction of new anti-cancer medicines (e.g., albumin-bound paclitaxel (182)). Unfortunately, the initial excitement was tempered by the limited specificity of the EPR effect (limited by the lack of cellular specificity, low vascular density, and early release of active agents (183)); tumor-to-tumor variability also limits EPR usefulness (184). An orthogonal approach to drug delivery that is enjoying popularity in areas as diverse as oncology, neurodegenerative

diseases, rare genetic disorders, and regenerative medicine takes advantage of existing transport networks within the organism. An example of a promising drug delivery system where opportunities to improve routing are frequently overlooked is Tf, an 80 kDa iron glycoprotein, the primary function of which is the delivery of iron to cells. It is one of very few plasma proteins that gain cellular entry by the process of receptor-mediated endocytosis (178), a fact that has long attracted attention of the drug design community (17,23,32,185).

For example, malignant cells have dramatically elevated iron demands to sustain their uncontrolled growth and overexpress TfR, making Tf an attractive candidate for the selective delivery of cytotoxic agents to cancer cells, where cytotoxins could be either small molecule drugs chemically attached to Tf surface (8,17,20), macromolecules (such as Tf-diphtheria toxin conjugate TransMID (186)), or nano-objects, such as Tf-functionalized nanoparticles for siRNA delivery (187). Above and beyond internalization via receptor-mediated endocytosis, Tf can traverse polar cells in the process of transcytosis (188), allowing it to cross physiological barriers (such as BBB (189) and the intestinal epithelial barrier (190)). Efforts aiming at exploitation of this unique trait for the purpose of targeted drug delivery are also underway, with the ultimate goal of developing therapeutic agents that can reach targets shielded from the vast majority of existing drugs (191,192). We have recently started exploring a possibility of conjugating a bacteriolytic enzyme to Tf for targeting microbial infections in the central nervous system (34,35).

Among the many challenges faced by development of such products is difficulty associated with the need to obtain accurate and quantitative data on biodistribution of exogenous (administered) Tf and/or Tf-based therapeutics on the background of very abundant and structurally similar (if not identical) endogenous Tf. Indeed, Tf concentration in serum of healthy human subjects ranges between 25 and 50 μM (193), at least two orders of magnitude above the serum concentration of exogenous Tf even if highly concentrated preparations are used for injection. Although radiolabeling (e.g., using ^{125}I) can be used to detect such levels of exogenous Tf (194), it requires protein modification, which may impact its receptor binding and, therefore, affect the biodistribution. Furthermore, since the endogenous Tf is expected in most relevant cases to be structurally very similar (if not identical) to the exogenous protein, this not only rules out the use of ELISA as a detection/quantitation tool (due to likely cross-reactivity), but also makes the use of many proteomics-inspired tools (e.g., using ^{18}O-labeling of proteolytic fragments (195) or entire protein (196)) highly problematic. Although in our previous work we were able to detect exogenous Tf in biological fluids using the ^{18}O-labeling strategy, we had to rely on the affinity purification step prior to MS detection taking advantage of the His-tag segment of the recombinant Tf (197). Presence of the abundant and structurally similar endogenous Tf in tissues would also make it impossible to use traditional MALDI MS imaging approach for localization studies of exogenous Tf and Tf-based drugs in tissues, which typically relies on *in situ* proteolysis of proteins followed by detection of fragment peptides (198).

An alternative approach to detection and quantitation of exogenous proteins in complex biological matrices relies on placing metal tags on proteins followed by their detection with ICP MS (199), although most of those applications were limited to model studies currently. ICP MS is a sensitive technique for measuring metal- and metalloid-containing compounds (125), and in the absence of interferences from ubiquitous metals and plasma-related ions it can allow the limits of detection to be achieved at low fmol level (126,127). However, covalent modification of the protein surface with metal-containing tags, (e.g., *p*-hydroxymercuribenzoic acid (200) or reactive metal chelates such as activated DTPA (201) and DOTA (202), which form strong complexes with multiple lanthanides (203)), is likely to exert at least some influence on protein interactions with its physiological partners. In the case of Tf and/or Tf-based therapeutics, covalent modification is likely to interfere with the receptor binding process, a key step in both endocytosis and transcytosis, thereby inevitably altering their trafficking patterns and rendering the biodistribution data meaningless.

Tf contains a “cognate” metal tag (iron), some isotopes of which can be detected by ICP MS with very high sensitivity, but it can hardly be used as a specific Tf tracer because of its ubiquity in all biological fluids (mostly from hemoglobin and endogenous Tf) and tissues (ferritin, myoglobin, cytochromes, *etc.*). While Tf is known to bind a wide range of other metals (204), the affinities vary greatly (102), and a good Tf tracer must be selected carefully. In addition to the iron binding site, we also explore the utility of the His-tag, a histidine-rich segment of the recombinant Tf (as well as many other recombinant proteins) as a potential site for metal tagging. In this study, we limited the

scope of inquiry by examining two noncognate metals (indium and gallium), the interaction of which with Tf at the iron-binding sites is well-documented (102), and nickel as ametal targeting the His-tag segment of the protein (205). Four criteria are used to select acceptable non-ferric Tf tracers with ICP MS detection: (1) the metal should form a stable complex with the protein, (2) the metal should not be removed from Tf by ubiquitous scavengers, such as serum albumin or iron-free endogenous Tf, (3) the presence of the metal should not affect the receptor binding properties of the protein, and (4) minimal interferences from ubiquitous metals and plasma-generated ions (such as Ar^+, ArO^+, $CaOH^+$, etc.).

3.2 Materials and Methods

3.2.1 Preparation and Characterization of Tf Tagged with Nonferrous Metals

A diferric form of human serum transferrin (Fe_2Tf) (Intergen, Purchase, NY, USA) was converted to the apo-form (apo-Tf) by washing it with 1 mM EDTA in 3% (v/v) CH_3CO_2H, followed by buffer exchange to 50 mM HEPES buffer at pH 7.5. Indium and gallium were purchased from Alfa Aesar (Ward Hill, MA, USA). In- and Ga-tagged Tf were produced by incubating apoTf with metal·nitrilotriacetate (NTA) complexes in 100 mM NH_4HCO_3 and 50 mM HEPES buffer at room temperature for 1 hour followed by buffer exchange to 150 mM ammonium acetate, pH 7.5. The extent of protein tagging was determined by native ESI MS using a SolariX Fourier transform ion cyclotron resonance (FT ICR) mass spectrometer (Bruker Daltonics, Billerica, MA, USA). The possibility of metal exchange between In- and Ga-tagged Tf and apo-Tf, as well as the receptor-

binding by Tf substituted with nonferrous metals, was examined by native ESI MS using a QStar XL (AB Sciex, Toronto, Canada) hybrid quadrupole/time-of-flight mass spectrometer equipped with a standard ESI source.

Recombinant human Fe_2Tf containing an N-terminal His-tag was generously provided by Professor Anne B. Mason (University of Vermont College of Medicine), and the nickel-tagged form of this protein was produced by incubating it with significant molar excess of $NiSO_4$ in 20 mM ammonium acetate at pH 7.5. The extent of Fe_2Tf tagging with Ni^{2+} was determined by native ESI MS using a SolariX FT ICR mass spectrometer (vide supra). Unlike most other glycoproteins, Tf exhibits surprisingly little heterogeneity (see Figure 3-6 in Supplementary Material), which makes the analysis of metal-binding measurements carried out by native ESI MS relatively straightforward. The efficiency of nickel transfer to albumin was determined by incubating the Ni-tagged protein with bovine serum albumin (Calbiochem, La Jolla, CA, USA) prior to the ESI MS analysis.

3.2.2 ICP MS

Limits of detection of In-tagged Tf (In_2Tf) by ICP MS were determined by spiking 1 mL of bovine serum (Equitech-Bio, Inc., Kerrville, TX, USA) with a measured amount of In_2Tf, followed by an overnight digestion using 2 mL of freshly prepared HNO_3/H_2O_2 mixture (3:1, v:v). Rhodium (Inorganic Ventures, Christiansburg, VA, USA) was used as an internal standard and was added to the serum prior to digestion. The digested samples were diluted with deionized water to a final volume of 20 mL. A series of

indium standard solutions (5, 2, 1, 0.5, 0.2, 0.1, 0.05, 0.02, 0.01, and 0 ppb) containing 10% HNO_3/H_2O_2 and spiked with internal standard were prepared before each experiment. All ICP MS measurements were carried out using a NexION 300X ICP mass spectrometer (PerkinElmer, Waltham, MA, USA).

3.2.3 Animal Models

Experiments were carried out at the animal facilities of the University of Massachusetts, Amherst, on 10-week-old male Wistar rats purchased from Charles River Laboratories (Wilmington, MA, USA). All In_2Tf samples were buffer-exchanged into 100 mM sterilized PBS buffer solution prior to injections. Rats were euthanized by CO_2 overdose 24 hours after the intravenous injection of 7.5 mg/kg dose of body weight of In_2Tf. Blood samples were collected in heparin coated tube to prevent coagulation. Organs of interest were harvested, rinsed in PBS, dried, weighed, and stored in a –80°C freezer.

3.2.4 Imaging LA-ICP MS

Organs of rats were embedded in Tissue-Tek O.C.T. compound (Sakura Finetek USA, Torrance, CA) and cryocut at –20°C into slices of 20 μm thickness with a LEICA CM1850 cryostat (Leica Microsystems GmbH, Wetzlar, Germany). The slices were placed on regular glass slides and air dried. Experiments were conducted with a CETAC LSX-213 G2 laser ablation system (Lincoln, NE, USA) coupled to the NexION 300X ICP mass spectrometer (vide supra). LA unit was synchronized with the ICP MS in external triggering mode. Organ sections were inserted into the cell and ablated line by line.

Elemental images were reconstructed using ImageJ, an open source image generator software (http://rsbweb.nih.gov/ij/), following the extraction and compilation of individual element list of pixels from raw data files, each of which was acquired from a single ablated line containing signal intensity values for all metals measured *(e.g.,* ^{57}Fe and ^{115}In).

3.3 Results and Discussion

3.3.1 Evaluation of Nickel as a Tracer of Recombinant Tf and Tf-Based Products

The recombinant form of Tf used in our work had an N-terminal His-tag, a short peptide containing a hexahistidine segment, which is frequently inserted into the wild-type protein sequence to facilitate its purification on Ni columns. Since the His-tag has high affinity to Ni^{2+} ions and at the same time does not participate in Tf interaction with its receptor, it might be considered as a possible location for placing a metal tag for ICP MS detection. Indeed, saturation of Tf solution with molar excess of $NiSO_4$ resulted in attachment of at least one metal ion to each Tf molecule, as evidenced by the disappearance of the Ni-free protein signal from the native ESI mass spectrum and appearance of protein ions, masses of which are consistent with formation of Ni adducts (Figure 3-1). Importantly, binding with nickel did not lead to a conformational change, as no high charge density ions (below *m/z* 3,000) were detected.

However, the ability of recombinant Tf to bind Ni^{2+} ions does not guarantee that this metal could be a reliable tracer of this protein in biological samples: should this metal be removed from Tf while in circulation by various scavengers, all information on

Tf distribution obtained by tracing Ni as a tracer using ICP MS would be meaningless. The stability of the Ni adducts of Fe_2Tf was evaluated by incubating Ni-saturated Fe_2Tf with equal amount of albumin, the principal nickel binding protein *in vivo* (206). Native ESI MS spectra acquired post-incubation provide unequivocal evidence that the majority of Ni^{2+} ions are readily removed from the His-Tag of recombinant Tf by albumin (Figure 3-1 inset, top trace), indicating that this metal cannot be used as a reliable tracer of Tf *in vivo*.

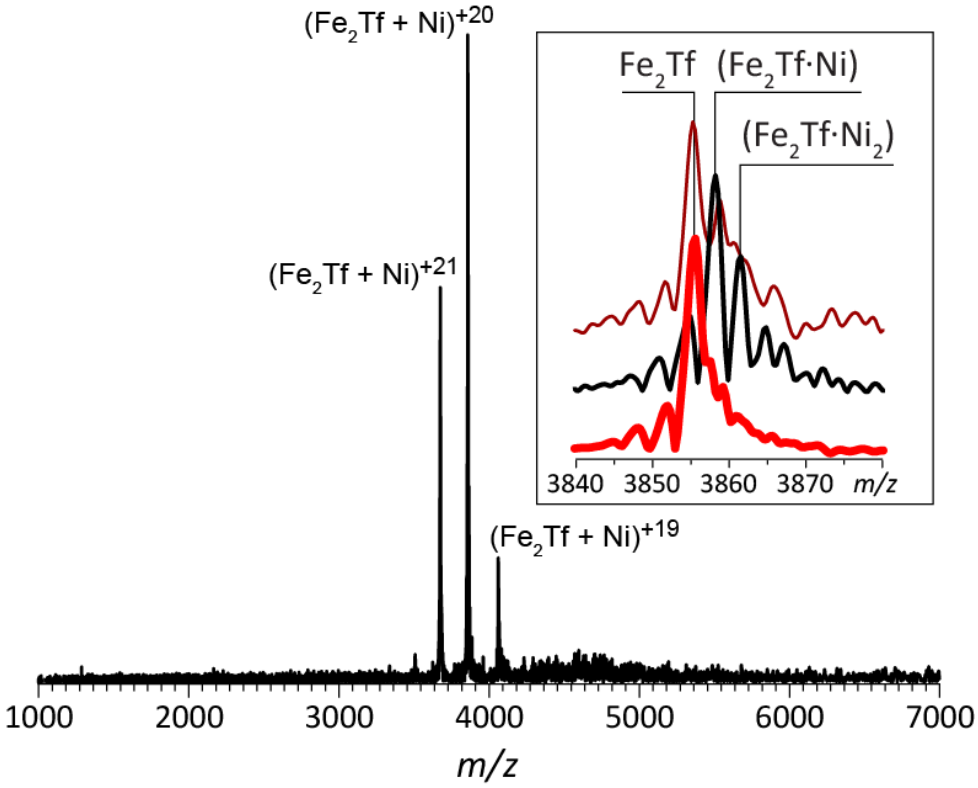

Figure 3-1 ESI mass spectrum of recombinant iron-saturated Tf incubated with $NiSO_4$. The inset shows ESI mass spectra of Tf before (red trace) and after (207) incubation with $NiSO_4$. The top trace shows the result of adding albumin to the solution of Tf incubated with $NiSO_4$. All mass spectra were acquired at near-physiological conditions (pH 7.5, 20 mM ammonium acetate). Only ion peaks at charge state +20 are shown for clarity.

3.3.2 Evaluation of Nonferrous Metals Associating with the Protein at the Iron Binding Sites: Gallium and Indium

Unlike nickel, which readily binds to iron-saturated Tf at the His-tag segment, a variety of metals can associate with the apo-form of Tf at the iron-binding sites (204). Indium and gallium in particular are known to have significant Tf affinity comparable to iron (204), and endogenous Tf has been implicated in transporting radioactive isotopes of these metals used in medicine as imaging agents (25). Although many other metals can form stable complexes with Tf, the significant difference in their ionic radii and that of Fe^{3+} results in significant distortions of the closed conformation of Tf (102,208), which is likely to have a pronounced influence on its receptor binding properties. Since our goal here is to design tracers of Tf and Tf-based therapeutics that would adequately reflect their biodistribution, we limited our search to In^{3+} and Ga^{3+} as their physical characteristics are sufficiently close to Fe^{3+} and, therefore, are less likely to alter the receptor binding properties. Preparation of In-saturated Tf at neutral pH results in formation of a complex where association of In^{3+} with each lobe of the protein is also accompanied by binding of a synergistic ion (CO_3^{2-}), mirroring the Fe^{3+} binding to this protein. Contrary to this, binding of only a single Ga^{3+} ion to Tf (accompanied by the synergistic anion) was observed under the identical conditions when Tf solution was saturated with gallium salt. While earlier spectroscopic work provided evidence of Ga/Tf complex formation with 2:1 stoichiometry (209,210), our results are consistent with the previous studies of Ga/Tf complexes using native ESI MS, where only 1:1 complexes were observed (102).

It may be argued that the absence of Ga_2Tf species in native ESI mass spectra could be a consequence of the failure of the metal binding to trigger cleft closure in one of the Tf lobes (which is likely to diminish the protein/metal complex stability in the gas phase, as is the case for Bi/Tf complex (102)). However, even if this is the case, and the Ga_2Tf species are indeed formed in solution but cannot be observed by native ESI MS because one of the protein lobes remains in the open conformation (characteristic of either the apo-form of Tf, or the holo-form of this protein at endosomal pH (211)), the receptor binding characteristics of such putative Ga_2Tf species would deviate from that of Fe_2Tf species, which makes Ga hardly suitable as a Tf tracer. Lastly, the Ga_xTf species are unstable *vis-à-vis* metal replacement in the presence of ferric ion stabilized by low-molecular weight chelators: 1 hour incubation of Ga-saturated Tf in Fe·NTA solution (with 10 times molar excess of Fe·NTA) results in complete displacement of Ga^{3+} ions and formation of diferric transferring, Fe_2Tf (Figure 3-2A). Therefore, should Ga-labeled Tf or Tf-based therapeutic product be exposed to a pool of low-molecular weight iron post-administration, there is a high likelihood that all metal labels will be lost, making it impossible to trace the exogenous Tf using ICP MS-based methods of detection.

Unlike gallium, indium shows vastly improved characteristics *vis-à-vis* Tf binding. First, a dimetal form of indium-saturated Tf (In_2Tf) can be readily prepared with no traces of apo-Tf or In_1Tf. Importantly, indium-saturated Tf also exhibits markedly improved stability when exposed to a pool of low-molecular weight iron *in vitro*: one of the In^{3+} ions remains to be bound to the protein even after 1 hour incubation of In_2Tf in solution of Fe·NTA (10 times molar excess of the latter) with no sign of formation of the

diferric Tf (Figure 3-2B). Lastly, In_2Tf is still capable of binding to transferrin receptor (TfR) with high affinity, as is evident from the mass spectrum of the In_2Tf/TfR mixture acquired under near-native conditions (Figure 3-3). The only two ionic species present in solution correspond to the free protein (which was present in slight excess) and its 2:1 complex with the receptor with no detectable signal corresponding to either free receptor or 1:1 In_2Tf/TfR complex.

While the ability of Tf to retain at least one bound In^{3+} ion even in the presence of a large pool of low-molecular weight iron is critical for the ability to track metal-labeled Tf in biological fluids and tissues, exchange of even a single In^{3+} ion from In_2Tf for ferric ion may create a pool of low-molecular weight indium (not associated with Tf), leading to false-positive signals if indium is used as a Tf reporter. Although one might expect that low-molecular weight indium should be removed from circulation very effectively by passing through the glomerular filters (in which case no false-positive signal would be generated), the circulation lifetime of indium not associated with Tf might be significantly increased as a result of binding to scavenger proteins (such as albumin), which would make quick passage through kidneys unlikely. In order to find ways to increase the stability of In_2Tf, we explored the utility of oxalate as an alternative synergistic anion. Oxalate has been shown in the past to increase iron affinity of Tf to a very significant extent (55,101,212), although its influence on stabilizing Tf complexes with nonferric metals remains unknown. We investigated the ability of oxalate to "lock" In^{3+} within Tf and prevent its exchange with low-molecular weight iron by preparing In_2Tf in which both carbonates acting as synergistic anions were replaced with oxalate

anions (see the Materials and Methods section for detail). The resulting complex $(In^{3+}C_2O_4^{2-})_2Tf$ was found to be remarkably stable with respect to metal retention, showing no signs of indium-to-iron exchange after 1 hour incubation in a pool of low-molecular weight iron (Figure 3-2C).

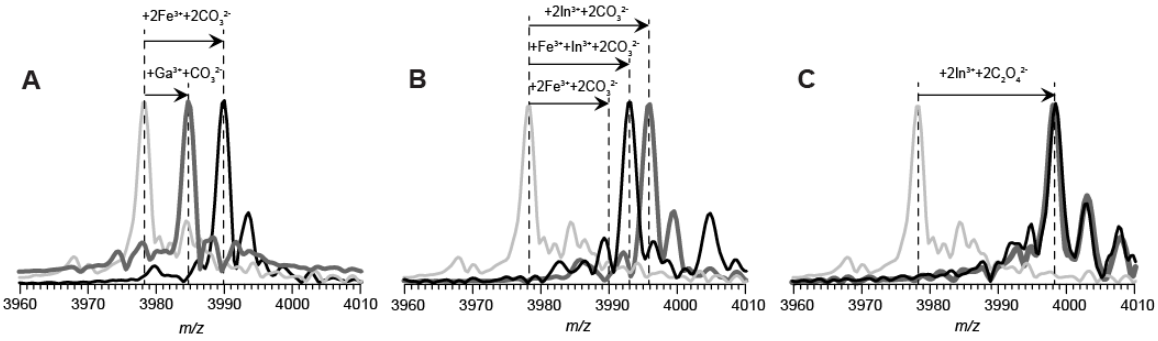

Figure 3-2 Replacement of noncognate metals from Tf by iron: native ESI mass spectra of Ga- (A) and In-saturated Tf (B) incubated with Fe·NTA. Only protein ion peaks at charge state +20 are shown for clarity (gray traces show reference ion peaks of apo-Tf). The effect of replacing carbonate with oxalate as a synergistic anion on metal exchange is shown in (C): In_2Tf ions (charge state +20) in native ESI mass spectra of In-saturated Tf before (gray) and after incubation with Fe·NTA (207).

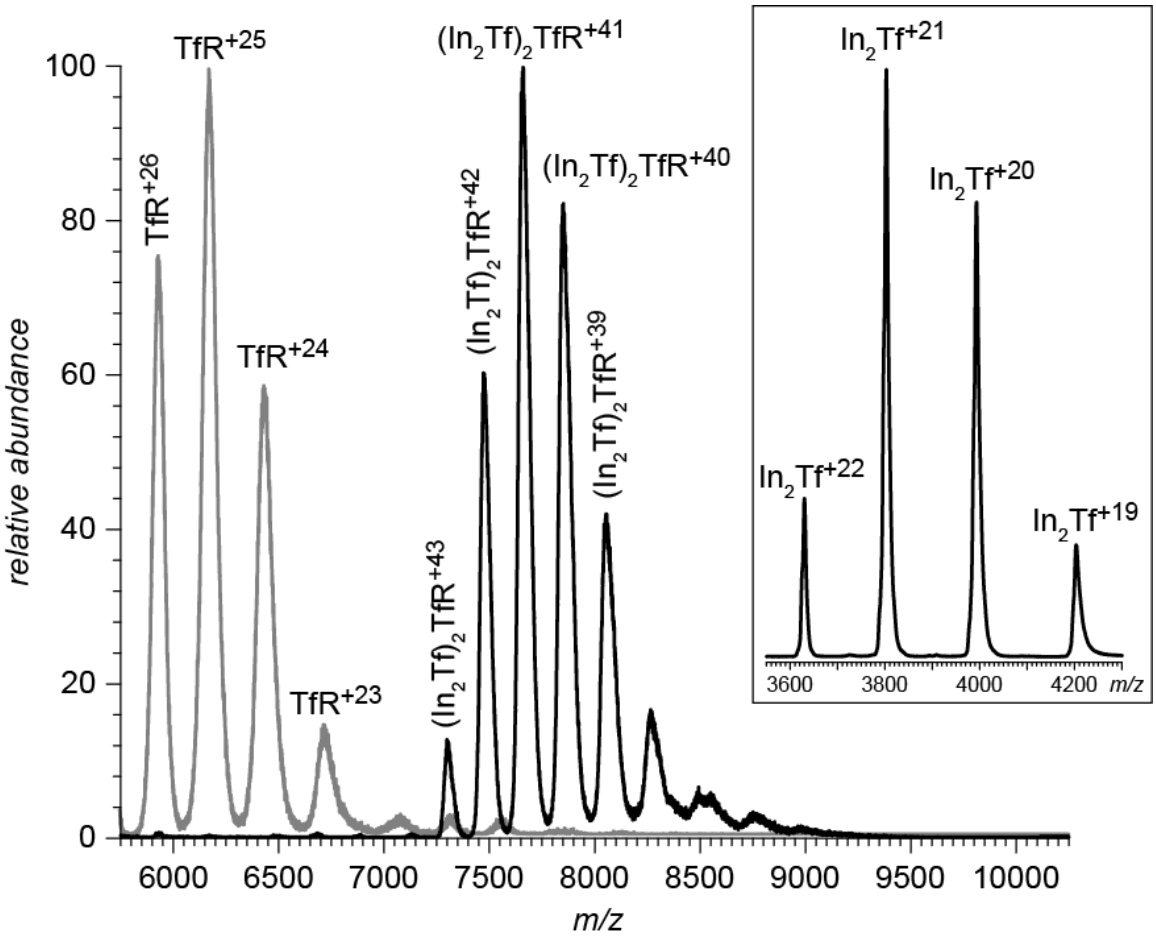

Figure 3-3 Nano-ESI mass spectrum of a mixture of In_2Tf (6 µM) and TfR (3 µM) in 150 mM ammonium acetate at pH 7.5. The gray trace shows the reference spectrum of TfR (acquired in the absence of Tf). Inset show the ionic signal representing the excess of free In_2Tf in solution.

3.3.3 Evaluation of Indium as a Tf Tracer in Biological Samples

Since indium has shown favorable characteristics *vis-à-vis* Tf binding and preserving the receptor recognition properties of this protein, it has been investigated as a tracer of exogenous Tf in biological samples both *in vitro* and *in vivo*. Possible matrix effects were evaluated and the limit of detection was determined by spiking the commercial bovine serum samples with small amounts of In_2Tf solution in 150 mM ammonium acetate, and comparing ICP MS spectra of these samples with the blank

indium-free commercial serum (spiked with 150 mM ammonium acetate solution containing no In-labeled protein). Indium has two stable isotopes (^{113}In and ^{115}In), and the only two metals that can potentially interfere with indium in ICP MS are cadmium and tin. While none of these metals is expected to occur naturally in mammals, heavy metals are frequently present in solvents and reagents (e.g., traces of tin may originate from using stannous chloride $SnCl_2$, a popular pre-reducing agent, in manufacturing commercial reagents used for processing biological samples prior to ICP MS analysis). Indeed, a scan of *m/z* region 50 – 150 by ICP MS reveals a surprising wealth of elements that were not necessarily expected to be detected in serum (Figure 3-4A). Fortunately, tin was found to be the only possible interfering element contributing very low abundance isotopes to ionic signal at *m/z* 113 and 115. The origin of tin was traced to the reagent-grade hydrogen peroxide used for sample digestion (see Figure 3-7 in Supplementary Material for more detail), and it might be possible to eliminate this interfering species from the ICP mass spectra altogether by selecting a higher-quality supplier of this reagent. Short of complete elimination of tin from the reagents, a correction to the intensities of ^{113}In and ^{115}In can be readily made based on the known abundance distribution of tin isotopes and the intensity of ^{116}Sn, ^{117}Sn, and other high-abundance tin isotopes in the ICP mass spectrum.

The signal for the most abundant indium isotope (^{115}In) was clearly discernible in the ICP mass spectrum of In_2Tf-spiked commercial serum sample where the final concentration of indium was as low as 0.01 ppb (corresponding to 0.04 nM protein concentration). A calibration curve for indium in serum constructed using rhodium as an

internal standard (Figure 3-4B) shows excellent linearity (R^2 > 0.99) up to 5 ppb, suggesting that In-labeling can be used for sensitive detection and quantitation of exogenous Tf and Tf-based therapeutics in biological fluids and tissue homogenates.

Measuring indium concentration in blood, cerebrospinal fluid, and other biological fluids following administration of Tf-based therapeutics labeled with this metal will be invaluable for obtaining reliable pharmacokinetic profiles of these protein drugs. However, a detailed picture of biodistribution of Tf-based therapeutics cannot be reconstructed from the average concentrations of indium in tissue homogenates, where all information on uneven distribution of the protein therapeutic across organ tissues would be lost during the homogenization process. However, biodistribution patterns of metals in organ cross-sections can be obtained by combining ICP MS with laser ablation (LA) (145), a technique that emerged in the past several years as a powerful tool to probe distribution of biometals in various tissues (213). In order to assess the feasibility of using LA-ICP MS as a means of obtaining biodistribution patterns of Tf-based therapeutics in tissues, a metal distribution map was generated for a cross-section of rat spleen harvested twenty-four hours after the injection of 2.5 mg of In_2Tf. The medium-resolution distribution maps of iron (^{57}Fe) and indium (^{115}In) differ significantly in absolute intensities, but the distribution patterns are very similar (Figure 3-5), suggesting that the sensitivity provided by LA-ICP MS is adequate for mapping biodistribution of Tf-based therapeutics under clinically relevant conditions.

While detection and quantitation of proteins (including biopharmaceuticals) in biological fluids can be carried out using commonly accepted approaches relying on

introducing isotopic labels (e.g., ^{18}O) either at the peptide (195) or the whole protein level (196), application of these procedures to Tf-based therapeutics is problematic because of the presence of very abundant endogenous protein, the amino acid sequence of which is very similar if not identical to that of the exogenous Tf. Therefore, the ability to selectively detect and quantitate exogenous protein will hinge on the ability to detect a proteolytic fragment unique to that protein, but absent from endogenous Tf. An alternative strategy would take advantage of a non-native segment within the recombinantly produced exogenous protein (such as a His-tag) to afford selective capture of that protein (197). However, even in these circumstances, we have found that the sensitivity afforded by ICP MS measurements of In_2Tf exceeds that of the commonly accepted techniques combining ^{18}O labeling and LC/MS detection by at least factor of three.

The advantages provided by indium labeling and ICP MS detection are even more significant when it comes to measuring biodistribution patterns of Tf-based biopharmaceuticals. While molecular imaging with MALDI MS (214) can produce protein distribution patterns in tissue cross-sections, the size of Tf places it outside of the mass range amenable to direct detection with MALDI TOF MS, and requires *in situ* digestion to be carried out prior to imaging (215). The very low levels of exogenous Tf in tissues under clinically relevant conditions and the presence of abundant endogenous Tf are very likely to prevent successful utilization of traditional MALDI MS imaging for characterization of biodistribution of Tf-based therapeutics in animal tissues.

Finally, indium labeling provides a possibility to multiplex the measurements, another very important advantage for both Tf quantitation and imaging studies. Although in this work all measurements were based on the intensity of ^{115}In, both stable isotopes of this metal are available commercially, and it is possible to produce and co-inject isotope-coded variants of Tf-based therapeutics and selectively track them in a single animal.

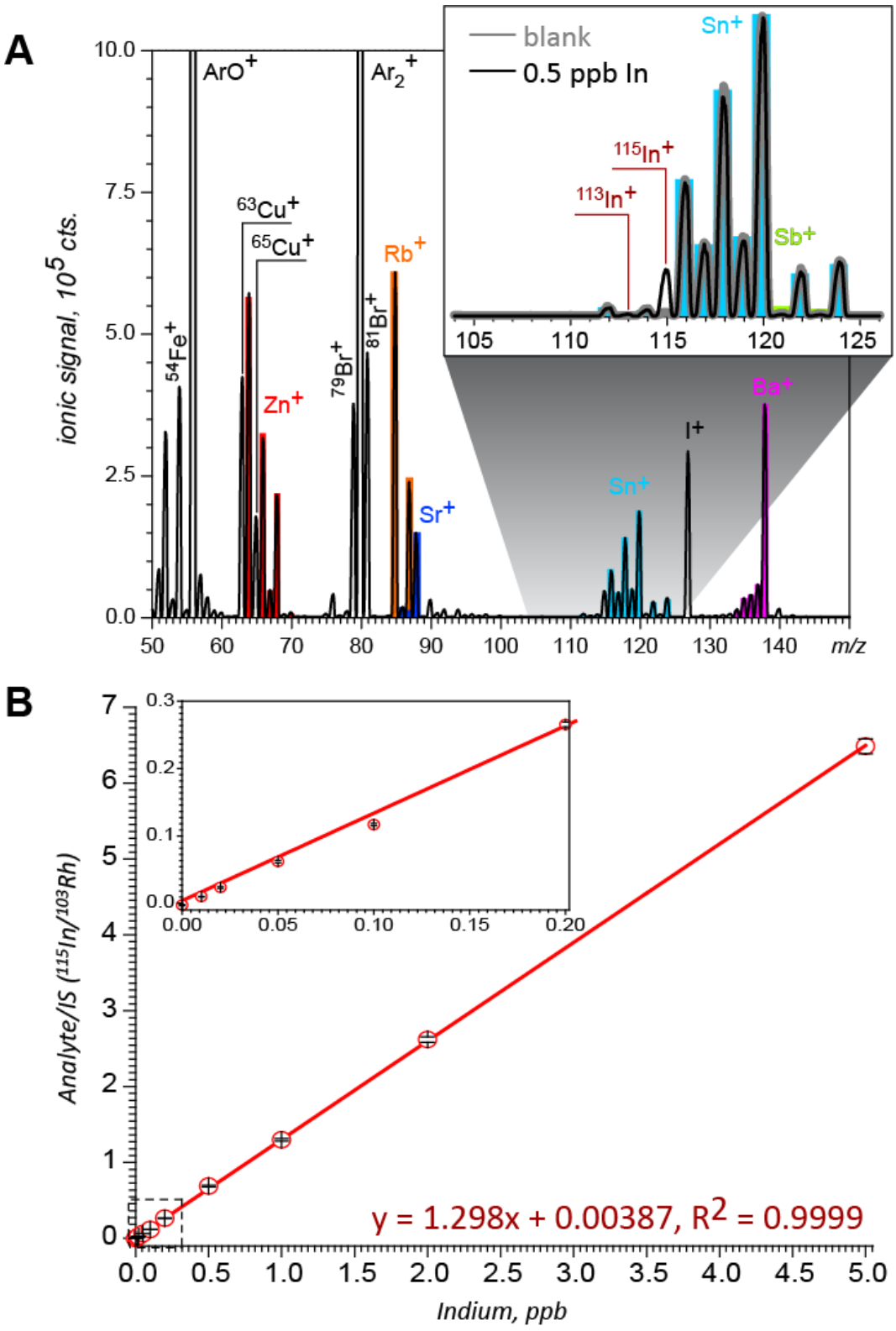

Figure 3-4 (A) ICP mass spectrum of bovine serum spiked with In_2Tf in 150 mM ammonium acetate (to a total indium concentration of 0.5 ppb). The inset shows a

zoomed view of the *m/z* region 104-126 for the spiked sample (black trace) and the blank (indium-free serum sample, gray trace) normalized to the intensity of ^{120}Sn signal. Colored bars represent natural isotopic distributions of select elements (labeled with the same color). (B) Calibration curve for indium (^{115}In) in serum obtained with rhodium as an internal standard. The inset is a zoomed view of the calibration curve below 0.2 ppb of indium.

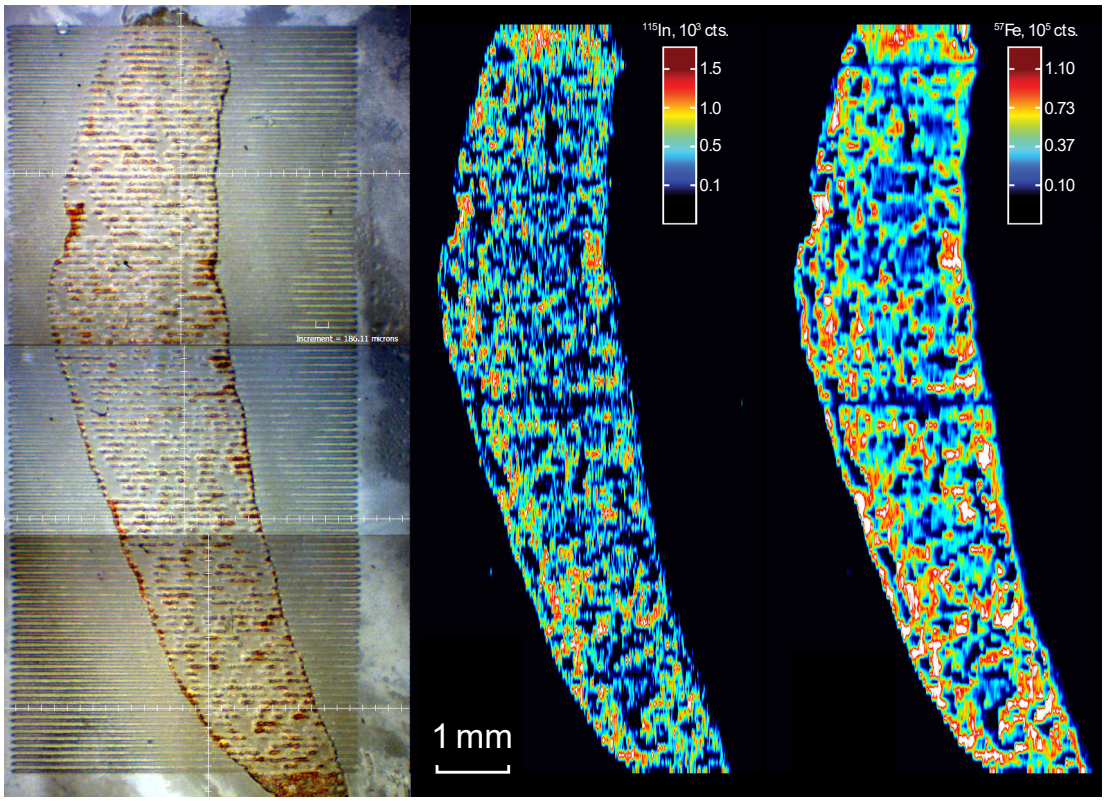

Figure 3-5 LA-ICP MS imaging of iron (^{57}Fe) and indium (^{115}In) distribution in the cross-section of spleen harvested from a rat 24 hours after the injection of In_2Tf. Shown on the left is a photograph of the spleen cross-section following completion of the imaging work with laser-etched lines.

3.4 Conclusion

The spectacular progress in the field of ICP MS in the past decade enabled probing of biometals (such as metals associated with proteins) in biological samples at unprecedented levels of detail, including sensitive detection and quantitation as well as spatially resolved measurements (2D-imaging) in tissues. Tf is a ferroprotein that is used

as a delivery vehicle in a range of therapies that are currently under development, and availability of a reliable analytical method to trace exogenous Tf in various biological samples would be a boon to the drug development efforts. While the cognate metal (iron) is hardly suitable for the role of Tf tracer due to its high abundance in all living organisms, it can be replaced with nonferrous metals, some of which can be used as Tf tracers. Numerous ESI MS-based methods have been developed in the past two decades to probe protein/metal complexes at a variety of levels (58,212,216-220), and many of these techniques have been used here to investigate three metals (Ni, Ga, and In) as potential tracers of Tf. One of them (In) has been found to be ideally suited for this role, as it binds strongly to both lobes of Tf, and allows the latter to retain its receptor-binding properties. Absence of strong interferences in ICP mass spectra allows indium to be detected with high sensitivity in complex biological matrices, enabling both quantitation of In_2Tf in biological fluids and tissue homogenates, and imaging of this protein in organ cross-sections. Although this work focuses on intact Tf (rather than Tf/drug conjugates), a follow-up paper will present the results of studies of biodistribution of a Tf-based antimicrobial agent (a Tf/bacteriolytic enzyme conjugate (34)) designed to target infections on the central nervous systems that are shielded from many antibiotics by a blood-brain barrier.

Further studies will be needed to determine if other nonferrous metals from the extensive list of Tf binders (204,221) as well as iron isotopes (222-224) can be used as tracers of this protein. Expanding the repertoire of Tf tracers will enable multiplexing in biodistribution studies of exogenous Tf and Tf-based therapies. Above and beyond Tf,

the strategy outlined in this work may also be used to facilitate pharmacokinetic and biodistribution studies of other drug candidates that utilize metalloproteins as vehicles for targeted delivery (such as the hemoglobin/haptoglobin complex (225)).

3.5 Supplementary Material

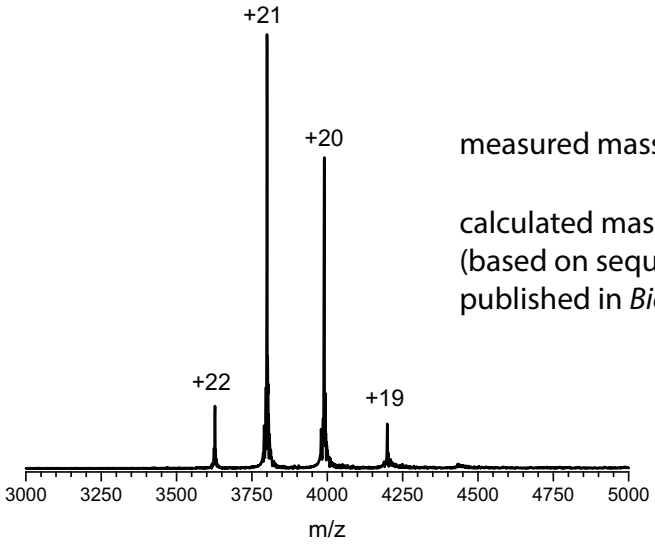

Figure 3-6 ESI mass spectrum of diferric human transferrin.

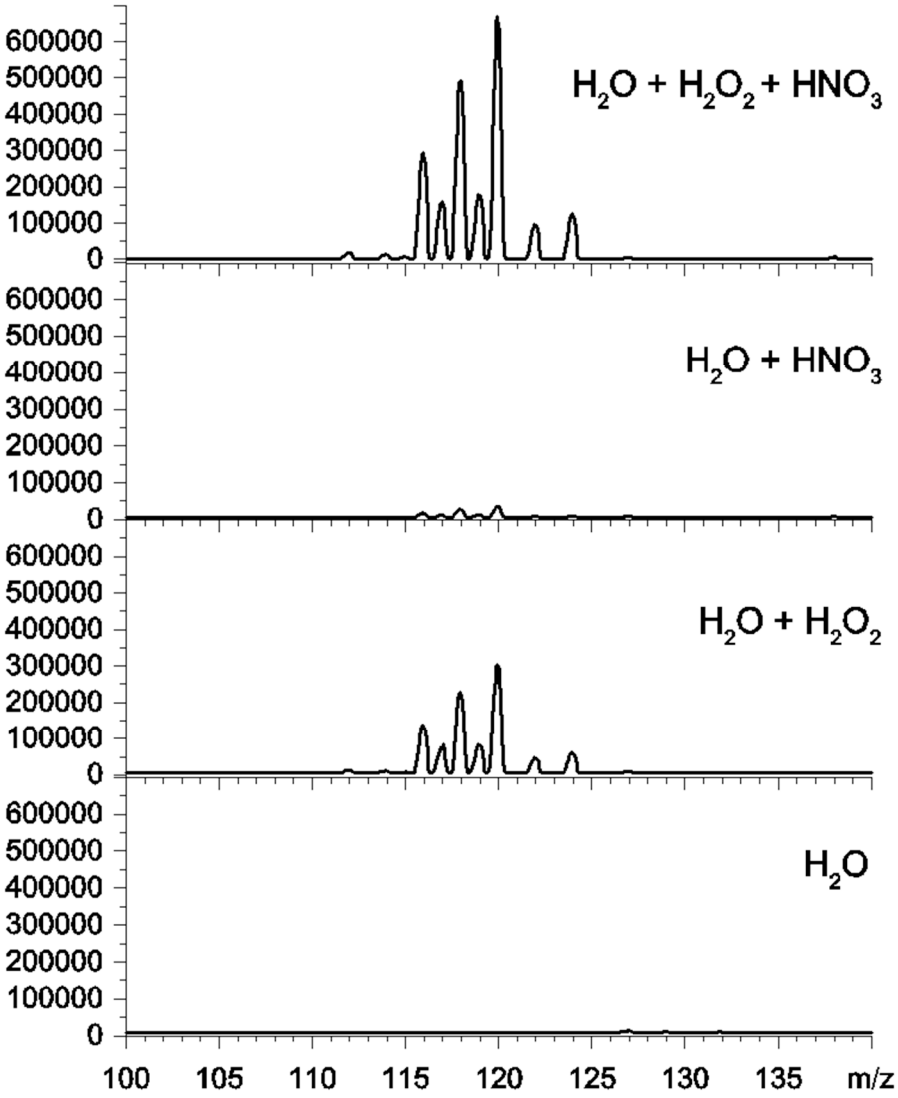

Figure 3-7 ICP mass spectra of solvents and reagents used in this work for quantitation of In-labeled Tf in biological fluids.

CHAPTER 4

CONCLUSIONS AND FUTURE DIRECTIONS

Mass spectrometry has become a powerful tool in proteomics for the studies of protein characterization, quantitation, modifications and protein/protein interactions. MS methods are also being developed to determine both higher order structure and the dynamics of proteins as well as protein complexes, which successfully complement other biophysical techniques, such as X-ray crystallography and NMR spectroscopy. In this work, we use several MS-based methods to investigate the biodistribution of Tf and characterize the molecular mechanism of the Tf/TfR system for the final purpose of devising highly efficient and selective Tf-drug delivery systems. The outcome of this work is:

(i) TfR conformational dynamics and its interactions with different forms of Tf have been investigated in this work by HDX MS. The functional significance of the conformational changes in TfR is described as its direct participation in the Tf binding and internalization and iron release. Analyzing the HDX protection patterns within TfR using several Tf/TfR models that mimic various stages encountered during endocytosis reveals a number of unique aspects of the conformational dynamics of TfR in the neutral and acidic pH that impact Tf binding properties. Binding with holoTf at pH 7.5 induces a movement at the TfR/TfR dimer interface and stabilizes the apical domain. Decreasing the pH to 5.5, the pH-induced conformational changes within the helical domain of TfR trigger a chain reaction that stabilize the C-lobe of Tf in an open conformation. The conformational change at Trp528 in the protease-like domain influences the position of

the Tf bridge whereby further accommodates Tf clefts opening. Moreover, site-specific interactions of Tf C1/TfR are characterized at both pH 7.5 and 5.5, responsible for its pH-dependent Tf binding preference.

The current sequence coverage is about 81% and this number is expected to increase due to the possibility of identifying the glycopeptides with their characteristic neutral mass loss (226). In addition, utilizing ion mobility separation which adds a structure-based separation to the measurements could also improve the ion signal sensitivity and enhance peptide ion identification. To further characterize the detailed site-specific Tf binding sites on TfR, higher resolution HDX MS/MS measurements with electron capture dissociation (ECD) or electron transfer dissociation (ETD) fragmentation using low HD scrambling instrument parameters (227) will be used to study the conformational dynamics of certain peptides of interest located at the Tf/TfR interface region at the amino acid resolution level. Obtaining such high spatial resolution backbone-amide protection map allows us to better understand the interactions between Tf/TfR that lead to stabilizing apoTf at acidic condition. Moreover, the presence of noncanonical states of Tf (211,212) might be also critical to the binding ability of TfR with apoTf at neutral pH and with holoTf at endosomal pH. This assumption will be evaluated by characterizing the receptor binding affinity orders of wild type Tf, Tf variants and non-canonical states of Tf at both neutral and endosomal pH levels by direct ESI MS. Although this work is more focused on investigating the conformation and dynamics of TfR, following experiments need to characterize the changes on different forms of Tf at neutral and endosomal pH to better understand the

Tf/TfR binding properties and the roles of iron release in the presence of TfR. Furthermore, in order to successfully design a rational drug delivery strategy, we need to further understand the properties of the therapeutic drug-Tf conjugates and their interactions with TfR by investigating whether the drug-Tf would affect the receptor binding properties and how do Tf and/or TfR modulate the drug in the endosome.

(ii) A new method, using indium as a potential tracer of Tf with ICP MS detection, is developed to quantitate the exogenous Tf in multiple biological fluids and tissues at picomol level. With this method, the exogenous Tf has been successfully detected and quantified in rat CSF after intravenous injection. Moreover, by applying LA-ICP MS, we are able to investigate the biodistribution of the exogenous Tf at the cellular level.

However, it should be noticed that the volume of CSF in the rat brain is only approximately 90 µL (228), and normally the amount of the fluid collected is much less than this. It is a challenge to collect enough CSF fluid without blood contamination. To avoid a false-positive result and confidently investigate the exogenous Tf in rat CSF rather than from the blood during sample collection process, mercury labeled rat albumin could be used as an indicator of the contamination of blood in CSF, as the albumin is only synthesized extrathecally (229). Rat albumin contains one free sulfhydryl group. Our preliminary study demonstrates that the mercury labeled albumin can be synthesized using *p*-hydroxymercuribenzoic acid (pHMB), a labeling reagent which is well-known to form covalent bonds to SH groups of peptide or proteins (Figure 4-1 and Figure 4-2B). By co-injecting the mercury labeled rat albumin with the indium labeled rat Tf into the rat, any mercury signal detected by ICP MS in the CSF sample could flag the

contamination of blood. Furthermore, this method can be further extended to study the biodistribution of the Tf-drug conjugates designed to target tumors (17) and CNS disorders (230). In addition, this method can provide a possibility to enable multiplexing by utilizing multiple metal ions (204) or isotopes (222-224) as tracers, so that different versions of Tf and Tf-based therapies can be analyzed simultaneously. For example, our group recently demonstrates the feasibility of using ruthenium as a protein tracer which can stably bind to the His-tag segment of a recombinant Tf without interfering the receptor binding ability (231). When selecting an acceptable Tf tracer, the behavior of the metal-Tf complex under conditions mimicking the endosomal environment (where the release of iron occurs) should be also considered, as the integrity of the complex should not be compromised (232). Above and beyond Tf, the strategy outlined in this work may also be applied to investigate the biodistribution of other metalloprotein-based drug systems (such as the hemoglobin/haptoglobin complex (233)).

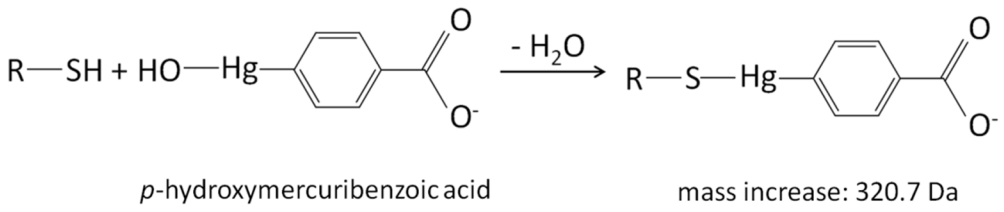

Figure 4-1 The mercury labeling strategy is using *p*-hydroxymercuribenzoic acid (pHMB) as a labeling reagent, follows the potential labeling of free sulfhydryl groups derived from cysteines ubiquitously present in protein.

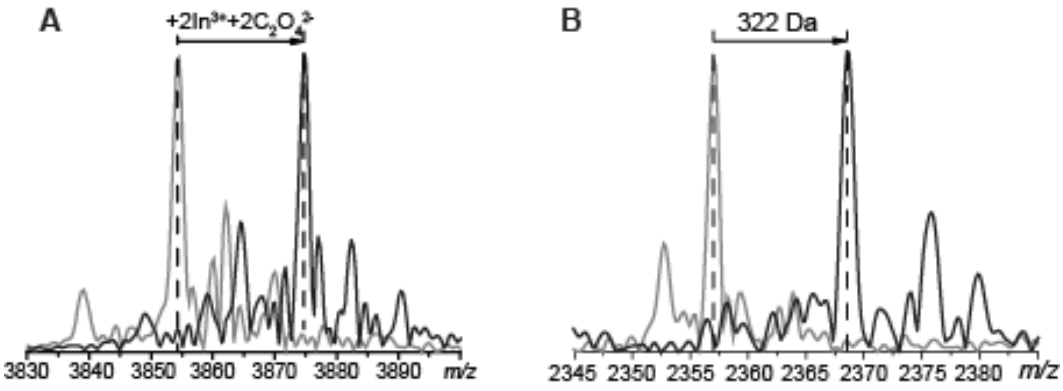

Figure 4-2 ESI MS spectra of (A) rat Tf labeling with indium and (B) rat serum albumin labeling with pHMB. Only protein ion peaks at charge state +20 for indium-Tf (A) and at charge state +28 for mercury-albumin labeling (B) are shown for clarity. Gray trace in each spectrum shows the reference ion peak of apo-protein. The theoretical mass increase of pHMB labeling is 320.7 Da.

BIBLIOGRAPHY

1. Goeddel, D. V.,Kleid, D. G.,Bolivar, F.,Heyneker, H. L.,Yansura, D. G.,Crea, R.,Hirose, T.,Kraszewski, A.,Itakura, K.,Riggs, A. D.: Expression in Escherichia coli of chemically synthesized genes for human insulin. Proc Natl Acad Sci U S A. 76, 106 (1979)

2. Lagasse, H. A.,Alexaki, A.,Simhadri, V. L.,Katagiri, N. H.,Jankowski, W.,Sauna, Z. E.,Kimchi-Sarfaty, C.: Recent advances in (therapeutic protein) drug development. F1000Res. 6, 113 (2017)

3. Usmani, S. S.,Bedi, G.,Samuel, J. S.,Singh, S.,Kalra, S.,Kumar, P.,Ahuja, A. A.,Sharma, M.,Gautam, A.,Raghava, G. P. S.: THPdb: Database of FDA-approved peptide and protein therapeutics. PLoS One. 12, e0181748 (2017)

4. Perez, J. H.,Branch, W. J.,Smith, L.,Mullock, B. M.,Luzio, J. P.: Investigation of endosomal compartments involved in endocytosis and transcytosis of polymeric immunoglobulin A by subcellular fractionation of perfused isolated rat liver. Biochem J. 251, 763 (1988)

5. Fishman, J. B.,Rubin, J. B.,Handrahan, J. V.,Connor, J. R.,Fine, R. E.: Receptor-mediated transcytosis of transferrin across the blood-brain barrier. J Neurosci Res. 18, 299 (1987)

6. Golden, P. L.,Maccagnan, T. J.,Pardridge, W. M.: Human blood-brain barrier leptin receptor. Binding and endocytosis in isolated human brain microvessels. J Clin Invest. 99, 14 (1997)

7. Ke, W.,Shao, K.,Huang, R.,Han, L.,Liu, Y.,Li, J.,Kuang, Y.,Ye, L.,Lou, J.,Jiang, C.: Gene delivery targeted to the brain using an Angiopep-conjugated polyethyleneglycol-modified polyamidoamine dendrimer. Biomaterials. 30, 6976 (2009)

8. Daniels, T. R.,Bernabeu, E.,Rodriguez, J. A.,Patel, S.,Kozman, M.,Chiappetta, D. A.,Holler, E.,Ljubimova, J. Y.,Helguera, G.,Penichet, M. L.: The transferrin receptor and the targeted delivery of therapeutic agents against cancer. Biochim Biophys Acta. 1820, 291 (2012)

9. Dufes, C.,Al Robaian, M.,Somani, S.: Transferrin and the transferrin receptor for the targeted delivery of therapeutic agents to the brain and cancer cells. Ther Deliv. 4, 629 (2013)

10. Tortorella, S.,Karagiannis, T. C.: Transferrin receptor-mediated endocytosis: a useful target for cancer therapy. J Membr Biol. 247, 291 (2014)

11. Fillet, G.,Beguin, Y.: Monitoring of erythropoiesis by the serum transferrin receptor and erythropoietin. Acta Clin Belg. 56, 146 (2001)

12. Li, H.,Qian, Z. M.: Transferrin/transferrin receptor-mediated drug delivery. Med Res Rev. 22, 225 (2002)

13. Ryschich, E.,Huszty, G.,Knaebel, H. P.,Hartel, M.,Buchler, M. W.,Schmidt, J.: Transferrin receptor is a marker of malignant phenotype in human pancreatic cancer and in neuroendocrine carcinoma of the pancreas. Eur J Cancer. 40, 1418 (2004)

14. Prutki, M.,Poljak-Blazi, M.,Jakopovic, M.,Tomas, D.,Stipancic, I.,Zarkovic, N.: Altered iron metabolism, transferrin receptor 1 and ferritin in patients with colon cancer. Cancer Lett. 238, 188 (2006)

15. Ponka, P.,Lok, C. N.: The transferrin receptor: role in health and disease. Int J Biochem Cell Biol. 31, 1111 (1999)

16. Wang, J.,Tian, S.,Petros, R. A.,Napier, M. E.,Desimone, J. M.: The complex role of multivalency in nanoparticles targeting the transferrin receptor for cancer therapies. Journal of the American Chemical Society. 132, 11306 (2010)

17. Daniels, T. R.,Delgado, T.,Helguera, G.,Penichet, M. L.: The transferrin receptor part II: targeted delivery of therapeutic agents into cancer cells. Clin Immunol. 121, 159 (2006)

18. Blumling Iii, J. P.,Silva, G. A.: Targeting the brain: advances in drug delivery. Curr Pharm Biotechnol. 13, 2417 (2012)

19. Xiao, G.,Gan, L. S.: Receptor-mediated endocytosis and brain delivery of therapeutic biologics. Int J Cell Biol. 2013, 703545 (2013)

20. Head, J. F.,Wang, F.,Elliott, R. L.: Antineoplastic drugs that interfere with iron metabolism in cancer cells. Adv Enzyme Regul. 37, 147 (1997)

21. Kato, M.,Kamiyama, H.,Okazaki, A.,Kumaki, K.,Kato, Y.,Sugiyama, Y.: Mechanism for the nonlinear pharmacokinetics of erythropoietin in rats. J Pharmacol Exp Ther. 283, 520 (1997)

22. Biessen, E. A.,van Teijlingen, M.,Vietsch, H.,Barrett-Bergshoeff, M. M.,Bijsterbosch, M. K.,Rijken, D. C.,van Berkel, T. J.,Kuiper, J.: Antagonists of the mannose receptor and

the LDL receptor-related protein dramatically delay the clearance of tissue plasminogen activator. Circulation. 95, 46 (1997)

23. Li, H.,Sun, H.,Qian, Z. M.: The role of the transferrin-transferrin-receptor system in drug delivery and targeting. Trends Pharmacol Sci. 23, 206 (2002)

24. De Domenico, I.,McVey Ward, D.,Kaplan, J.: Regulation of iron acquisition and storage: consequences for iron-linked disorders. Nat Rev Mol Cell Biol. 9, 72 (2008)

25. Kratz, F.,Elsadek, B.: Clinical impact of serum proteins on drug delivery. J Control Release. 161, 429 (2012)

26. Vincent, J. B.,Love, S.: The binding and transport of alternative metals by transferrin. Biochim Biophys Acta. 1820, 362 (2012)

27. Ha-Duong, N. T.,Hemadi, M.,Chikh, Z.,Chahine, J. M.: Kinetics and thermodynamics of metal-loaded transferrins: transferrin receptor 1 interactions. Biochem Soc Trans. 36, 1422 (2008)

28. Wiley, D. T.,Webster, P.,Gale, A.,Davis, M. E.: Transcytosis and brain uptake of transferrin-containing nanoparticles by tuning avidity to transferrin receptor. Proc Natl Acad Sci U S A. 110, 8662 (2013)

29. Yu, Y. J.,Watts, R. J.: Developing therapeutic antibodies for neurodegenerative disease. Neurotherapeutics. 10, 459 (2013)

30. Bien-Ly, N.,Yu, Y. J.,Bumbaca, D.,Elstrott, J.,Boswell, C. A.,Zhang, Y.,Luk, W.,Lu, Y.,Dennis, M. S.,Weimer, R. M.,Chung, I.,Watts, R. J.: Transferrin receptor (TfR) trafficking determines brain uptake of TfR antibody affinity variants. J Exp Med. 211, 233 (2014)

31. Zhang, Y.,Pardridge, W. M.: Rapid transferrin efflux from brain to blood across the blood-brain barrier. J Neurochem. 76, 1597 (2001)

32. Luck, A. N.,Mason, A. B.: Structure and dynamics of drug carriers and their interaction with cellular receptors: focus on serum transferrin. Adv Drug Deliv Rev. 65, 1012 (2013)

33. Paterson, J.,Webster, C. I.: Exploiting transferrin receptor for delivering drugs across the blood-brain barrier. Drug Discov Today Technol. 20, 49 (2016)

34. Nguyen, S. N.,Bobst, C. E.,Kaltashov, I. A.: Mass spectrometry-guided optimization and characterization of a biologically active transferrin-lysozyme model drug conjugate. Mol Pharm. 10, 1998 (2013)

35. Kaltashov, I. A.,Bobst, C. E.,Nguyen, S. N.,Wang, S.: Emerging mass spectrometry-based approaches to probe protein-receptor interactions: focus on overcoming physiological barriers. Adv Drug Deliv Rev. 65, 1020 (2013)

36. Feder, J. N.,Gnirke, A.,Thomas, W.,Tsuchihashi, Z.,Ruddy, D. A.,Basava, A.,Dormishian, F.,Domingo, R., Jr.,Ellis, M. C.,Fullan, A.,Hinton, L. M.,Jones, N. L.,Kimmel, B. E.,Kronmal, G. S.,Lauer, P.,Lee, V. K.,Loeb, D. B.,Mapa, F. A.,McClelland, E.,Meyer, N. C.,Mintier, G. A.,Moeller, N.,Moore, T.,Morikang, E.,Prass, C. E.,Quintana, L.,Starnes, S. M.,Schatzman, R. C.,Brunke, K. J.,Drayna, D. T.,Risch, N. J.,Bacon, B. R.,Wolff, R. K.: A novel MHC class I-like gene is mutated in patients with hereditary haemochromatosis. Nat Genet. 13, 399 (1996)

37. Parkkila, S.,Waheed, A.,Britton, R. S.,Bacon, B. R.,Zhou, X. Y.,Tomatsu, S.,Fleming, R. E.,Sly, W. S.: Association of the transferrin receptor in human placenta with HFE, the protein defective in hereditary hemochromatosis. Proc Natl Acad Sci U S A. 94, 13198 (1997)

38. Gross, C. N.,Irrinki, A.,Feder, J. N.,Enns, C. A.: Co-trafficking of HFE, a nonclassical major histocompatibility complex class I protein, with the transferrin receptor implies a role in intracellular iron regulation. J Biol Chem. 273, 22068 (1998)

39. Hemadi, M.,Kahn, P. H.,Miquel, G.,El Hage Chahine, J. M.: Transferrin's mechanism of interaction with receptor 1. Biochemistry. 43, 1736 (2004)

40. Lambe, T.,Simpson, R. J.,Dawson, S.,Bouriez-Jones, T.,Crockford, T. L.,Lepherd, M.,Latunde-Dada, G. O.,Robinson, H.,Raja, K. B.,Campagna, D. R.,Villarreal, G., Jr.,Ellory, J. C.,Goodnow, C. C.,Fleming, M. D.,McKie, A. T.,Cornall, R. J.: Identification of a Steap3 endosomal targeting motif essential for normal iron metabolism. Blood. 113, 1805 (2009)

41. Donovan, A.,Roy, C. N.,Andrews, N. C.: The ins and outs of iron homeostasis. Physiology (Bethesda). 21, 115 (2006)

42. Anderson, G. J.,Frazer, D. M.: Hepatic iron metabolism. Semin Liver Dis. 25, 420 (2005)

43. Sargent, P. J.,Farnaud, S.,Evans, R. W.: Structure/function overview of proteins involved in iron storage and transport. Curr Med Chem. 12, 2683 (2005)

44. Leverence, R.,Mason, A. B.,Kaltashov, I. A.: Noncanonical interactions between serum transferrin and transferrin receptor evaluated with electrospray ionization mass spectrometry. Proc Natl Acad Sci U S A. 107, 8123 (2010)

45. Yoon, D. J.,Chu, D. S.,Ng, C. W.,Pham, E. A.,Mason, A. B.,Hudson, D. M.,Smith, V. C.,MacGillivray, R. T.,Kamei, D. T.: Genetically engineering transferrin to improve its in vitro ability to deliver cytotoxins. J Control Release. 133, 178 (2009)

46. Lambert, L. A.,Perri, H.,Meehan, T. J.: Evolution of duplications in the transferrin family of proteins. Comp Biochem Physiol B Biochem Mol Biol. 140, 11 (2005)

47. Barber, M. F.,Kronenberg, Z.,Yandell, M.,Elde, N. C.: Antimicrobial Functions of Lactoferrin Promote Genetic Conflicts in Ancient Primates and Modern Humans. PLoS Genet. 12, e1006063 (2016)

48. Ward, P. P.,Mendoza-Meneses, M.,Cunningham, G. A.,Conneely, O. M.: Iron status in mice carrying a targeted disruption of lactoferrin. Mol Cell Biol. 23, 178 (2003)

49. Adlerova, L.,Bartoskova, A.,Faldyna, M.: Lactoferrin: a review. Veterinarni Medicina. 53, 457 (2008)

50. Lambert, L. A.: Molecular evolution of the transferrin family and associated receptors. Biochim Biophys Acta. 1820, 244 (2012)

51. Roopenian, D. C.,Akilesh, S.: FcRn: the neonatal Fc receptor comes of age. Nat Rev Immunol. 7, 715 (2007)

52. Aisen, P.,Leibman, A.,Zweier, J.: Stoichiometric and site characteristics of the binding of iron to human transferrin. J Biol Chem. 253, 1930 (1978)

53. Schlabach, M. R.,Bates, G. W.: The synergistic binding of anions and Fe3+ by transferrin. Implications for the interlocking sites hypothesis. J Biol Chem. 250, 2182 (1975)

54. Bates, G. W.,Schlabach, M. R.: The nonspecific binding of Fe3+ to transferrin in the absence of synergistic anions. J Biol Chem. 250, 2177 (1975)

55. Halbrooks, P. J.,Mason, A. B.,Adams, T. E.,Briggs, S. K.,Everse, S. J.: The oxalate effect on release of iron from human serum transferrin explained. J Mol Biol. 339, 217 (2004)

56. Luck, A. N.,Bobst, C. E.,Kaltashov, I. A.,Mason, A. B.: Human serum transferrin: is there a link among autism, high oxalate levels, and iron deficiency anemia? Biochemistry. 52, 8333 (2013)

57. Baldwin, G. S.: Comparison of transferrin sequences from different species. Comp Biochem Physiol B. 106, 203 (1993)

58. Gumerov, D. R.,Mason, A. B.,Kaltashov, I. A.: Interlobe communication in human serum transferrin: metal binding and conformational dynamics investigated by electrospray ionization mass spectrometry. Biochemistry. 42, 5421 (2003)

59. Rinaldo, D.,Field, M. J.: A computational study of the open and closed forms of the N-lobe human serum transferrin apoprotein. Biophys J. 85, 3485 (2003)

60. Dewan, J. C.,Mikami, B.,Hirose, M.,Sacchettini, J. C.: Structural evidence for a pH-sensitive dilysine trigger in the hen ovotransferrin N-lobe: implications for transferrin iron release. Biochemistry. 32, 11963 (1993)

61. Halbrooks, P. J.,He, Q. Y.,Briggs, S. K.,Everse, S. J.,Smith, V. C.,MacGillivray, R. T.,Mason, A. B.: Investigation of the mechanism of iron release from the C-lobe of human serum transferrin: mutational analysis of the role of a pH sensitive triad. Biochemistry. 42, 3701 (2003)

62. McClelland, A.,Kuhn, L. C.,Ruddle, F. H.: The human transferrin receptor gene: genomic organization, and the complete primary structure of the receptor deduced from a cDNA sequence. Cell. 39, 267 (1984)

63. Lawrence, C. M.,Ray, S.,Babyonyshev, M.,Galluser, R.,Borhani, D. W.,Harrison, S. C.: Crystal structure of the ectodomain of human transferrin receptor. Science. 286, 779 (1999)

64. Byrne, S. L.,Leverence, R.,Klein, J. S.,Giannetti, A. M.,Smith, V. C.,MacGillivray, R. T.,Kaltashov, I. A.,Mason, A. B.: Effect of glycosylation on the function of a soluble, recombinant form of the transferrin receptor. Biochemistry. 45, 6663 (2006)

65. Eckenroth, B. E.,Steere, A. N.,Chasteen, N. D.,Everse, S. J.,Mason, A. B.: How the binding of human transferrin primes the transferrin receptor potentiating iron release at endosomal pH. Proc Natl Acad Sci U S A. 108, 13089 (2011)

66. Giannetti, A. M.,Snow, P. M.,Zak, O.,Bjorkman, P. J.: Mechanism for multiple ligand recognition by the human transferrin receptor. PLoS Biol. 1, E51 (2003)

67. Mason, A. B.,Byrne, S. L.,Everse, S. J.,Roberts, S. E.,Chasteen, N. D.,Smith, V. C.,MacGillivray, R. T.,Kandemir, B.,Bou-Abdallah, F.: A loop in the N-lobe of human serum transferrin is critical for binding to the transferrin receptor as revealed by mutagenesis, isothermal titration calorimetry, and epitope mapping. J Mol Recognit. 22, 521 (2009)

68. Verrijt, C. E.,Kroos, M. J.,Huijskes-Heins, M. I.,Cleton-Soeteman, M. I.,van Run, P. R.,van Eijk, H. G.,van Dijk, J. P.: Accumulation and release of iron in polarly and non-polarly cultured trophoblast cells isolated from human term placentas. Eur J Obstet Gynecol Reprod Biol. 86, 73 (1999)

69. Dautry-Varsat, A.,Ciechanover, A.,Lodish, H. F.: pH and the recycling of transferrin during receptor-mediated endocytosis. Proc Natl Acad Sci U S A. 80, 2258 (1983)

70. Giannetti, A. M.,Halbrooks, P. J.,Mason, A. B.,Vogt, T. M.,Enns, C. A.,Bjorkman, P. J.: The molecular mechanism for receptor-stimulated iron release from the plasma iron transport protein transferrin. Structure. 13, 1613 (2005)

71. Lebron, J. A.,Bennett, M. J.,Vaughn, D. E.,Chirino, A. J.,Snow, P. M.,Mintier, G. A.,Feder, J. N.,Bjorkman, P. J.: Crystal structure of the hemochromatosis protein HFE and characterization of its interaction with transferrin receptor. Cell. 93, 111 (1998)

72. Cheng, Y.,Zak, O.,Aisen, P.,Harrison, S. C.,Walz, T.: Structure of the human transferrin receptor-transferrin complex. Cell. 116, 565 (2004)

73. Hall, D. R.,Hadden, J. M.,Leonard, G. A.,Bailey, S.,Neu, M.,Winn, M.,Lindley, P. F.: The crystal and molecular structures of diferric porcine and rabbit serum transferrins at resolutions of 2.15 and 2.60 A, respectively. Acta Crystallogr D Biol Crystallogr. 58, 70 (2002)

74. Wally, J.,Halbrooks, P. J.,Vonrhein, C.,Rould, M. A.,Everse, S. J.,Mason, A. B.,Buchanan, S. K.: The crystal structure of iron-free human serum transferrin provides insight into inter-lobe communication and receptor binding. J Biol Chem. 281, 24934 (2006)

75. Sakajiri, T.,Yamamura, T.,Kikuchi, T.,Yajima, H.: Computational structure models of apo and diferric transferrin-transferrin receptor complexes. Protein J. 28, 407 (2009)

76. Bennett, M. J.,Lebron, J. A.,Bjorkman, P. J.: Crystal structure of the hereditary haemochromatosis protein HFE complexed with transferrin receptor. Nature. 403, 46 (2000)

77. Steere, A. N.,Miller, B. F.,Roberts, S. E.,Byrne, S. L.,Chasteen, N. D.,Smith, V. C.,MacGillivray, R. T.,Mason, A. B.: Ionic residues of human serum transferrin affect binding to the transferrin receptor and iron release. Biochemistry. 51, 686 (2012)

78. Byrne, S. L.,Steere, A. N.,Chasteen, N. D.,Mason, A. B.: Identification of a kinetically significant anion binding (KISAB) site in the N-lobe of human serum transferrin. Biochemistry. 49, 4200 (2010)

79. Lambert, L. A.,Mitchell, S. L.: Molecular evolution of the transferrin receptor/glutamate carboxypeptidase II family. J Mol Evol. 64, 113 (2007)

80. Camaschella, C.,Roetto, A.,Cali, A.,De Gobbi, M.,Garozzo, G.,Carella, M.,Majorano, N.,Totaro, A.,Gasparini, P.: The gene TFR2 is mutated in a new type of haemochromatosis mapping to 7q22. Nature Genetics. 25, 14 (2000)

81. West, A. P., Jr.,Bennett, M. J.,Sellers, V. M.,Andrews, N. C.,Enns, C. A.,Bjorkman, P. J.: Comparison of the interactions of transferrin receptor and transferrin receptor 2 with transferrin and the hereditary hemochromatosis protein HFE. J Biol Chem. 275, 38135 (2000)

82. Kleven, M. D.,Jue, S.,Enns, C. A.: Transferrin Receptors TfR1 and TfR2 Bind Transferrin through Differing Mechanisms. Biochemistry. 57, 1552 (2018)

83. Silver, D. A.,Pellicer, I.,Fair, W. R.,Heston, W. D.,Cordon-Cardo, C.: Prostate-specific membrane antigen expression in normal and malignant human tissues. Clin Cancer Res. 3, 81 (1997)

84. Chang, S. S.,Reuter, V. E.,Heston, W. D.,Bander, N. H.,Grauer, L. S.,Gaudin, P. B.: Five different anti-prostate-specific membrane antigen (PSMA) antibodies confirm PSMA expression in tumor-associated neovasculature. Cancer Res. 59, 3192 (1999)

85. Rajasekaran, A. K.,Anilkumar, G.,Christiansen, J. J.: Is prostate-specific membrane antigen a multifunctional protein? Am J Physiol Cell Physiol. 288, C975 (2005)

86. Rahn, K. A.,Slusher, B. S.,Kaplin, A. I.: Glutamate in CNS neurodegeneration and cognition and its regulation by GCPII inhibition. Curr Med Chem. 19, 1335 (2012)

87. Rajasekaran, S. A.,Anilkumar, G.,Oshima, E.,Bowie, J. U.,Liu, H.,Heston, W.,Bander, N. H.,Rajasekaran, A. K.: A novel cytoplasmic tail MXXXL motif mediates the internalization of prostate-specific membrane antigen. Mol Biol Cell. 14, 4835 (2003)

88. Davis, M. I.,Bennett, M. J.,Thomas, L. M.,Bjorkman, P. J.: Crystal structure of prostate-specific membrane antigen, a tumor marker and peptidase. Proc Natl Acad Sci U S A. 102, 5981 (2005)

89. Mahon, P.,Bateman, A.: The PA domain: a protease-associated domain. Protein Sci. 9, 1930 (2000)

90. Luo, X.,Hofmann, K.: The protease-associated domain: a homology domain associated with multiple classes of proteases. Trends Biochem Sci. 26, 147 (2001)

91. O'Keefe, D. S.,Bacich, D. J.,Huang, S. S.,Heston, W. D. W.: A Perspective on the Evolving Story of PSMA Biology, PSMA-Based Imaging, and Endoradiotherapeutic Strategies. J Nucl Med. 59, 1007 (2018)

92. Helguera, G.,Jemielity, S.,Abraham, J.,Cordo, S. M.,Martinez, M. G.,Rodriguez, J. A.,Bregni, C.,Wang, J. J.,Farzan, M.,Penichet, M. L.,Candurra, N. A.,Choe, H.: An antibody recognizing the apical domain of human transferrin receptor 1 efficiently inhibits the entry of all new world hemorrhagic Fever arenaviruses. J Virol. 86, 4024 (2012)

93. Goodman, L. B.,Lyi, S. M.,Johnson, N. C.,Cifuente, J. O.,Hafenstein, S. L.,Parrish, C. R.: Binding site on the transferrin receptor for the parvovirus capsid and effects of altered affinity on cell uptake and infection. J Virol. 84, 4969 (2010)

94. Montemiglio, L. C.,Testi, C.,Ceci, P.,Falvo, E.,Pitea, M.,Savino, C.,Arcovito, A.,Peruzzi, G.,Baiocco, P.,Mancia, F.,Boffi, A.,des Georges, A.,Vallone, B.: Cryo-EM structure of the human ferritin-transferrin receptor 1 complex. Nat Commun. 10, 1121 (2019)

95. Mesters, J. R.,Barinka, C.,Li, W.,Tsukamoto, T.,Majer, P.,Slusher, B. S.,Konvalinka, J.,Hilgenfeld, R.: Structure of glutamate carboxypeptidase II, a drug target in neuronal damage and prostate cancer. EMBO J. 25, 1375 (2006)

96. Wasinger, V. C.,Cordwell, S. J.,Cerpa-Poljak, A.,Yan, J. X.,Gooley, A. A.,Wilkins, M. R.,Duncan, M. W.,Harris, R.,Williams, K. L.,Humphery-Smith, I.: Progress with gene-product mapping of the Mollicutes: Mycoplasma genitalium. Electrophoresis. 16, 1090 (1995)

97. Aebersold, R.,Mann, M.: Mass spectrometry-based proteomics. Nature. 422, 198 (2003)

98. Anderson, N. L.,Anderson, N. G.: Proteome and proteomics: New technologies, new concepts, and new words. Electrophoresis. 19, 1853 (1998)

99. Kaltashov, I. A.,Abzalimov, R. R.: Do ionic charges in ESI MS provide useful information on macromolecular structure? J Am Soc Mass Spectrom. 19, 1239 (2008)

100. Daniel, J. M.,Friess, S. D.,Rajagopalan, S.,Wendt, S.,Zenobi, R.: Quantitative determination of noncovalent binding interactions using soft ionization mass spectrometry. International Journal of Mass Spectrometry. 216, 1 (2002)

101. Gumerov, D. R.,Kaltashov, I. A.: Dynamics of iron release from transferrin N-lobe studied by electrospray ionization mass spectrometry. Analytical Chemistry. 73, 2565 (2001)

102. Zhang, M.,Gumerov, D. R.,Kaltashov, I. A.,Mason, A. B.: Indirect detection of protein-metal binding: interaction of serum transferrin with In3+ and Bi3+. J Am Soc Mass Spectrom. 15, 1658 (2004)

103. Karas, M.,Bahr, U.,Dulcks, T.: Nano-electrospray ionization mass spectrometry: addressing analytical problems beyond routine. Fresen J Anal Chem. 366, 669 (2000)

104. Wang, L.,Pan, H.,Smith, D. L.: Hydrogen exchange-mass spectrometry: optimization of digestion conditions. Mol Cell Proteomics. 1, 132 (2002)

105. Kaltashov, I. A.,Eyles, S. J.: Crossing the phase boundary to study protein dynamics and function: combination of amide hydrogen exchange in solution and ion fragmentation in the gas phase. J Mass Spectrom. 37, 557 (2002)

106. Engen, J. R.,Smith, D. L.: Investigating protein structure and dynamics by hydrogen exchange MS. Anal Chem. 73, 256A (2001)

107. Wales, T. E.,Engen, J. R.: Hydrogen exchange mass spectrometry for the analysis of protein dynamics. Mass Spectrom Rev. 25, 158 (2006)

108. Weis, D. D. *Hydrogen Exchange Mass Spectrometry of Proteins*; Wiley Online Library, 2015.

109. Kaltashov, I. A.,Bobst, C. E.,Abzalimov, R. R.: Hydrogen/Deuterium Exchange Mass Spectrometry (HDX MS) in the Studies of Architecture, Dynamics, and Interactions of Biopharmaceutical Products. Mass Spectrometry Handbook. 7, 227 (2012)

110. Yang, H.,Smith, D. L.: Kinetics of cytochrome c folding examined by hydrogen exchange and mass spectrometry. Biochemistry. 36, 14992 (1997)

111. Engen, J. R.,Wales, T. E.: Analytical Aspects of Hydrogen Exchange Mass Spectrometry. Annu Rev Anal Chem (Palo Alto Calif). 8, 127 (2015)

112. Kaltashov, I. A.,Bobst, C. E.,Abzalimov, R. R.,Wang, G.,Baykal, B.,Wang, S.: Advances and challenges in analytical characterization of biotechnology products: mass spectrometry-based approaches to study properties and behavior of protein therapeutics. Biotechnol Adv. 30, 210 (2012)

113. Percy, A. J.,Rey, M.,Burns, K. M.,Schriemer, D. C.: Probing protein interactions with hydrogen/deuterium exchange and mass spectrometry-a review. Anal Chim Acta. 721, 7 (2012)

114. Marcsisin, S. R.,Engen, J. R.: Hydrogen exchange mass spectrometry: what is it and what can it tell us? Anal Bioanal Chem. 397, 967 (2010)

115. Woodward, C.: Advances in protein hydrogen exchange by mass spectrometry. Journal of the American Society for Mass Spectrometry. 10, 672 (1999)

116. Smith, D. L.,Deng, Y.,Zhang, Z.: Probing the non-covalent structure of proteins by amide hydrogen exchange and mass spectrometry. J Mass Spectrom. 32, 135 (1997)

117. Suchanova, B.,Tuma, R.: Folding and assembly of large macromolecular complexes monitored by hydrogen-deuterium exchange and mass spectrometry. Microb Cell Fact. 7, 12 (2008)

118. Walters, B. T.,Ricciuti, A.,Mayne, L.,Englander, S. W.: Minimizing back exchange in the hydrogen exchange-mass spectrometry experiment. J Am Soc Mass Spectrom. 23, 2132 (2012)

119. Hvidt, A.,Nielsen, S. O.: Hydrogen exchange in proteins. Adv Protein Chem. 21, 287 (1966)

120. Kaltashov, I. A.,Eyles, S. J.: Secondary Mass Spectrometry-Based Approaches to Study Biomolecular Dynamics: Equilibrium Intermediates. (eds.) Mass Spectrometry in Biophysics, p. 183. John Wiley & Sons, Inc., (2005)

121. Gertsman, I.,Komives, E. A.,Johnson, J. E.: HK97 maturation studied by crystallography and H/2H exchange reveals the structural basis for exothermic particle transitions. J Mol Biol. 397, 560 (2010)

122. Garcia, N. K.,Guttman, M.,Ebner, J. L.,Lee, K. K.: Dynamic changes during acid-induced activation of influenza hemagglutinin. Structure. 23, 665 (2015)

123. Kaltashov, I. A.,Bobst, C. E.,Abzalimov, R. R.,Berkowitz, S. A.,Houde, D.: Conformation and dynamics of biopharmaceuticals: transition of mass spectrometry-based tools from academe to industry. J Am Soc Mass Spectrom. 21, 323 (2010)

124. Bantscheff, M.,Lemeer, S.,Savitski, M. M.,Kuster, B.: Quantitative mass spectrometry in proteomics: critical review update from 2007 to the present. Anal Bioanal Chem. 404, 939 (2012)

125. Profrock, D.,Prange, A.: Inductively coupled plasma-mass spectrometry (ICP-MS) for quantitative analysis in environmental and life sciences: a review of challenges, solutions, and trends. Appl Spectrosc. 66, 843 (2012)

126. Sanz-Medel, A.,Montes-Bayón, M.,Bettmer, J.,Fernández-Sanchez, M. L.,Encinar, J. R.: ICP-MS for absolute quantification of proteins for heteroatom-tagged, targeted proteomics. TrAC Trends in Analytical Chemistry. 40, 52 (2012)

127. Liu, R.,Lv, Y.,Hou, X.,Yang, L.,Mester, Z.: Protein quantitation using Ru-NHS ester tagging and isotope dilution high-pressure liquid chromatography–inductively coupled plasma mass spectrometry determination. Analytical Chemistry. 84, 2769 (2012)

128. Thomas, R. *Practical guide to ICP-MS: a tutorial for beginners*; Second ed.; CRC press, 2013.

129. Amr, M. A.: The collision/reaction cell and its application in inductively coupled plasma mass spectrometry for the determination of radioisotopes: A literature review. Adv. Appl. Sci. Res. 3, 2179 (2012)

130. Chen, R.,Jiang, X.,Conaway, M. C.,Mohtashemi, I.,Hui, L.,Viner, R.,Li, L.: Mass spectral analysis of neuropeptide expression and distribution in the nervous system of the lobster Homarus americanus. J Proteome Res. 9, 818 (2010)

131. Jones, E. A.,Shyti, R.,van Zeijl, R. J.,van Heiningen, S. H.,Ferrari, M. D.,Deelder, A. M.,Tolner, E. A.,van den Maagdenberg, A. M.,McDonnell, L. A.: Imaging mass spectrometry to visualize biomolecule distributions in mouse brain tissue following hemispheric cortical spreading depression. J Proteomics. 75, 5027 (2012)

132. Shanta, S. R.,Kim, T. Y.,Hong, J. H.,Lee, J. H.,Shin, C. Y.,Kim, K. H.,Kim, Y. H.,Kim, S. K.,Kim, K. P.: A new combination MALDI matrix for small molecule analysis: application to imaging mass spectrometry for drugs and metabolites. Analyst. 137, 5757 (2012)

133. Touboul, D.,Brunelle, A.: MALDI mass spectrometry imaging of lipids and primary metabolites on rat brain sections. Methods Mol Biol. 1203, 41 (2015)

134. Ait-Belkacem, R.,Sellami, L.,Villard, C.,DePauw, E.,Calligaris, D.,Lafitte, D.: Mass spectrometry imaging is moving toward drug protein co-localization. Trends Biotechnol. 30, 466 (2012)

135. Chew, Y. V.,Holmes, A. J.,Cliff, J. B.: Visualization of metabolic properties of bacterial cells using nanoscale secondary ion mass spectrometry (NanoSIMS). Methods Mol Biol. 1096, 133 (2014)

136. Kim, Y. P.,Shon, H. K.,Shin, S. K.,Lee, T. G.: Probing nanoparticles and nanoparticle-conjugated biomolecules using time-of-flight secondary ion mass spectrometry. Mass Spectrom Rev. 34, 237 (2015)

137. Boxer, S. G.,Kraft, M. L.,Weber, P. K.: Advances in imaging secondary ion mass spectrometry for biological samples. Annu Rev Biophys. 38, 53 (2009)

138. Fletcher, J. S.,Vickerman, J. C.: Secondary ion mass spectrometry: characterizing complex samples in two and three dimensions. Analytical Chemistry. 85, 610 (2013)

139. Prideaux, B.,Stoeckli, M.: Mass spectrometry imaging for drug distribution studies. J Proteomics. 75, 4999 (2012)

140. Becker, J. S. *Inorganic mass spectrometry : principles and applications*; John Wiley & Sons: Chichester, England; Hoboken, NJ, 2007.

141. Becker, J. S.,Becker, J. S.,Dressler, V. L.,Wu, B.,Zoriy, M.: Imaging of metals and metal-containing species in biological tissues and on gels by laser ablation inductively coupled plasma mass spectrometry (LA-ICP-MS): a new analytical strategy for applications in life sciences. Pure and Applied Chemistry. 80, 2643 (2008)

142. Ifa, D. R.,Wiseman, J. M.,Song, Q.,Cooks, R. G.: Development of capabilities for imaging mass spectrometry under ambient conditions with desorption electrospray ionization (DESI). International Journal of Mass Spectrometry. 259, 8 (2007)

143. Robichaud, G.,Barry, J. A.,Garrard, K. P.,Muddiman, D. C.: Infrared matrix-assisted laser desorption electrospray ionization (IR-MALDESI) imaging source coupled to a FT-ICR mass spectrometer. J Am Soc Mass Spectrom. 24, 92 (2013)

144. Cooks, R. G.,Ouyang, Z.,Takats, Z.,Wiseman, J. M.: Ambient Mass Spectrometry. Science. 311, 1566 (2006)

145. Becker, J. S.,Zoriy, M.,Matusch, A.,Wu, B.,Salber, D.,Palm, C.: Bioimaging of metals by laser ablation inductively coupled plasma mass spectrometry (LA-ICP-MS). Mass Spectrom Rev. 29, 156 (2010)

146. Bonta, M.,Lohninger, H.,Marchetti-Deschmann, M.,Limbeck, A.: Application of gold thin-films for internal standardization in LA-ICP-MS imaging experiments. Analyst. 139, 1521 (2014)

147. Gray, A. L.: Solid sample introduction by laser ablation for inductively coupled plasma source mass spectrometry. Analyst. 110, 551 (1985)

148. Jackson, S. E.,Longerich, H. P.,Dunning, G. R.,Fryer, B. J.: The application of laser-ablation microprobe-inductively coupled plasma-mass spectrometry (LAM-ICP-MS) to in situ trace-element determinations in minerals. Canadian Mineralogist. 30, 1049 (1992)

149. Niehoff, A. C.,Moosmann, A.,Sobbing, J.,Wiehe, A.,Mulac, D.,Wehe, C. A.,Reifschneider, O.,Blaske, F.,Wagner, S.,Sperling, M.,von Briesen, H.,Langer, K.,Karst, U.: A palladium label to monitor nanoparticle-assisted drug delivery of a photosensitizer into tumor spheroids by elemental bioimaging. Metallomics. 6, 77 (2014)

150. Konz, I.,Fernandez, B.,Fernandez, M. L.,Pereiro, R.,Gonzalez-Iglesias, H.,Coca-Prados, M.,Sanz-Medel, A.: Quantitative bioimaging of trace elements in the human lens by LA-ICP-MS. Anal Bioanal Chem. 406, 2343 (2014)

151. Noinaj, N.,Easley, N. C.,Oke, M.,Mizuno, N.,Gumbart, J.,Boura, E.,Steere, A. N.,Zak, O.,Aisen, P.,Tajkhorshid, E.,Evans, R. W.,Gorringe, A. R.,Mason, A. B.,Steven, A. C.,Buchanan, S. K.: Structural basis for iron piracy by pathogenic Neisseria. Nature. 483, 53 (2012)

152. Houde, D.,Berkowitz, S. A.,Engen, J. R.: The utility of hydrogen/deuterium exchange mass spectrometry in biopharmaceutical comparability studies. J Pharm Sci. 100, 2071 (2011)

153. Englander, S. W.,Kallenbach, N. R.: Hydrogen exchange and structural dynamics of proteins and nucleic acids. Q Rev Biophys. 16, 521 (1983)

154. Bai, Y.,Milne, J. S.,Mayne, L.,Englander, S. W.: Primary structure effects on peptide group hydrogen exchange. Proteins. 17, 75 (1993)

155. Connelly, G. P.,Bai, Y.,Jeng, M. F.,Englander, S. W.: Isotope effects in peptide group hydrogen exchange. Proteins. 17, 87 (1993)

156. Huang, W.,Groothuys, S.,Heredia, A.,Kuijpers, B. H.,Rutjes, F. P.,van Delft, F. L.,Wang, L. X.: Enzymatic glycosylation of triazole-linked GlcNAc/Glc-peptides: synthesis, stability and anti-HIV activity of triazole-linked HIV-1 gp41 glycopeptide C34 analogues. Chembiochem. 10, 1234 (2009)

157. Hamuro, Y.,Coales, S. J.,Molnar, K. S.,Tuske, S. J.,Morrow, J. A.: Specificity of immobilized porcine pepsin in H/D exchange compatible conditions. Rapid Commun Mass Spectrom. 22, 1041 (2008)

158. Pan, J.,Han, J.,Borchers, C. H.,Konermann, L.: Hydrogen/deuterium exchange mass spectrometry with top-down electron capture dissociation for characterizing structural transitions of a 17 kDa protein. J Am Chem Soc. 131, 12801 (2009)

159. Kaltashov, I. A.,Eyles, S. J.: Studies of biomolecular conformations and conformational dynamics by mass spectrometry. Mass Spectrom Rev. 21, 37 (2002)

160. Ahmad, S.,Gromiha, M.,Fawareh, H.,Sarai, A.: ASAView: database and tool for solvent accessibility representation in proteins. BMC Bioinformatics. 5, 51 (2004)

161. Chu, X.,Wang, J.: Specificity and affinity quantification of flexible recognition from underlying energy landscape topography. PLoS Comput Biol. 10, e1003782 (2014)

162. James, N. G.,Byrne, S. L.,Mason, A. B.: Incorporation of 5-hydroxytryptophan into transferrin and its receptor allows assignment of the pH induced changes in intrinsic fluorescence when iron is released. Biochim Biophys Acta. 1794, 532 (2009)

163. Tsutsui, Y.,Liu, L.,Gershenson, A.,Wintrode, P. L.: The conformational dynamics of a metastable serpin studied by hydrogen exchange and mass spectrometry. Biochemistry. 45, 6561 (2006)

164. Laskowski, R. A.,Gerick, F.,Thornton, J. M.: The structural basis of allosteric regulation in proteins. Febs Lett. 583, 1692 (2009)

165. Zhang, Q.,Chen, J.,Kuwajima, K.,Zhang, H. M.,Xian, F.,Young, N. L.,Marshall, A. G.: Nucleotide-induced conformational changes of tetradecameric GroEL mapped by H/D exchange monitored by FT-ICR mass spectrometry. Sci Rep. 3, 1247 (2013)

166. Zheng, J.,Yong, H. Y.,Panutdaporn, N.,Liu, C.,Tang, K.,Luo, D.: High-resolution HDX-MS reveals distinct mechanisms of RNA recognition and activation by RIG-I and MDA5. Nucleic Acids Res. 43, 1216 (2015)

167. Wagner, J. R.,Lee, C. T.,Durrant, J. D.,Malmstrom, R. D.,Feher, V. A.,Amaro, R. E.: Emerging Computational Methods for the Rational Discovery of Allosteric Drugs. Chem Rev. 116, 6370 (2016)

168. Livingstone, C. D.,Barton, G. J.: Protein sequence alignments: a strategy for the hierarchical analysis of residue conservation. Comput Appl Biosci. 9, 745 (1993)

169. Williams, A. M.,Enns, C.: A region of the C-terminal portion of the human transferrin receptor contains an asparagine-linked glycosylation site critical for receptor structure and function. Journal of Biological Chemistry. 268, 12780 (1993)

170. Wang, W.,Antonsen, K.,Wang, Y. J.,Wang, D.: pH dependent effect of glycosylation on protein stability. european journal of pharmaceutical sciences. 33, 120 (2008)

171. Byrne, S. L.,Chasteen, N. D.,Steere, A. N.,Mason, A. B.: The unique kinetics of iron release from transferrin: the role of receptor, lobe-lobe interactions, and salt at endosomal pH. J Mol Biol. 396, 130 (2010)

172. Steere, A. N.,Chasteen, N. D.,Miller, B. F.,Smith, V. C.,MacGillivray, R. T.,Mason, A. B.: Structure-based mutagenesis reveals critical residues in the transferrin receptor participating in the mechanism of pH-induced release of iron from human serum transferrin. Biochemistry. 51, 2113 (2012)

173. Xu, G.,Liu, R.,Zak, O.,Aisen, P.,Chance, M. R.: Structural allostery and binding of the transferrin*receptor complex. Mol Cell Proteomics. 4, 1959 (2005)

174. Liao, S. M.,Du, Q. S.,Meng, J. Z.,Pang, Z. W.,Huang, R. B.: The multiple roles of histidine in protein interactions. Chem Cent J. 7, 44 (2013)

175. D'Souza, S. E.,Ginsberg, M. H.,Plow, E. F.: Arginyl-glycyl-aspartic acid (RGD): a cell adhesion motif. Trends Biochem Sci. 16, 246 (1991)

176. Ruoslahti, E.: RGD and other recognition sequences for integrins. Annu Rev Cell Dev Biol. 12, 697 (1996)

177. Hentze, M. W.,Muckenthaler, M. U.,Galy, B.,Camaschella, C.: Two to tango: regulation of Mammalian iron metabolism. Cell. 142, 24 (2010)

178. Luck, A. N.,Mason, A. B.: Transferrin-mediated cellular iron delivery. Curr Top Membr. 69, 3 (2012)

179. Wally, J.,Buchanan, S. K.: A structural comparison of human serum transferrin and human lactoferrin. Biometals. 20, 249 (2007)

180. Abdizadeh, H.,Atilgan, A. R.,Atilgan, C.: Detailed molecular dynamics simulations of human transferrin provide insights into iron release dynamics at serum and endosomal pH. J Biol Inorg Chem. 20, 705 (2015)

181. Bertrand, N.,Wu, J.,Xu, X.,Kamaly, N.,Farokhzad, O. C.: Cancer nanotechnology: the impact of passive and active targeting in the era of modern cancer biology. Adv Drug Deliv Rev. 66, 2 (2014)

182. Kratz, F.: A clinical update of using albumin as a drug vehicle - a commentary. J Control Release. 190, 331 (2014)

183. Nehoff, H.,Parayath, N. N.,Domanovitch, L.,Taurin, S.,Greish, K.: Nanomedicine for drug targeting: strategies beyond the enhanced permeability and retention effect. Int J Nanomedicine. 9, 2539 (2014)

184. Ruoslahti, E.,Bhatia, S. N.,Sailor, M. J.: Targeting of drugs and nanoparticles to tumors. J Cell Biol. 188, 759 (2010)

185. Qian, Z. M.,Li, H.,Sun, H.,Ho, K.: Targeted drug delivery via the transferrin receptor-mediated endocytosis pathway. Pharmacol Rev. 54, 561 (2002)

186. Rainov, N. G.,Soling, A.: Technology evaluation: TransMID, KS Biomedix/Nycomed/Sosei/PharmaEngine. Curr Opin Mol Ther. 7, 483 (2005)

187. Davis, M. E.: The first targeted delivery of siRNA in humans via a self-assembling, cyclodextrin polymer-based nanoparticle: from concept to clinic. Mol Pharm. 6, 659 (2009)

188. Broadwell, R. D.,Baker-Cairns, B. J.,Friden, P. M.,Oliver, C.,Villegas, J. C.: Transcytosis of protein through the mammalian cerebral epithelium and endothelium. III. Receptor-mediated transcytosis through the blood-brain barrier of blood-borne transferrin and antibody against the transferrin receptor. Exp Neurol. 142, 47 (1996)

189. Pardridge, W. M.: Re-engineering biopharmaceuticals for delivery to brain with molecular Trojan horses. Bioconjug Chem. 19, 1327 (2008)

190. Amet, N.,Wang, W.,Shen, W. C.: Human growth hormone-transferrin fusion protein for oral delivery in hypophysectomized rats. J Control Release. 141, 177 (2010)

191. Jones, A. R.,Shusta, E. V.: Blood-brain barrier transport of therapeutics via receptor-mediation. Pharm Res. 24, 1759 (2007)

192. Smith, M. W.,Gumbleton, M.: Endocytosis at the blood-brain barrier: from basic understanding to drug delivery strategies. J Drug Target. 14, 191 (2006)

193. Ashwood, E. R.,Burtis, C. A.,Tietz, N. W. *Tietz textbook of clinical chemistry*; third ed.; WB Saunders Company: Philadelphia, 1999.

194. Mayle, K. M.,Le, A. M.,Kamei, D. T.: The intracellular trafficking pathway of transferrin. Biochim Biophys Acta. 1820, 264 (2012)

195. Fenselau, C.,Yao, X.: 18O2-labeling in quantitative proteomic strategies: a status report. J Proteome Res. 8, 2140 (2009)

196. Wang, S.,Kaltashov, I. A.: A new strategy of using O18-labeled iodoacetic acid for mass spectrometry-based protein quantitation. J Am Soc Mass Spectrom. 23, 1293 (2012)

197. Wang, S.,Bobst, C. E.,Kaltashov, I. A.: A new liquid chromatography-mass spectrometry-based method to quantitate exogenous recombinant transferrin in cerebrospinal fluid: a potential approach for pharmacokinetic studies of transferrin-based therapeutics in the central nervous systems. Eur J Mass Spectrom (Chichester, Eng). 21, 369 (2015)

198. Angel, P. M.,Caprioli, R. M.: Matrix-assisted laser desorption ionization imaging mass spectrometry: in situ molecular mapping. Biochemistry. 52, 3818 (2013)

199. Kutscher, D. J.,Busto, M. E. D.,Zinn, N.,Sanz-Medel, A.,Bettmer, J.: Protein labelling with mercury tags: fundamental studies on ovalbumin derivatised with p-hydroxymercuribenzoic acid (pHMB). J Anal Atom Spectrom. 23, 1359 (2008)

200. Kutscher, D. J.,del Castillo Busto, M. E.,Zinn, N.,Sanz-Medel, A.,Bettmer, J.: Protein labelling with mercury tags: fundamental studies on ovalbumin derivatised with p-hydroxymercuribenzoic acid (pHMB). J Anal Atom Spectrom. 23, 1359 (2008)

201. Patel, P.,Jones, P.,Handy, R.,Harrington, C.,Marshall, P.,Evans, E. H.: Isotopic labelling of peptides and isotope ratio analysis using LC-ICP-MS: a preliminary study. Anal Bioanal Chem. 390, 61 (2008)

202. Ahrends, R.,Pieper, S.,Kuhn, A.,Weisshoff, H.,Hamester, M.,Lindemann, T.,Scheler, C.,Lehmann, K.,Taubner, K.,Linscheid, M. W.: A metal-coded affinity tag approach to quantitative proteomics. Mol Cell Proteomics. 6, 1907 (2007)

203. Thibon, A.,Pierre, V. C.: Principles of responsive lanthanide-based luminescent probes for cellular imaging. Anal Bioanal Chem. 394, 107 (2009)

204. Sun, H. Z.,Li, H. Y.,Sadler, P. J.: Transferrin as a metal ion mediator. Chemical Reviews. 99, 2817 (1999)

205. Hochuli, E.,Dobeli, H.,Schacher, A.: New metal chelate adsorbent selective for proteins and peptides containing neighbouring histidine residues. J Chromatogr. 411, 177 (1987)

206. Glennon, J. D.,Sarkar, B.: Nickel(II) transport in human blood serum. Studies of nickel(II) binding to human albumin and to native-sequence peptide, and ternary-complex formation with L-histidine. Biochem J. 203, 15 (1982)

207. Sharma, S.,Grobe, A. C.,Wiseman, D. A.,Kumar, S.,Englaish, M.,Najwer, I.,Benavidez, E.,Oishi, P.,Azakie, A.,Fineman, J. R.,Black, S. M.: Lung antioxidant enzymes are regulated by development and increased pulmonary blood flow. Am J Physiol Lung Cell Mol Physiol. 293, L960 (2007)

208. Vidaud, C.,Gourion-Arsiquaud, S.,Rollin-Genetet, F.,Torne-Celer, C.,Plantevin, S.,Pible, O.,Berthomieu, C.,Quemeneur, E.: Structural consequences of binding of UO2(2+) to apotransferrin: can this protein account for entry of uranium into human cells? Biochemistry. 46, 2215 (2007)

209. Harris, W. R.,Pecoraro, V. L.: Thermodynamic binding constants for gallium transferrin. Biochemistry. 22, 292 (1983)

210. Li, Y.,Liu, B.,Ge, Z.,Yang, B.: Spectroscopic analysis of the interaction between gallium(III) and apoovotransferrin. J Photochem Photobiol B. 91, 137 (2008)

211. Bobst, C. E.,Zhang, M.,Kaltashov, I. A.: Existence of a noncanonical state of iron-bound transferrin at endosomal pH revealed by hydrogen exchange and mass spectrometry. J Mol Biol. 388, 954 (2009)

212. Kaltashov, I. A.,Bobst, C. E.,Zhang, M.,Leverence, R.,Gumerov, D. R.: Transferrin as a model system for method development to study structure, dynamics and interactions of metalloproteins using mass spectrometry. Biochim Biophys Acta. 1820, 417 (2012)

213. Becker, J. S.,Matusch, A.,Wu, B.: Bioimaging mass spectrometry of trace elements - recent advance and applications of LA-ICP-MS: A review. Anal Chim Acta. 835, 1 (2014)

214. Lietz, C. B.,Gemperline, E.,Li, L.: Qualitative and quantitative mass spectrometry imaging of drugs and metabolites. Adv Drug Deliv Rev. 65, 1074 (2013)

215. Gessel, M. M.,Norris, J. L.,Caprioli, R. M.: MALDI imaging mass spectrometry: spatial molecular analysis to enable a new age of discovery. J Proteomics. 107, 71 (2014)

216. Zaia, J.,Fabris, D.,Wei, D.,Karpel, R. L.,Fenselau, C.: Monitoring metal ion flux in reactions of metallothionein and drug-modified metallothionein by electrospray mass spectrometry. Protein Sci. 7, 2398 (1998)

217. Kaltashov, I. A.,Zhang, M.,Eyles, S. J.,Abzalimov, R. R.: Investigation of structure, dynamics and function of metalloproteins with electrospray ionization mass spectrometry. Anal Bioanal Chem. 386, 472 (2006)

218. Hartinger, C. G.,Groessl, M.,Meier, S. M.,Casini, A.,Dyson, P. J.: Application of mass spectrometric techniques to delineate the modes-of-action of anticancer metallodrugs. Chem Soc Rev. 42, 6186 (2013)

219. Yu, X. L.,Wojciechowski, M.,Fenselau, C.: Assessment of Metals in Reconstituted Metallothioneins by Electrospray Mass-Spectrometry. Analytical Chemistry. 65, 1355 (1993)

220. Fabris, D.,Fenselau, C.: Characterization of allosteric insulin hexamers by electrospray ionization mass spectrometry. Analytical Chemistry. 71, 384 (1999)

221. Li, H.,Sadler, P. J.,Sun, H.: Rationalization of the strength of metal binding to human serum transferrin. Eur J Biochem. 242, 387 (1996)

222. Konz, I.,Fernandez, B.,Fernandez, M. L.,Pereiro, R.,Sanz-Medel, A.: Absolute quantification of human serum transferrin by species-specific isotope dilution laser ablation ICP-MS. Analytical Chemistry. 83, 5353 (2011)

223. Busto, M. E.,Montes-Bayon, M.,Sanz-Medel, A.: Accurate determination of human serum transferrin isoforms: Exploring metal-specific isotope dilution analysis as a quantitative proteomic tool. Analytical Chemistry. 78, 8218 (2006)

224. Feng, L.,Zhang, D.,Wang, J.,Shen, D.,Li, H.: A novel quantification strategy of transferrin and albumin in human serum by species-unspecific isotope dilution laser ablation inductively coupled plasma mass spectrometry (ICP-MS). Anal Chim Acta. 884, 19 (2015)

225. Nielsen, M. J.,Moestrup, S. K.: Receptor targeting of hemoglobin mediated by the haptoglobins: roles beyond heme scavenging. Blood. 114, 764 (2009)

226. Bobst, C. E.,Thomas, J. J.,Salinas, P. A.,Savickas, P.,Kaltashov, I. A.: Impact of oxidation on protein therapeutics: conformational dynamics of intact and oxidized acid-beta-glucocerebrosidase at near-physiological pH. Protein Sci. 19, 2366 (2010)

227. Abzalimov, R. R.,Bobst, C. E.,Kaltashov, I. A.: A new approach to measuring protein backbone protection with high spatial resolution using H/D exchange and electron capture dissociation. Analytical Chemistry. 85, 9173 (2013)

228. Davson, H.: Secondary The cerebrospinal fluid. (eds.) Handbook of neurochemistry, p. 23. Springer, (1969)

229. Nadal, A.,Fuentes, E.,Pastor, J.,Mcnaughton, P. A.: Plasma-Albumin Is a Potent Trigger of Calcium Signals and DNA-Synthesis in Astrocytes. P Natl Acad Sci USA. 92, 1426 (1995)

230. Choudhury, H.,Pandey, M.,Chin, P. X.,Phang, Y. L.,Cheah, J. Y.,Ooi, S. C.,Mak, K. K.,Pichika, M. R.,Kesharwani, P.,Hussain, Z.,Gorain, B.: Transferrin receptors-targeting nanocarriers for efficient targeted delivery and transcytosis of drugs into the brain tumors: a review of recent advancements and emerging trends. Drug Deliv Transl Res. 8, 1545 (2018)

231. Ren, C.,Bobst, C. E.,Kaltashov, I. A.: Exploiting His-Tags for Absolute Quantitation of Exogenous Recombinant Proteins in Biological Matrices: Ruthenium as a Protein Tracer. Anal Chem. 91, 7189 (2019)

232. Bonvin, G.,Bobst, C. E.,Kaltashov, I. A.: Interaction of transferrin with non-cognate metals studied by native electrospray ionization mass spectrometry. International Journal of Mass Spectrometry. 420, 74 (2017)

233. Xu, S.,Kaltashov, I. A.: Evaluation of Gallium as a Tracer of Exogenous Hemoglobin-Haptoglobin Complexes for Targeted Drug Delivery Applications. J Am Soc Mass Spectrom. 27, 2025 (2016)